NTNU – Trondheim
Norwegian University of
Science and Technology

Fatigue Lifetime Assessment of Typical Longitudinal/End Connections for Large Offshore Service Construction Vessels (OSCVs).

Application of Finite Element Method
Software and Rule Loads

Mads Vambheim Steffensen

Marine Technology (2-year)
Submission date: June 2015
Supervisor: Bernt Johan Leira, IMT

Norwegian University of Science and Technology
Department of Marine Technology

Master thesis, Spring 2015

for

Master Student Mads Vambheim Steffensen

Fatigue Lifetime Assessment of Typical Longitudinal/End Connections for Large Offshore Service Construction Vessels (OSCVs)

Estimering av Utmattingslevetid for Typiske Longitudinaler/Endeforbindelser for store OSCV fartøy

The largest Offshore Subsea Construction Vessels (OSCVs) today are around 180 meters and designed with high strength steel. The design of local hull structure details are based on smaller offshore vessels such as traditional Platform Supply Vessels (PSVs) with length around 80 meters. This situation makes it highly interesting to assess the fatigue lifetime of the vessel.

One specific vessel, or alternatively a more generic detail based on experience from previous design analyses will be studied in more detail.

It is proposed that the work is performed according to the following plan:

1. A literature survey is performed with respect to the historic development and design of past and present OSCVs. In addition, a research and evaluation of the general operational pattern for such vessel, shall be carried out. This should result in a description of the background for the present work and motivation for further development of analysis methods.
2. Existing rules, standards and guidelines for design of such vessels are to be described. Focus is on the DNV GL set of rules.

3. A global Finite Element Model of the hull is to be established. Computation of the stress distribution throughout the hull is to be performed for relevant fatigue load cases. Specific structural details in a region with high dynamic stress amplitudes are to be considered in some more detail, and the local stresses and stress concentrations are to be computed.
4. The relevant DNV GL standard shall first be applied in order to estimate the fatigue lifetime. The expected lifetime values for both worldwide operation and north Atlantic operation shall be estimated.

The work-scope may prove to be larger than initially anticipated. Subject to approval from the supervisor, topics may be deleted from the list above or reduced in extent.

In the thesis the candidate shall present his personal contribution to the resolution of problems within the scope of the thesis work. Theories and conclusions should be based on mathematical derivations and/or logic reasoning identifying the various steps in the deduction. The candidate should utilize the existing possibilities for obtaining relevant literature.

The thesis should be organized in a rational manner to give a clear exposition of results, assessments, and conclusions. The text should be brief and to the point, with a clear language. Telegraphic language should be avoided.

The thesis shall contain the following elements: A text defining the scope, preface, list of contents, summary, main body of thesis, conclusions with recommendations for further work, list of symbols and acronyms, references and (optional) appendices. All figures, tables and equations shall be numerated.

The supervisor may require that the candidate, at an early stage of the work, presents a written plan for the completion of the work. The plan should include a budget for the use of computer and laboratory resources which will be charged to the department. Overruns shall be reported to the supervisor.

The original contribution of the candidate and material taken from other sources shall be clearly defined. Work from other sources shall be properly referenced using an acknowledged referencing system.

The thesis shall be submitted in electronic form:

- Signed by the candidate
- The text defining the scope included
- Drawings and/or computer prints can be organized in a separate folder.

Supervisor: Professor Bernt J. Leira Contact person at Vard: Lars Erik Nygård

Start: January 16th, 2015

Deadline: June 15th, 2015

Trondheim, 19 January 2015

Bernt J. Leira

Abstract

In the last decades there has a major development of the Offshore Service Construction Vessels (OSCV) where high tensile steel has been introduced to increase the dead weight, but also to increase the allowable stress level. In the same period the average main dimensions have increased, leading to greater wave induced hull girder moments. This development has made it interesting to check the expected fatigue lifetime of the structure.

In this thesis, the aim is to assess the expected fatigue lifetime of a longitudinal stiffener (HP-profile) at a typical end support for an OSCV designed by VARD Design AS. The analysis has been according DNV standards with special focus on the Classification Notes No. 30.7 – Fatigue Assessment of Ship Structures.

As a part of the work, the operational pattern for OSCVs has been investigated to determine - in the best possible way - the long term sea environment, in addition to how frequently the general OSCV is at sea where dynamic loading occurs. The result showed that the vessel spend between 60 and 70 % of the time at sea, and that the long-term sea environment is fairly difficult to determine in the design phase. However, worldwide trade assumption appears to be more correct than North Atlantic assumption, based on the fact that these vessels operate when the significant wave height, H_s is small.

Regarding fatigue lifetime of the longitudinal at a typical end support, the analyzes showed that the main deck longitudinals are more critical with respect to fatigue compared to a bottom longitudinals, since the latter are subject to mean stress effect, i.e. the stress cycles are in compression. When applying the operational profile, the calculation shows that the fatigue life of a longitudinal in main deck is about 37 years when assuming North Atlantic environment and 20 years' service life.

The studies have also shown that detail design is important for preventing fatigue damage. Using a soft (radius-ed) bracket will provide lower hot spot stress (/stress concentration factor) compared to a straight edged bracket.

Sammendrag

I løpet av de siste ti-år har det vært en betydelig utvikling for konstruksjonskipene som utfører tjenester for offshore industrien. For å kunne øke lastekapasiteten og kunne tillate høyere spenningsnivå i skrogbjelken, har det blitt vanlig å benytte høyfast stål som skrogmateriale. Samtidig har også hoveddimensjonene økt. Det har medført til at det globale bølgemomentet på skipene har også økt. Som følge av det vil det være interessant å beregne forventet levetid for slike båter, med tanke på utmatting.

I denne oppgaven er målet å estimere den forventede levetiden for en langskipsstiver (Bulb-profil) ved en typisk endeforbindelse (sveiseforbindelse mellom stiver og kneplate). Analysen er utført for et konstruksjonsskip designet av VARD Design AS, og skal utføres i henhold til *DNV Classification Note No. 30.7 – Fatigue Assessment of Ship Structures*.

Som en del av arbeidet, er en undersøkelse av det generelle operasjonsmønsteret til konstruksjonsskipene gjennomført. Målet er da å finne ut hvilket bølgemiljø skipstypen opplever over tid. I tillegg, har studiet som mål å finne ut hvor hyppig skipstypen er til havs hvor de dynamiske lastene opptrer. Resultatet viser at konstruksjonsskipene tilbringer mellom 60 og 70 % av tiden til sjøs, og at langtids bølgemiljø er vanskelig å stadfeste i designfasen. Likevel, tyder resultatet i studiet på at «*worldwide trade*» fremstår som mer riktig å anta fremfor et nordatlantisk bølgemiljø. Det er ikke bare basert på de geografiske områdene skipstypen operer i, men også det faktum at de opererer under rolige sjøtilstander (lav signifikante bølgehøyden).

Angående utmattingslevetid for longitudinaler ved typiske endeforbindelser, viser resultatet at utmatting er mest kritisk for longitudinaler i styrkedekket (hoveddekket). For longitudinaler i bunnen av skroget, viser beregningene at de er utsatt for en statisk kompresjonsspenning i en størrelsesorden som medfører at spenningssyklusen skjer i kompresjon. Som følge av det, er spenningsvidden redusert med 70 % i henhold til klassenotasjonen til DNV GL.

Basert på operasjonsprofilen funnet i oppgaven, viser beregningene at levetiden til longitudinalen i hoveddekket er 37 år. Dette estimatet er basert på antagelse om et 20 år langt operasjonsliv, tillegg til antagelse om at skipet operer i et nordatlantisk bølgemiljø over tid.

Som en del av analysen, ble også to typiske kneplatedesign sammenlignet med tanke på konsentrasjonsfaktoren som er presentert ved tåen av kneplatene. Analysen viste at den ene kneplaten som er designet med en buet kant gir lavere konsentrasjonsfaktor enn den andre som er designet med en rett kant.

Preface

This report is a result of my master thesis work in marine constructions at the Department of Marine Technology at The Norwegian University of Science and Technology, NTNU. The thesis has been written during the spring of 2015.

The focus in the work on this thesis has been to carry out a fatigue lifetime analysis for a longitudinal at a typical end support detail in the hull structure of an OSCV. Through the work, I have gained knowledge about the fatigue phenomenon and the necessary steps that are required to assess the fatigue damage.

I have also gained experience with finite element modelling of ship structures in the finite element method software, Sesam GeniE. The learning part of the FEM software was very time consuming and a lot of time was needed to complete the model. A lot of effort was also used in improving poor meshing and fixing errors in the model.

There have been many contributors to this thesis. First, I want to thank my supervisor at NTNU, Professor Bernt Johan Leira for the thesis guidance and Lars Erik Nygård in VARD Design AS for letting me use their design, and also for the advices and information he has given me. I also want to send a special thanks to Eivind Tørset Magnussen in DNV GL for the help he has given me regarding the finite element modelling, and the many good discussions we've had. In addition, I want to thank Olav Aagaard for the assistance in the initial phase of the FE modelling where he gave me information about applications in Sesam GeniE and different strategies for modelling.

My final gratitude goes to my parents Jarle Steffensen and Sidsel Vambheim for their support during the spring, but also for the overall support during the years of study at the Department of Marine Technology at NTNU.

Trondheim, June 18, 2015

Mads Vambheim Steffensen

Table of Contents

List of figures

List of tables

Terms and Definitions

Base Material	
FPSO	Floating, Production, Storage and Offloading unit (Dokkum, 2011)
Longitudinal	Longitudinal stiffener of the hull girder.
Marine Operation	A non-routine operation of a limited defined duration related to handling of object(s) and/or vessel(s) in the marine environment (inshore/offshore waters, subsea, quay areas and construction sites) during temporary phases (Larsen, 2015).
Mobilization	Out-fitting and re-engineering aspects of a vessel to change its primary purpose, often for only a temporary period (http://www.intermarineuk.com/shipping-mobilisation.htm)
Operational profile	The same as operational trading pattern
OSV	Offshore Service Vessel. It is a common term for the vessels that are providing the offshore oil & gas industry with different services like supply, anchor handling and lifting (Dokkum, 2011).
Rules	DNV Rules for Classification of Ships
Superstructure	A decked structure on the freeboard deck
Scatter diagram	Statistical distribution of the different amplitudes of significant wave height with corresponding wave frequency. It is used to present sea environments in a concise way, typically as environmental input for hydrodynamic and statistical analysis.
Shear lag (-effect)	The effective area in resisting tension/compression. This may be less than the net area.
Strength deck	The uppermost continuous deck in the hull girder (DNV, 2014c).
Merchant vessels	Term about the ship types presented in section 3, DNV CN No. 30.7 – Fatigue Assessment of Ship Structures (DNV, 2014a); tankers, gas carriers, bulk carriers, ore carriers, container ships and roll on / roll off- and car carriers.

Abbreviations

#[number]	Frame number
[modified]	Modifications are made to the original figure/table
[re-drawn]	The figure/table is drawn from scratch based on a reference drawing
AIS	Automatic Identification System
AP	After Perpendicular
BC	Boundary Condition
CL	Center Line
CN	Classification Note

DNV	Det Norske Veritas
dof	Degree(s) of freedom
FE	Finite Element
FEA	Finite Element Analysis
FEM	Finite Element Method
FLS	Fatigue Limit State
FP	Forward Perpendicular
FCL	From Center Line
GM	Metacentric height
HTS	High Tensile Steel
IMR	Inspection, Maintenance & Repair
LC	Load Condition
N/A	Not Applicable or Not Available
NA	Neutral Axis
NF	Not Found
OS	Offshore Standard
ROP	Read Out Point
RP	Recommended Practice
ULS	Ultimate Limit State

Greek Symbols

A	Cross sectional area
B	Greatest moulded breadth of the ship
D	Fatigue damage
C_B	Block coefficient
I	Moment of inertia
K_g	Stress concentration factor
M_{wo}	Vertical wave bending moment amplitude
N	Number of cycles to failure in relation to S-N curves
L	Rule length of the ship
a	Local / global load combination factor
a_i	Acceleration in direction i.
b	Local / global load combination factor
f_e	Environmental reduction factor
f_m	Mean stress reduction factor
f_r	Transformation factor from 10^{-8} to 10^{-4} probability level of exceedance
g	Acceleration of gravity (=9.81 m/s^2)
h	Weibull shape parameter
l	Stiffener length
m	S-N fatigue parameter

p	Lateral pressure
p_n	Sailing rate = fraction of design life at sea
q	Weibull scale parameter
s	Stiffener spacing
t	thickness
T_d	Design service life, normally not to be taken less than 20 years (DNV, 2014c)

Latin Symbols

ν_o	Long-term average zero up-crossing frequency
ρ	Density
ρ_p	Average correlation between sea pressure loads and internal pressure loads
σ	Stress amplitude
σ_2	Secondary stress amplitude
σ_3	Tertiary stress amplitude
σ_e	Total local stress amplitude due to external loads
σ_i	Total local stress amplitude due to internal loads
$\sigma_{nominal}$	Nominal stress amplitude
σ_v	Wave induced vertical hull girder stress
σ_{yield}	Yield stress level of the base material (= 355 N/mm2)
η	Fatigue usage factor
$\Delta\sigma$	Stress range
$\Delta\sigma_g$	Global stress range
$\Delta\sigma_l$	Local stress range
$\Gamma(\ )$	Gamma function

1 Introduction

Fatigue cracks and fatigue damages have been known to ship designers for several decades and a lot of data based on experience have been made available by among others the classification societies (DNV, 2014a). However, in the last decades there has been a major development of the Offshore Service Construction Vessels (OSCV) where high tensile steel has been introduced to increase the dead weight, but also to increase the allowable stress level (VARD, 2015). In the same period the average main dimensions have increased, leading to greater wave induced hull girder moments. This development has made it interesting to check the fatigue life of the OSCV. In this respect the fatigue capacity of the hull is a matter of fatigue capacity of each structural detail.

However, some features regarding the operational pattern are of such character that they may provide lower dynamic loading on the hull. This may for example be the limits for a marine operation with respect to the significant wave height. In addition, the history shows that it often takes weeks and months to mobilize (prepare) the vessel for the next mission (VARD, 2015). So, compared to merchant ships that are normally assumed to spend 85 % of their lifetime at sea where dynamic loads occur, the OSCV is claimed to spend less time, but how much is uncertain.

In this project the expected fatigue lifetime of longitudinals at typical end supports for an OSCV designed by VARD Design AS will be assessed according to DNV GL standards, with basis in *Classification Notes No. 30.7 – Fatigue Assessment of Ship Structures*. As a part of the work, the operational pattern will be investigated to determine - in the best possible way - the long term sea environment, in addition to how frequently the general OSCV is at sea.

The fatigue evaluation will be based on a “simple” method presented in the classification note, where the long-term stress range is based on dynamic loading as specified in the DNV rules and then postulated to follow a Weibull distribution.

It should be noted that the classification note is well suited for merchant ships like tankers, bulk carriers and container vessels due to the vast experience base. It provides operational profiles and structural elements that are of possible interest for fatigue evaluation, for the different kinds. OSCVs, nor Offshore Service Vessels in general, are presented in the document. Thus, the thesis work will see how the classification note applies for OSCVs and to highlight the differences compared to traditional vessels with respect to operational profile, and the fraction of life time spent at sea.

The work is divided into three parts:

- First the DNV Classification Notes No. 30.7 – Fatigue Assessment of Ship Structures is reviewed including a description of the fatigue phenomenon. Other DNV documents dealing with the same topic are also included when relevant.
- The features of OSCVs are described, including an investigation of the operation profile of such vessel. The study will be used as basis for the determination of long-term wave environment and how frequently the vessel is at sea.
- A FE model of the hull is established to calculate the stresses, based on the rule loads. First, the extent of the model, boundaries and load application are presented, in addition to element types and methods for hot spot stress derivation. Then an analysis of the model is carried out where many potential details are given fine mesh directly in the model. Details that turn out to be non-interesting will then be omitted from a further investigation. Two typical bracket designs for longitudinals crossing transverse bulkheads in main deck are also analyzed to see which of them provides the lowest stress concentration factor. Difference between two methods for hot spot stress derivation are specially considered.

2 DNV CN 30.7 - Fatigue Assessment of Ship Structures

The fatigue calculation method that is introduced in the classification note is basically based on application of S-N curves and estimation of cumulative damage (Palmgren – Miner's rule). By employing S-N curves the analyst can determine the number of cycles to failure based on the calculated stress range. These curves are based on fatigue test where a material have been exposed to constant cyclic load until failure (Almar-Næss, 1985).

When determining the long-term stress range, the classification note describes two methods: simplified analysis and direct analysis. The difference is that the simple analysis postulates the long-term stress range distribution with a stress range based on dynamic loading as specified in the rules, while the direct analysis estimates the long-term stress range by use of spectral method. The latter is not going to be explained herein

The stress range obtained in the simple analysis, before estimating the long-term stress range, is a combination of different stress components. Each of these components are the structural stress response to a single load, e.g. hull girder wave moment, internal dynamic tank pressure, or external dynamic wave pressure. Further and more detailed description of the items above, including the fatigue mechanism, are going to be described in the following.

2.1 Fatigue Mechanism

"Fatigue may be defined as a process of cycle by cycle accumulation of damage in a material undergoing fluctuating stresses and strains. A significant feature of fatigue is that the load is not large enough to cause immediate failure. Instead, failure occurs after a certain number of load fluctuations have been experienced, i.e. after the accumulated damage has reached a critical level" (Almar-Næss, 1985).

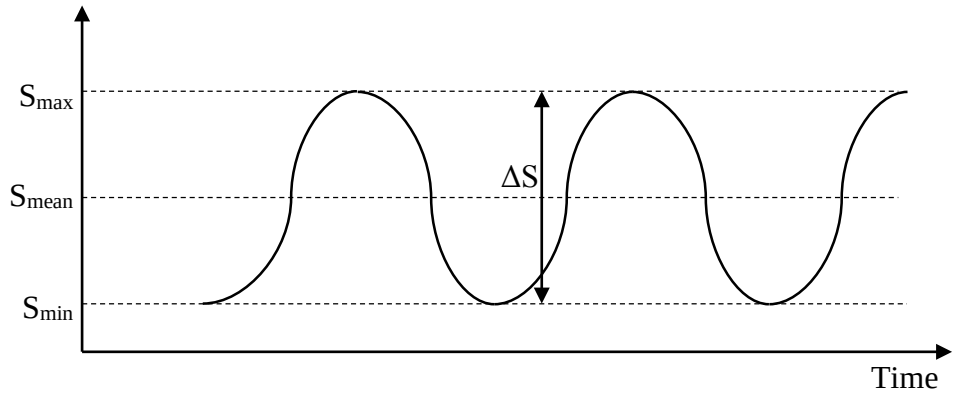

Figure 2.1: Fatigue load history and symbols (Berge, 2006) [re-drawn].

The fluctuating component, also termed stress or strain range, is the most important load effect parameter. It is defined as the difference between a load peak and the subsequently valley. The mean or peaks levels of loading are of relatively minor importance compared to the stress/strain range (Almar-Næss, 1985). Other parameters that affect the fatigue life is the corrosiveness of the environment and the magnitude of stress concentration factors for the structural details (see Hot Spot Stress, section 2.2).

The procedure for fatigue analysis in the classification note is based on the assumption that it is only necessary to consider the ranges of cyclic stress in determining the fatigue endurance. In other words it does not distinguish between compression and tension stresses, but only consider the range between lowest and highest stress value. However, it opens for some reduction in the fatigue damage accumulation when parts of the stress cycle range are in compression. In such case the mean stress effect is considered. A description of this is given in section 2.11.3 on page 17.

2.2 Hot Spot Stress

The hot spot stress is defined as the geometric stress that includes stress rising effects due to significant changes in the geometry such as structural discontinuities and presence of attachments (DNV, 2014a). For hot spot stress at a weld toe it is important to exclude the localized stress due to the presence of the weld itself. If not, the stress is defined as notch stress (see Figure 2.2).

In practical engineering it is common to establish the relation between hot spot stress and the nominal stress at the hot spot. This relation is termed to as stress concentration factor (SCF) and is taken as (DNV, 2014a):

$$SCF = \frac{\sigma_{hot\ spot}}{\sigma_{nominal}} \quad (1)$$

The factor is used to describe how much stress raise the particular detail cause. For practical engineering, it can be used to compare alternative details and used as basis for what details that can be used in the design. In the classification note this factor is denoted as K-factor and the document provides tabulated K-factor values for standard stiffener supports, flange connections and cut outs. Application of these in relation to this thesis work is discussed in section 2.9 on page 13.

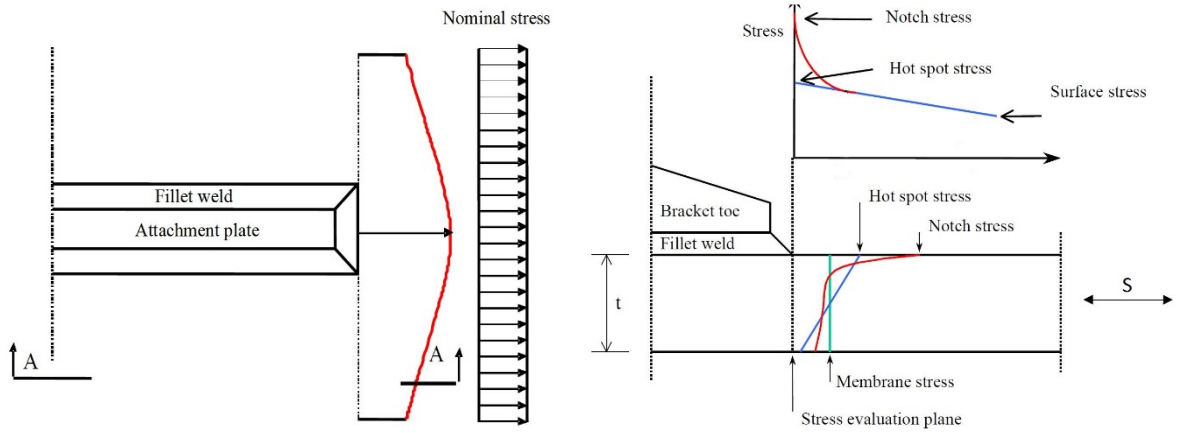

Figure 2.2: Schematic stress distribution at hot spot located at the weld toe of a bracket terminating on a plate (DNV, 2014a) [modified].

2.3 S-N Curves

Assessment of fatigue life is normally assessed by S-N curves that gives the number of cycles to failure based on a given stress range (Almar-Næss, 1985). Such curves are based on testing of metallic components undergoing constant amplitude loading till failure. In this respect loading may be force, strain, or displacement controlled. The S-N plot will in most cases have a span over several decades in cycles, hence plotted on log-log format.

In (DNV, 2014a) the S-N curves are based on the mean-minus-two-standard-deviation curves for experimental data. As a result, they are associated with a 97.6% probability of survival.

With respect to the yield stress of the material, the S-N curves are applicable for both normal and high strength steels used in construction of hull structures. For welded joints, they include the effect of the local weld notch (hot spot S-N curves). Therefore, the S-N curves herein are compatible with calculated stresses that do not include the notch stress due to the weld.

$$\log N = \log \bar{a} - m \log \Delta\sigma \quad (2)$$

N	= predicted number of cycles to failure for stress range $\Delta\sigma$
$\Delta\sigma$	= stress range
m	= negative inverse slope of S-N curve
$\log \bar{a}$	= intercept of log N-axis by S-N curve
	= log a – 2s, where:
	a = constant relating to mean S-N curve
	s = standard deviation of log N; = 0.2

Table 2.1: S-N parameters for air or with cathodic protection (DNV, 2014a) [re-drawn].

S-N curve	Material	$N \leq 10^7$		$N > 10^7$	
		$\log \bar{a}$	m	$\log \bar{a}$	m
I	Welded joint	12.164	3.0	15.606	5.0
III	Base material	15.117	4.0	17.146	5.0
IV	Base material*	12.436	3.0		

)* In corrosive environment – one slope SN curve.

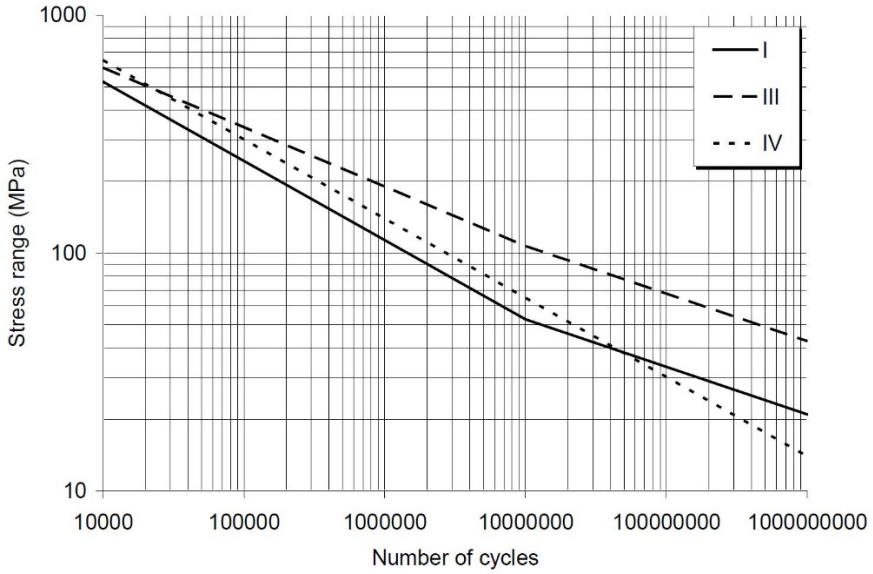

Figure 2.3: S-N curves

2.4 Ship Accelerations and Motions

The formula for ship accelerations and motions in the classification note are derived from the Rules for classification of ships (DNV, 2014c). In this document, the motions and acceleration are extreme values at the probability level 10^{-8}, i.e. value exceeded once in 10^8

wave reversals. As a ship is normally expected to be designed for a lifetime of 20 years (Mürer, 1995), during which period it is assumed that 15 % is spent not sailing (port calls, docking, repairs), the following expression for the lifetime wave encounters is given as:

$$N_l = 0.85 T_1 / 4 \log L \quad (3)$$

T_1 = lifetime in sec. = 3600 x 24 x 365 x 20 = 6.3072 x 10^8 sec.

L= ship length [m]

For a ship of 134.0 meters the number of lifetime encounters thus becomes 6.3 x10^7.

When fatigue life is considered, the number of lifetime encounters will be reduced to a probability level of daily exceedance (10^{-4}) (DNV, 2014a), by application of a transformation factor.

2.5 Dynamic Loads

For a ship at sea it is the wave loads and inertia loads (acceleration of mass) due to motion that cause dynamic loading on the hull structure (DNV, 2014a). Initially, the vessel cargo is causing static loads on the structure, but when the vessel is at sea and subject to waves of a significant level, then the cargo contributes to dynamic loading due to the accelerations. A typical example is the combination of heave, pitch and roll motion.

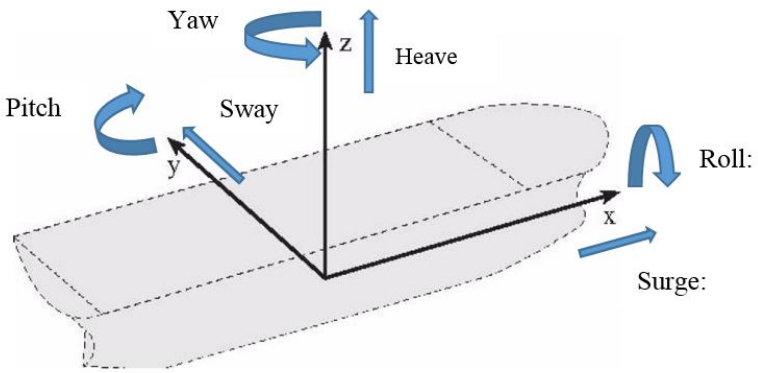

Figure 2.4: Definition of coordinate system and rigid-body motion modes (DNV, 2014a) [modified].

According to the classification note, the dynamic load amplitude does not only depend on the properties of the waves, but also the present properties of the vessel like draught, speed and load distribution. It is therefore necessary to consider all the frequently used loading

conditions in the fatigue evaluation. Loading conditions that are rarely used can be neglected (DNV, 2014a).

2.5.1 Rule wave induced hull girder moment

For fatigue lifetime assessment the classification note calculates a wave moment that has a 10^{-4} probability level of exceedance which correspond to about a daily return period (DNV, 2014b). It uses the same formula as specified in the (DNV, 2014c) and multiplies it by a factor f_r that transform the load from 10^{-8} to 10^{-4} probability level. Consequently, the vertical wave induced moments in sagging and hogging are taken as

$$M_{wo,s} = -0.11 f_r k_{wm} C_w L^2 B (C_B + 0.7) \quad [kNm] \tag{4}$$

$$M_{wo,h} = 0.19 f_r k_{wm} C_w L^2 B C_B \quad [kNm] \tag{5}$$

where
C_w = wave coefficient
k_{wm} = moment distribution factor

The wave coefficient is according to (Mürer, 1995) an expression for the wave height at 80 % level of the extreme waves, in the North Atlantic.

The moment distribution factor is equal to 1.0 in the midship interval 0.4L from AP to 0.65L from AP. According to Figure 2.5 the factor can also be equal to 1.2. This is for ships that have large flare in the fore body and/or designed for high speed (DNV, 2014c). The classification note says only that k_{wm} is equal 1.0, but is stating that this only applies for ships with low/moderate speed. This indicates that the adjustment of k_{wm} in the specified region shall also be considered in a fatigue assessment in accordance with (DNV, 2014a).

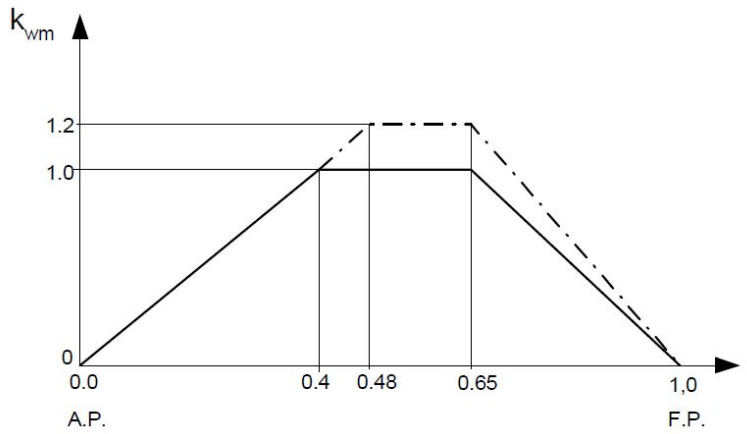

Figure 2.5: Wave bending moment distribution (DNV, 2014c).

2.5.2 Rule horizontal wave bending moment

Similar to the vertical hull girder moment the horizontal wave bending moment is also based on the rule load and transformed from 10^{-8} to 10^{-4} probability level by the transformation factor f_r. However, unlike the vertical moment that is constant (at its maximum) between 0.4L and 0.65 L from AP, the horizontal moment is varying with the length from AP and is taken as:

$$M_{wo,s} = 0.22 f_r L^{9/4}(T_{act}+0.3B)C_B(1-\cos(2\pi x/L)) \quad [kNm] \qquad (6)$$

where

x = distance from AP to section considered.

T_{act} = actual draught in considered load conditions

2.6 Operational Trading Pattern (Operational Profile)

The classification note provides standard values for the operational trading pattern of traditional ship types like oil tankers, bulk carriers and container ships. Common feature for these ships is that they are assumed, based on *normal, worldwide trading*, to spend 85 percent of their lifetime at sea and 15 percent of their lifetime at ports (port calls, docking, repairs). Tabulated values of the fraction of lifetime operating under each loading condition are provided as well, and are reflecting the assumed operational trading pattern for such ships. However, the document opens for that the designer can use his own values, if desired.

Table 2.2: Oil tankers: Fraction of time at sea in loaded and in ballast condition (DNV, 2014a) [re-drawn and modified].

	Time fraction in loading condition, P_n:
Loaded condition, P_1:	0.425
Ballast condition, P_2:	0.425
SUM, P_{tot}:	0.85

Since this project is not dealing with a ship type that is mentioned above, but an OSCV, it is necessary to carry out a study of the operational trading pattern. Its aim is to determine the same type of values as described above, and what loading conditions to be considered in the fatigue evaluation, i.e. the frequently used loading condition.

Instead of using the term operational trading pattern in accordance with the classification note, the term *operational profile* will be used hereafter.

2.7 Stress Components

When performing the simplified fatigue calculation, the final hot spot stress is a sum of many stress components. It is therefore important to make sure that all loads that affect the stress level at the hot spot, are considered. A schematic overview of the stress components caused by the external pressure load is shown in Figure 2.6. However, it is not only the pressure that causes stress. Relative deflection between boundaries is also a source to stresses at the hot spot, as illustrated in Figure 2.7.

It is important to notice that the stress magnitude of the local stress components, in addition to the horizontal hull girder stress, σ_h vary from one loading condition to another. This is because the rule loads are based on the actual draught and the metacentric height, which are often different between the loading conditions. Thus, all frequently used loading conditions need to be considered (DNV, 2014a).

Compression stresses are given negative sign and tension stresses are given positive sign in the calculation.

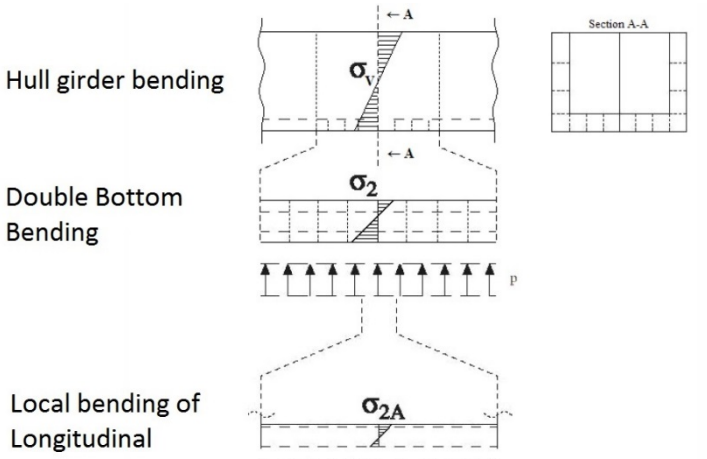

Figure 2.6: Definition of stress components (DNV, 2014a) [modified].

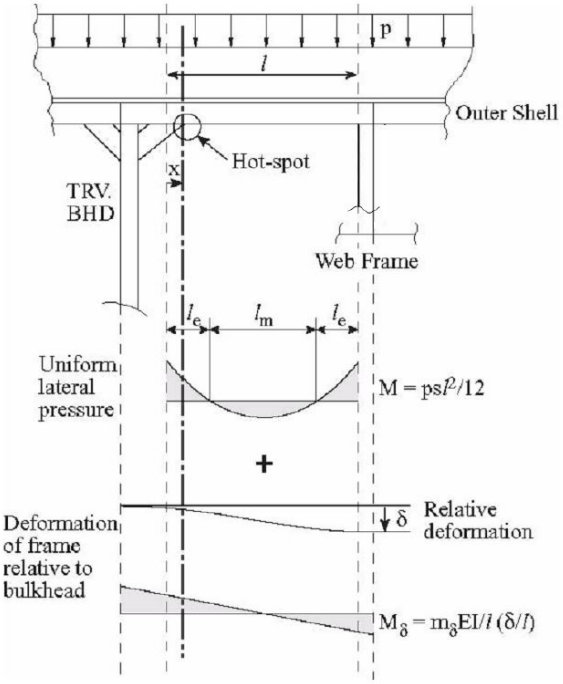

Figure 2.7: Stresses in stiffener subject to bending and relative deflection between the boundaries (DNV, 2014a).

2.8 Screening - Selection of Structural Details for Further Analysis

Similarly to the operational profile, the classification note also provides experienced based information about structural elements that are of possible interest for fatigue evaluation. It also provides information about the loads that need to be considered when checking the hot

spot stress at the specified details. The table below presents an outline of such information regarding the plating and longitudinals in a tanker.

Table 2.3: Possible fatigue critical areas in Oil tankers (DNV, 2014a) [modified].

Structure member	*Structural detail*	*Load type*
Side-, bottom- and deck plating and longitudinals	Butt joint, deck openings and attachment to transverse webs, transverse bulkheads, hopper knuckles and intermediate longitudinal girders	Hull girder bending, stiffener lateral pressure load and support deformation

Regarding OSCVs, such information is not provided by the classification note, thus this experienced based may not be regarded as 100 percent applicable for OSCVs. Consequently, fatigue screening by use of FE model of the hull should be conducted to ensure that all critical details are highlighted (DNV, 2012). In such selective work it is the amplitude of stress range that decides whether further analysis is necessary, or not. So, if the largest stress cycle is below the fatigue limit, then further analysis can be omitted (DNV, 2014a).

However, there may be some similarities between OSCVs and the merchant ships since they share some common design features like longitudinal stiffening of the hull girder. In other words, longitudinals that are supported by transverse members such as bulkheads, girders or floors in the double bottom, are also present in OSCV design. This implies that the advises given in Table 2.3 may also be applicable for OSCV designs if fatigue is an issue.

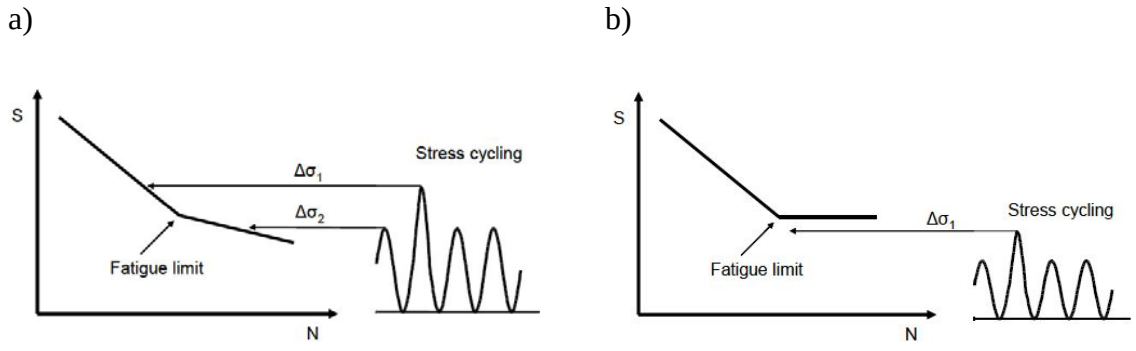

Figure 2.8: Figure a) illustrates where a detailed fatigue assessment is required, while b) shows when further fatigue assessment can be omitted (DNV, 2014a) [Modified].

2.9 Approaches for Assessment of HS stress

Often, the structural details are standard ones and have been analyzed before. Tabulated SCFs are then available for the designer provided that previous analyze results are archived. Such typical details in ship structures, based on the vast experience, are presented in the classification note. The fatigue calculation will then be limited to the validity of the SCFs.

If tabulated values are not available, it will be necessary to make local FE model of the detail in accordance with the requirements to the hot spot method (DNV, 2012).

2.10 Combination of Stress Components

When all the stress components are calculated they need to be combined. All stress components due to local loads, and all stress components due to global loads are then combined separately in accordance with eq. (7) and (8). Since the load components are not at their maximum simultaneously, a correlation coefficient, ρ is applied (eq.(9)). This coefficient is equal to 0.1 when combing the global stress components, while it is a variable for local stress components.

$$\Delta\sigma_l = \sqrt{\Delta\sigma_e^2 + \Delta\sigma_i^2 + 2\rho_p\sigma_e\sigma_i} \tag{7}$$

$$\Delta\sigma_g = \sqrt{\Delta\sigma_v^2 + \Delta\sigma_{hg}^2 + 2\rho_{vh}\Delta\sigma_v\Delta\sigma_{hg}} \tag{8}$$

$$\rho_p = \frac{1}{2} - \frac{z}{10\cdot T_{act}} + \frac{|x|}{4\cdot L} + \frac{|y|}{4\cdot B} - \frac{|x|\cdot z}{5\cdot L\cdot T_{act}} \tag{9}$$

where x, y and z are longitudinal, transverse and vertical distance from origin to load point considered. The origin of the coordinate system ha co-ordinates midship, center line and base line, as shown in Figure 2.4 on page 7.

Regarding the combination of stresses caused by local loads, the local stress amplitudes due to external and internal pressure loads are determined by summarizing the individual local stress components as follows

$$\sigma_{e,i}=\sigma_2+\sigma_{2A}+\sigma_3 \quad (10)$$

where σ_e and σ_i is the total local stress components for external and internal pressure, respectively.

The final step is to combine the local stress range with the global stress range to obtain the total stress range, $\Delta\sigma$ at the hot spot. The total stress range is then taken as

$$\Delta\sigma=\max\begin{cases}\Delta\sigma_g+b\Delta\sigma_l\\ a\Delta\sigma_G+\Delta\sigma_l\end{cases} \quad (11)$$

where a = b = 0.6.

2.11 Long Term Stress Distribution

A two parameter Weibull distribution is assumed for the long term stress ranges. The shape parameter h and scale parameter q are found by empirical formulas that are based on results from (Hovem, 1993). They are as follows:

$$q=\frac{\Delta\sigma_0}{(\ln n_0)^{1/h_n}} \quad (12)$$

$h = h_0$ for deck longitudinals

$h = h_0-0.005T_{act}$ for longitudinal and transverse bulkheads (13)

$$h_0= 2.21-0.54\log_{10}(L) \quad (14)$$

The stress range $\Delta\sigma_0$ used in the equation for the scale parameter is the combined global and local stress where the long term sailing route and high tensile steel quality is accounted for, in addition to the effect of mean stresses. The stress range is taken as

$$\Delta\sigma_0=f_m f_{HT} f_e \Delta\sigma \quad (15)$$

where

f_{HT} Reduction factor on derived combined stress range accounting for the high tensile steel quality for base material fatigue, see section 2.11.1.

f_e Reduction factor accounting for the long-term operational environment / sailing routes. The classification note use 1.0 for operation in North Atlantic

environment, and 0.8 for worldwide operation. The basis for the two values is described in the following section 2.11.2.

f_m Reduction factor for the effect of mean stress. This factor is described in section 2.11.3 on page 17.

The reference stress range value is then used in the S-N curve to determine the corresponding number of cycles to failure.

2.11.1 Reduction factor accounting for HTS quality

According to the classification note, steel material with increased yield stress level will have increased resistance towards cracking in the base material. The derived stress range can then be multiplied by the following factor accounting for this effect.

$$f_{HT} = \frac{1200}{965 + \sigma_{yield}}, \text{ minimum } 0.82 \qquad (16)$$

It should be noted that this effect does not apply for welded joints. This is explained by an experiment presented by A. Almar-Næss which shows fatigue endurance data for steels as a function of yield strength (Figure 2.9). The test shows that the effect of yield strength is large for machined plates and comparatively smaller for as-rolled plates. For welded joints, the fatigue strength is nearly independent of the yield strength.

As a comment to this it should be mentioned that the invariance of fatigue strength to yield strength may therefore have negative consequence on design regarding welded joints. The main reason for using HTSs is basically to be able to increase the allowable stress. In design against an ultimate load, this may be acceptable. A consequence of an increased stress level is, however, a reduced fatigue life. Therefore, the use of high strength steels may lead to fatigue problems. For structural components which are fatigue critical, there is no advantage in using HTS (Almar-Næss, 1985).

Actions that solve particular fatigue problems may be reduction of the stress level, post weld treatment, or by inserting cast components in the critical area. The decrease in stress level may be achieved by improved design of the weld detail (soften the geometric changes), or by increasing the section modulus of the structural members involved.

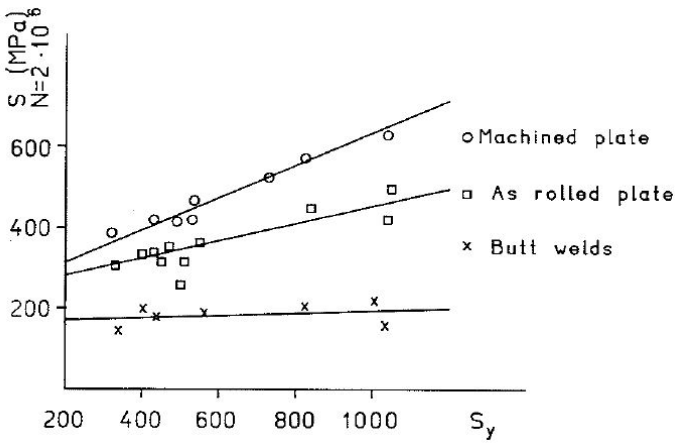

Figure 2.9: Fatigue strength of machined steel plate, as-rolled steel plate, and steel butt welds, as functions of yield stress (Almar-Næss, 1985).

2.11.2 Reduction factor accounting for the long-term sailing routes

The way that the classification note applies the long-term environment is to multiply the stress range by an environmental factor: 1.0 for North Atlantic environment and 0.8 for worldwide operation. This reduction factor is based on direct calculations of fatigue by application of hydrodynamic analyses and input from respectively worldwide and North Atlantic sea environment (Hovem, 1993). It is an approximate factor that varies from detail to detail based on the load. As an example, the factor is necessarily not the same in strength deck where vertical bending moment dominates as in the shipside where dynamic sea pressure dominates. Therefore, this factor may provide inaccurate results depending in the detail to be analyzed.

In the report (Hovem, 1993), the result showed that there is about 10% difference in extreme values between the two scatter diagrams. A consistent reduction in the Weibull parameter was also observed. Based on that, it was concluded to scale the stress level at 10-4 probability level by a factor of 0.8, to account for worldwide operation, hence the reduction factor f_e equal to 0.8 for worldwide operation, in the classification note.

If one is to apply a fatigue analysis on a small vessel that operates in another trade than North Atlantic and worldwide trade statistics, then a new f_e can be estimated provided that one carry out a component stochastic fatigue analysis (DNV, 2014a). In the latter case it is sufficient to only consider vertical wave bending moment. The new environmental factor is then obtained by the following principle (DNV, 2014a):

$$f_{e,new} = \left(\frac{D_a p_a}{D_{NA} p_{NA}}\right)^{\frac{1}{m}} \quad (17)$$

where

D_a = Damage in actual trade

p_a = part time at sea in actual trade

D_{NA} = Damage in North Atlantic

p_{NA} = part time at sea in North Atlantic

m = inverse slope of the SN curve – typ. Taken as 3 for most welded details

2.11.3 Reduction factor for the effect of mean stress

Even though the stress cycle at the hot spot is in tension it may be that the static stress (the mean stress of the stress cycle) is in compression. The magnitude of the compression stress will then decide how great part of the stress cycle will be in compression. This phenomenon is referred to as the mean stress effect and is credited for by multiplying the stress range by the reduction factor f_m (see eq. (15)), which is calculated by the following equation:

$$f_m = \frac{\sigma_t + f \cdot |\sigma_c|}{\sigma_t + |\sigma_c|} \quad (18)$$

f = 0.6 for hotspots in base material not significantly affected by residual stresses due to welding.
= 0.7 for hotspots in base material affected by residual stresses due to welding and construction.

σ_t = tension stress

$$= \max \begin{cases} \sigma_{static} + \frac{\Delta\sigma}{2} \\ 0 \end{cases}$$

σ_c = compression stress

$$= \min \begin{cases} \sigma_{static} - \frac{\Delta\sigma}{2} \\ 0 \end{cases}$$

As seen in equation (18) and Figure 2.10 on next page, the mean stress factor cannot be smaller than 0.6 or 0.7, depending on level of residual stresses from welding. These minimum values are valid when the tension stress is equal to zero, i.e. the absolute value of the static stress in compression is larger than the stress range divided by two.

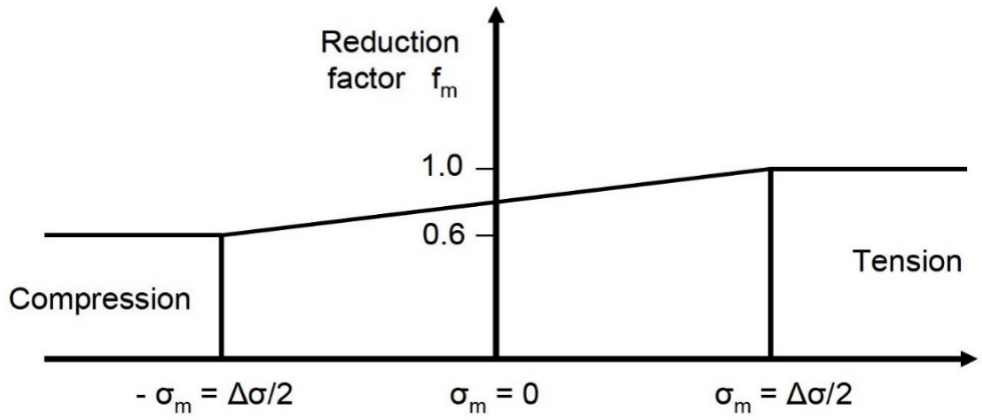

Figure 2.10: Stress range reduction factor (DNV, 2014a).

2.12 Fatigue Damage Calculation

When applying the two-slope SN curve described in section 2.3, the cumulative fatigue damage is calculated by the following equation (DNV, 2014a):

$$D = P_n v_0 T_d \left[\frac{q^{m_1}}{\bar{a}_1} \Gamma\left(1 + \frac{m_1}{h}; \left(\frac{S_1}{q}\right)^h\right) + \frac{q^{m_2}}{\bar{a}_2} \gamma\left(1 + \frac{m_2}{h}; \left(\frac{S_1}{q}\right)^h\right)\right] \quad (19)$$

where

P_n = fraction of design life in load condition n.

v_0 = $\frac{1}{4 \cdot \log_{10}(L)}$

T_d = design life of ship in seconds.

S_1 = Stress range for which change of slope of S-N curve occur.

$\bar{a}_1, m_1$ = S-N fatigue parameters for $N<10^7$ cycles (air condition).

$\bar{a}_2, m_2$ = S-N fatigue parameters for $N>10^7$ cycles (air condition).

$\Gamma(\ )$ = Weibull stress range scale distribution parameter for load condition n.

$\Gamma(\ ;\ )$ = Complementary Incomplete Gamma function, to be found in standard tables.

3 Offshore Service Construction Vessel (OSCV)

One important step in a fatigue evaluation is to determine the expected operational pattern of the ship: How much time is spent at ports, and how much time is spent at sea? These are important questions since the vessel is not subject to dynamic loading while in ports and other closed areas. Furthermore, it is important to consider the loading conditions since the dynamic wave loading on the hull varies with the draught and load distribution in the hull (DNV, 2014a). The stress range level that a structural detail is subject to may therefore vary significantly between the different loading conditions the vessel operates in.

In the classification note tabulated values for the questions above are given for merchant vessels like tankers, bulk carriers and container vessels, but not for OSCVs, and Offshore Service Vessels (OSVs) in general. Hence, this thesis work will seek to find the operational profile for OSCVs, on a general level. Furthermore, the result will be compared to the operational profile of merchant vessels provided in the classification note.

Regarding the investigation of operational profile for OSCVs, the approach is to analyze historical data (AIS data) of a similar operating vessel, and to do an interview with the ship owner/operator about operation of OSCVs in general. Such information is provided by DOF Management AS who has the management responsibility of the vessels owned by the DOF Group and other ship owning companies. The fleet contains of 27 operating subsea vessels and many of these are designed by VARD Design AS (DOF, 2015).

All text about the operational profile of OSCV is based on information provided by (Espen Venge, 2015), but before describing this, general information about the ship type is given. This also includes the historical development over the 10-15 years, based on OSCVs built at Norwegian ship yards since 2002. This information is gathered from maritimt.com.

3.1 About OSCV

Offshore Subsea Construction Vessel (OSCV) is a type of vessel that is very new to the maritime industry. The vessel is based on the typical offshore service vessel (OSV) design which is characterized by a high bow, superstructure in the front and a cargo deck stretching over the mid and aft ship. In addition, it is equipped with an offshore crane (sometimes two) to provide lifting capacity with respect to installation of subsea units, but also for maintenance and repair (Dokkum, 2011).

Often, the vessel is given more functions than just lifting capacity. Such vessels are often referred to as Multi Service Vessels (MSV) because of the large variety of task it can be used for (Dokkum, 2011) and typical features are:

- Survey work (e.g. seabed, pipeline, sub-sea structure);
- (Sub-sea) construction, installation and maintenance and repair work (IMR);
- Trenching of cables or pipelines;
- Installation of flexibles;
- Well intervention and work over services.

Figure 3.1: Illustration of an OSCV in operation by SMSC[1]

3.1.1 Historical Development of OSCV

A research of the historical development of the OSCV is carried out. The work is based on ship reviews by (Magasin, 2014) back to year 2002, which are mainly about ships built at Norwegian yards.

The research shows that there has been a major development of the Offshore Service Construction Vessel from the early 2000, both with respect to dimension and lifting capacity. In the beginning, the lengths were about 100 meters and below, but from 2006 and forward there has been a significant increase in the average length where the longest ones are around

[1] http://www.smsc.no/custom-simulations/lifting-operations

160 meters. The average lifting capacity has been increasing as well in the same period. In the early 2000, 100 tons lifting capacity was the common capacity, but during the last 8 years the typical value appears to be 250 tons, and 400 tons for the biggest ones. Regarding ships under construction, the features seem to have increased even more, as shown in Figure 3.2 and Figure 3.3.

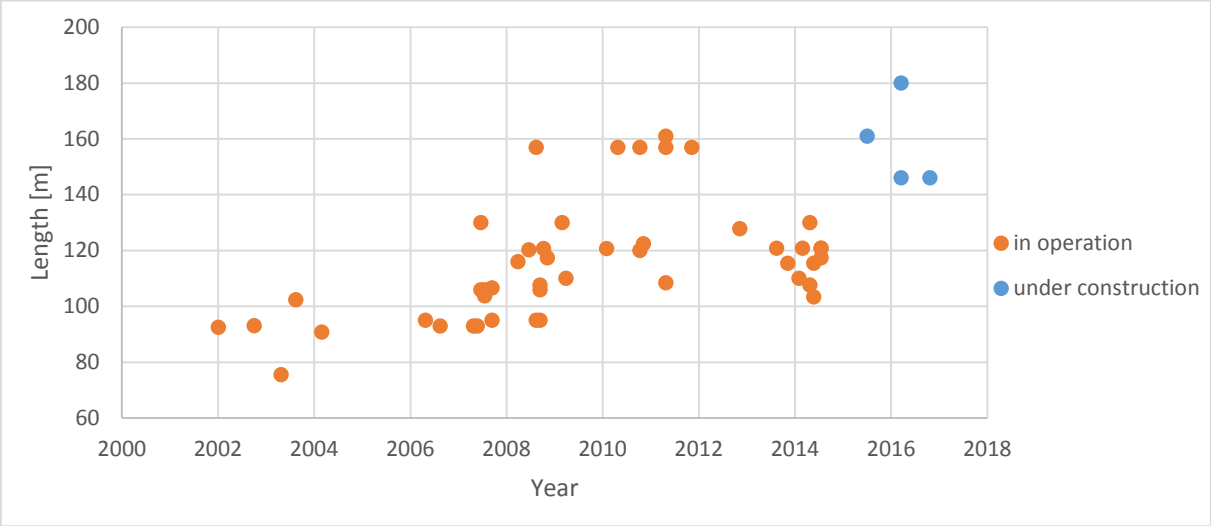

Figure 3.2: Historical development of OSCVs with respect to length (Magasin, 2014).

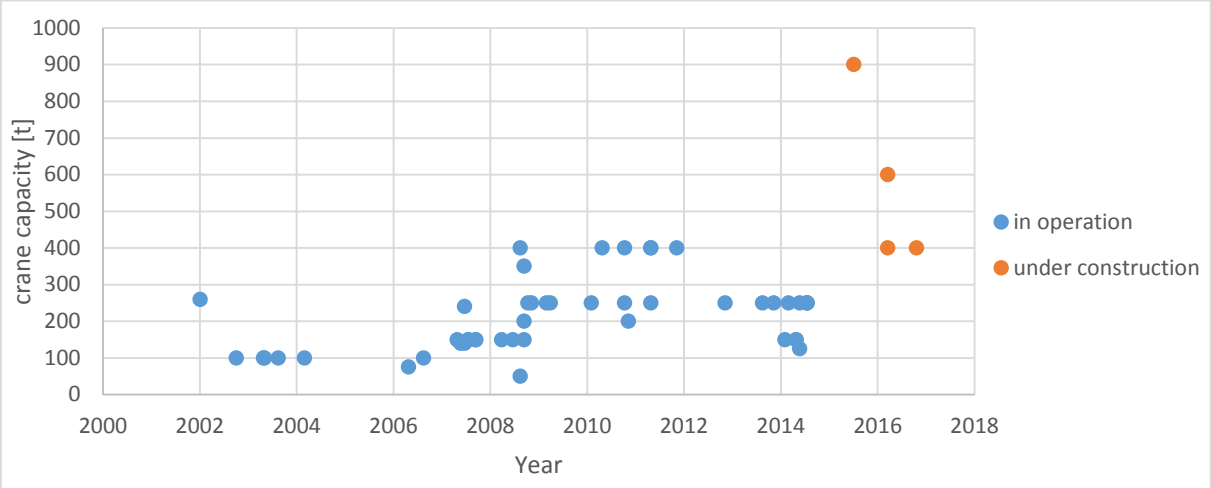

Figure 3.3: Historical development of OSCVs with respect to lifting capacity (Magasin, 2014).

3.1.2 Consequences of the development

The development of the OSCVs has led to a demand for high strength steels in order to meet the requirement of high load capacity (increased dead weight), to increase the allowable stress level, and the eager to improve the strength/weight ratio. To reduce production costs (less

filler material in welds) is also a reason (VARD, 2015). In summary, these factors have led to a general increase in the stress level. As described in section 2.11.1 on page 15, this development leads to a more imminent fatigue problem for welded joints.

In addition, the increased main dimensions, especially the ship length, lead to larger wave induced hull girder moments, according to (DNV, 2014a). It is, however, not the magnitude of the wave bending moment itself that is decisive, but how big it is relative to the still water bending moment.

3.2 How OSCVs Operates

A typical trading pattern for a merchant vessel can be back and forth between west Europe and China, sailing through the Suez Canal. In such case it is easy to determine the operation profile and the long-term sailing environment. The loading condition used during the sailing may also be easy to predict since the ship is expected to carry commercial goods in both directions, or only in one direction and ballast condition in return.

For an OSCV, the operation pattern is not that predictable. During a year the vessel is often operating in many geographical areas and the missions may vary a lot, as shown in the following. It may also have spent significant time in ports preparing for next mission (mobilization).

In the following these topics will be discussed based on interview with (Espen Venge, 2015), (Group, 2015) and AIS data from an operating OSCV, provided by the same company.

3.2.1 Geographical areas

The OSCVs in the Dof Group fleet operate many places around the world where there is oil and gas production off shore. These places are typically in the North Sea (and Norwegian Sea), Gulf of Mexico, the Indian Ocean outside Australia, Brazil and Africa (Namibia and Angola). On what date the vessel is heading for a particular area, and how long it is going to operate there, is not known for fleet management. Only the next few are known.

This implies that the fraction of time in different geographical sea areas during the lifetime of the vessel, is difficult to predict for the designer, and the fleet management. So, what does this have to do with fatigue calculation?

The sea environment differs around the world. The North Sea is characterized as a harsh environment compared to the Gulf of Mexico which is considered to be a benign environment (DNV, 2010). This means that the long-term wave load in the North Sea is greater than the

long-term wave load in the Gulf of Mexico. Of course, on one particular day the significant wave height can be bigger in the Gulf of Mexico than in the North Sea, but in the long run, the average significant wave in higher in the North Sea. Hence, the long-term average stress range on a structural detail will be greater when the vessel operates in the North Sea compared to operation in the Gulf of Mexico.

To know how frequently the OSCVs operates in different areas is therefore important for the accuracy of the fatigue lifetime estimation. One could of course only consider the harshest environment in the evaluation, but then the vessel may be "over-dimensioned".

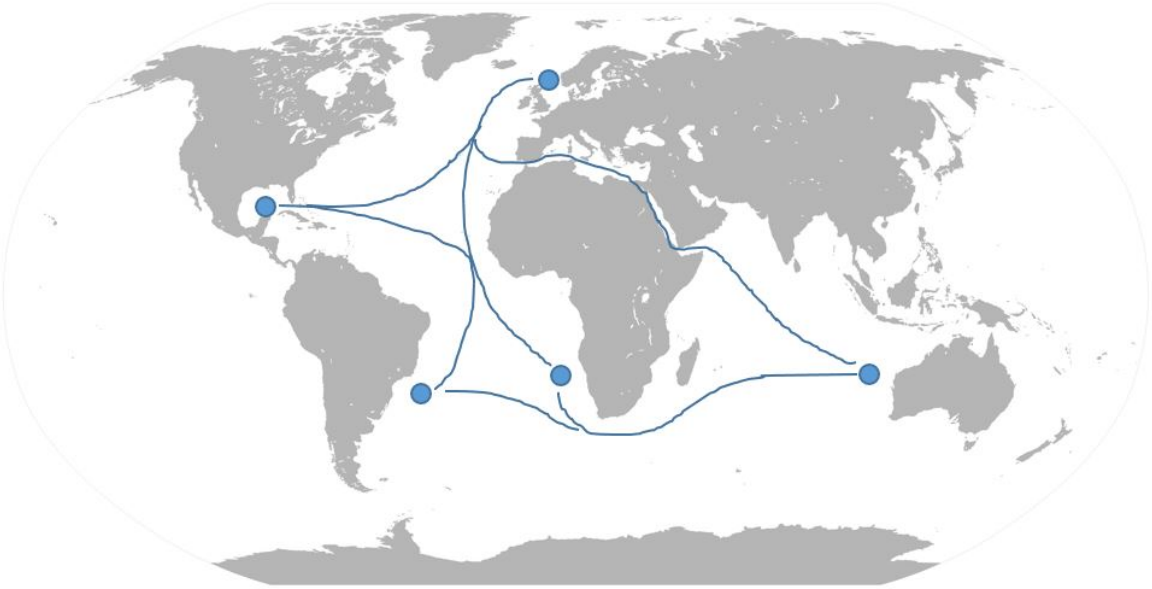

Figure 3.4: Illustration of operational pattern for OSCVs.

3.2.2 During operation

Up to now the different sea areas and the effect they have on the fatigue life (stress range) have been highlighted, but the sailing and maneuvering "inside" the sea area affects the fatigue life as well.

Marine operations – in this context the lifting and installation of subsea units– are depending on many factors with respect to carry out the mission in a successive way, where the success criteria is to bring an object from one defined safe condition[2] to another safe condition. Knowledge about vessel motion, lift dynamics & hydrodynamic loads, crane heave

[2] Safe condition: "a condition where the object is considered exposed to "normal" risk for damage or loss. "Normal" in this context is a risk similar to the risk expected during in-place condition." (Larsen, 2015)

compensation system and operability & moonpool operations is therefore important (Larsen, 2015). All these items have their limitation with respect to the environment (waves, wind, current, temperature, ice) and make the frame for what weather and sea conditions that can be accepted. Hence, the operator knows what weather window to wait for.

While waiting on weather - provided that the vessel already is at the field and has stopped the operation - the vessel either sails to nearest port, or “move to side” in standby and waiting for better sea condition. The decision depends on the extent and the level of the bad weather, economy, and especially safety.

The vessels often sail to nearest port when operating in the North Sea due to short distances, but outside Africa it is normal to lay in standby at the field due to long distances. A lot of paper work due to national requirements is also a reason. When working at fields far of shore e.g. fields outside Africa, the crew is normally transported by helicopters, while operating in other areas where the distance is short the crew is normally picked up by the vessel itself.

3.2.3 Mobilization (at port)

When the OSCVs starts on a new mission it has to mobilize, i.e. remove cargo and equipment from the previous mission and equip the vessel with necessary equipment and cargo for the next one. This process can take one day, or it can take weeks, or even months. Often the vessel just pick up one or two subsea modules and changing the crew. Other times it has to fill up the cable drum(s), mount some additional launching equipment and secure storage units on deck.

Based on this the OSCV appears to use significantly time at ports (mobilization). One may ask if these vessels use more time in ports compared to merchant vessels that are assumed to sail 85% of its lifetime, i.e. 15 % of the lifetime is spent at ports (DNV, 2014a). If so, this should be credited when calculating the fatigue life.

3.2.4 Transit

In transit the vessels follow the loading manual of the vessel, which is approved by the classification society. Often, the vessels are given additional dynamic loading due to special needs in a mission (also needs to be approved by the classification society). These additional loads are objects that are welded to the hull structure and are not part of the initial loading conditions in the manual. Instead they are introduced during the operational life, leading to alternation of the loading manual.

The speed under transit is based on the economy, but this may change depending on the client. Sometimes the project schedules are tight and to save time is an advantage. High utilization of the engine capacity is then normal. Skandi Acergy, that is an OSCV with L=146.0m and B=27m (DOF, 2015) sails typically in 15 knots during transit when choosing an economic speed.

How frequently the loading conditions are used in transit is unknown, besides that loading arrival and ballast are two commonly used conditions. Other loading conditions may be used, but rather rarely.

3.3 AIS Data from an Operating OSCV

An excel-file containing AIS data of an operating OSCV is provided from Dof Management AS. It contains daily information with dates about status and graphical location. The data goes back to 08-19-2011 and is sorted by geographical location and status which is presented in Table 3.1.

The result shows that a major part of the time has been spent in the North Sea. 854 days has been spent there which is about 63 % of the total days (1354). Rest of the days have mostly been spent in the Indian Ocean outside Australia, and some few in the Atlantic Ocean, Baltic Sea and Norwegian Sea. However, when only considering the status “in field” it is only the Indian Ocean and the North Sea that has been operated in.

Regarding the time spent under the operational statuses, the result shows that 68 % present of the time is spent in port, 18 % in transit and 48 % in fields. It also shows that 2 % of the time is spent anchored. Whether this is in offshore or inshore waters is not stated.

Table 3.1: Operational profile based on AIS data from an operating OSCV in the time period 08-19-2011 to 04-15-2015 (Espen Venge, 2015).

GEO: \	Total days:	In port:	Anchored:	Transit:	Field:
Atlantic ocean:	20	1	0	19	0
Baltic Sea:	36	33	0	3	0
Bay of Bengal:	1	0	0	1	0
Indian ocean (outside Australia):	361	36	9	54	262
Jawa Sea:	6	0	0	6	0
Mallacca Strait:	3	0	0	3	0
Mediterrenean:	6	0	1	5	0
North Atlantic:	3	0	0	3	0
North Sea:	854	315	6	141	392
Norwegian Sea:	15	11	3	1	0
Red Sea:	4	0	0	4	0
Singapore Strait:	45	38	4	3	0
SUM:	1354	434	23	243	654
Fractions:	1.00	0.32	0.02	0.18	0.48

In the report (IMO, 2009) an estimation of the fuel consumption in 2009 by international shipping have been carried out. AIS data from operating vessels of all kinds have been gathered and used as input. Among these the offshore service vessels can be found, but the OSCV is not presented here. However, there is one type termed “Pipe (various)”. According to the data, this type of vessel spends 233 days at during one year, and the statistic is based on many vessel. This corresponds to about 64 % which is very close to the 66 % found for the OSCV in Table 3.1.

3.4 Project Design

The vessel that is going to be evaluated in this thesis is designed for subsea construction, pipe laying and IMR services up to 3000 m depth (DOF, 2015). It is based on the VARD 3-serie design which is described as follows (VARD, 2015): “*The hull is designed with focus on good station-keeping and excellent maneuverability and sea-keeping characteristics. The design allows for flexible configuration with respect to the different operations this kind of vessels may be outfitted and arranged for, typically:*

- *Subsea construction and installation;*
- *Inspection, maintenance and repair;*
- *Flexible pipe laying;*
- *Well intervention;*
- *Diving support*»

The current configuration is with respect to pipe laying (VARD, 2015). The hull is equipped with a relatively “small” offshore crane with lifting capacity of 50 tons, even though it is featured with the capacity to have a larger offshore crane. In addition, the vessel is equipped with a VLS tower (shown in yellow on Figure 3.5) capable for 650 tons tension from the product.

The main perpendiculars and the hull material are presented in Table 3.2 and Table 3.3 on next page.

Figure 3.5: NB 823 (DOF, 2015)

Table 3.2: Main perpendiculars of NB 823.

Length over all, L_{oa}:	146.0	[m]
Length between perpendiculars, L_{pp}:	134.3	[m]
Rule length, L:	134.3	[m]
Breadth, B:	30.0	[m]
Depth to main deck, D:	13.0	[m]
Scantling draught, T:	8.6	[m]
Displacement (T=8.6m):	25 216	[tones]
Block coefficient, C_B (T=8.6m):	0.710	[-]
Speed, V:	14.0	[knots]
Frame spacing:	0.70 / 0.60[3]	[m]

Table 3.3: Hull material NB 823.

Hull material: NV-36	
σ_{yield}	= 355 MPa

[3] Aft of frame #6 and forward from #148

4 Part-ship FE model

It is decided to establish a part-ship FE model and in the areas where hot spot stresses are to be considered fine mesh areas are modelled directly into the part-ship model by using suitable element transitions meshes to come down from coarse to finer meshes.

Traditionally, the hot spot area is not an integrated part of the part-ship model assembly but a stand-alone model (DNV, 2014a). This requires that the boundaries of the sub-model coincide with those elements in the part-ship model from which the sub-model boundary conditions are extracted. The approach leads to a fairly small set of equations to be solved simultaneously compared to direct technique that is going to be used herein.

An example of the direct meshing approach is the container vessel shown in Figure 4.1 where the six hatch corner models initially were put directly into the global model and analyzed together in order to determine hot-spot stresses in the hatch corners.

The background for modelling a part-ship model instead of a global model as shown in Figure 4.1, is that it is only the midship area (from 0.4L from AP to 0.65L from AP) that is of interest in this thesis work. Modelling the complete extent of the hull (global model) is therefore considered as more time consuming than necessary.

To only model a certain part of the complete length is however, considered as efficient and effective in a fatigue design phase, and likewise the global model it provides nominal global stress of high accuracy in the hull girder (DNV, 2014a).

However, shear lag effects may not be as accurately captured as for a global model and need to be addressed when using a part-ship model (DNV, 2012). On the other hand the part-ship model - in addition to cargo hold models – provide more accurate relative deflection magnitudes for updating the nominal stresses for the longitudinal stiffeners that intersect a transverse bulkhead or transverse web (DNV, 2012). This make the model well suited for a *fatigue screening* which is the process where critical locations (hot spots) are identified.

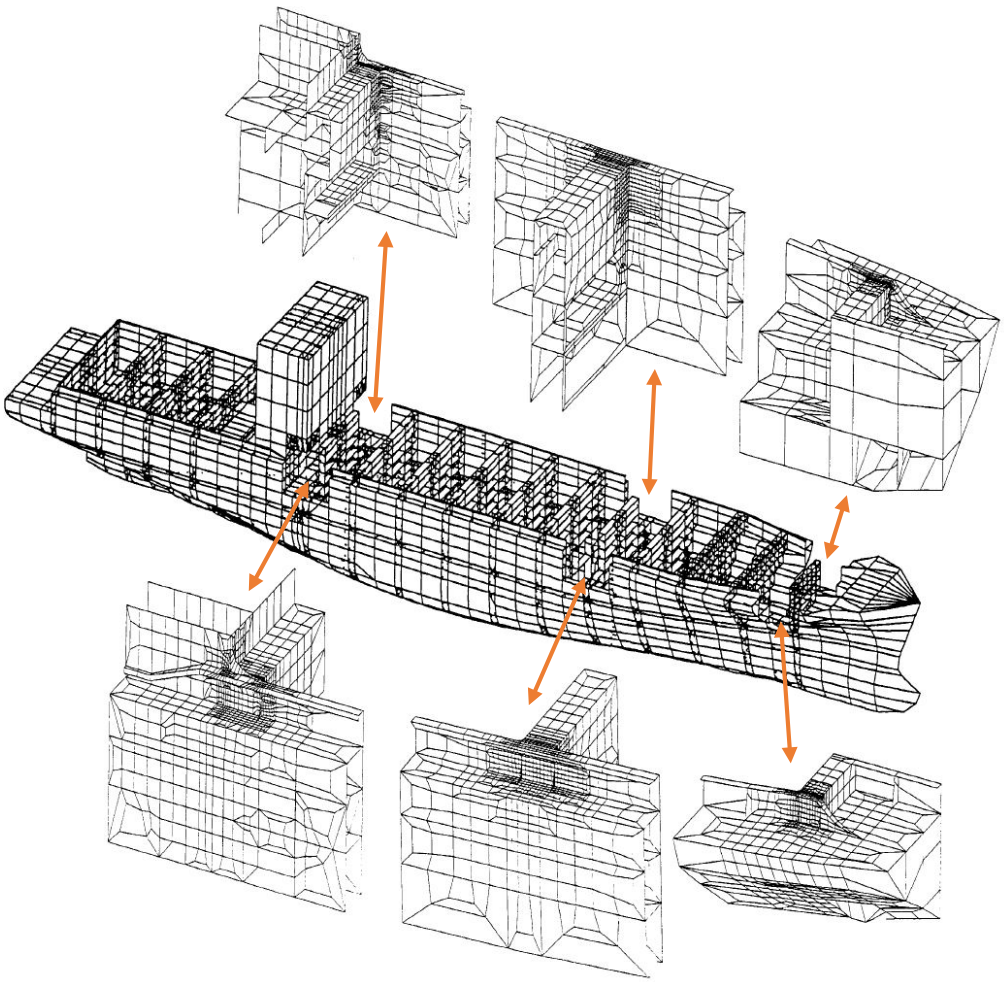

Figure 4.1: Global hull FE model of container vessel with fine mesh in areas directly in the model. In the illustration the areas with fine mesh are taken out of the global model so the fine mesh can be seen (DNV, 2014a) [modified].

4.1 Model Extent

The model is decided to extend from Frame no. 23 to Frame no. 127 and the decision is based upon consideration of the following three features:

- Distribution of maximum vertical rule wave bending moment
- Limit the influence of the boundary conditions on the results
- Provide for the correct stress distribution in the hull area of interest.

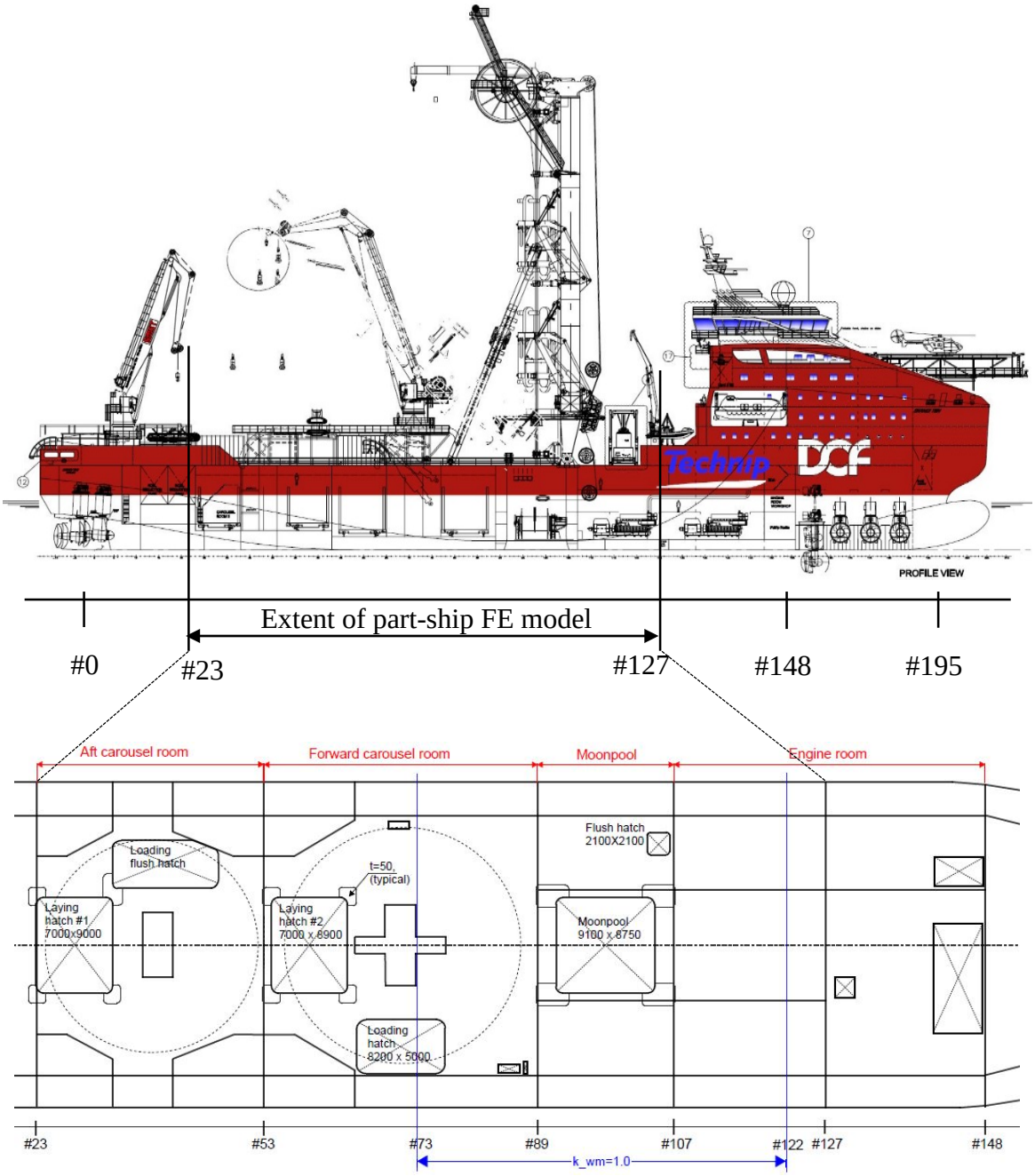

Figure 4.2: Extent of the part-ship FE model shown in profile view (drawing no. 823-100-001)[modified] and main deck view from above (drawing no. 823-200-011)[re-drawn].

4.1.1 Maximum rule wave bending moment

According to (DNV, 2014a), the moment distribution factor, k_{wm} of the rule wave bending moment is equal to 1.0 between 0.40L(53.720m) and 0.65L(87.295m) from A.P. Outside these limits the factor reduces linearly to zero at AP and FP, respectively (see section 2.5.1).

For NB 823 the interval of the maximum distribution value corresponds to between #73 and #122. Hence, the extent of the Part-ship model needs to at least extend over this length.

4.1.2 Boundary conditions

The Part-ship model typically consists of three complete compartments (DNV, 2012), where the primary fatigue calculations will be completed for the middle compartment as shown in Figure 4.3. The other compartments are to be included to limit the influence of the boundary conditions on the result, but also to provide the correct stress distribution towards the middle compartment.

For the evaluation herein it is not a specific compartment that is of interest, but a certain length interval where the rule wave bending moment is at its maximum. This interval stretches from around the middle of the forward carousel room compartment to the middle of the machine room. In other words, it touches 3 compartments: Forward carousel room compartment, moonpool compartment and the engine room compartment. However, regarding the latter there is a partly transverse bulkhead including pillars at Frame 127 (Figure 4.4). Hence, the engine room may be considered to be built up by two compartments: #107 - #127 and #127 - #148. By doing this, the recommendation (DNV, 2012) about having a complete transverse bulkhead at the aft and forward end of the model, is satisfied.

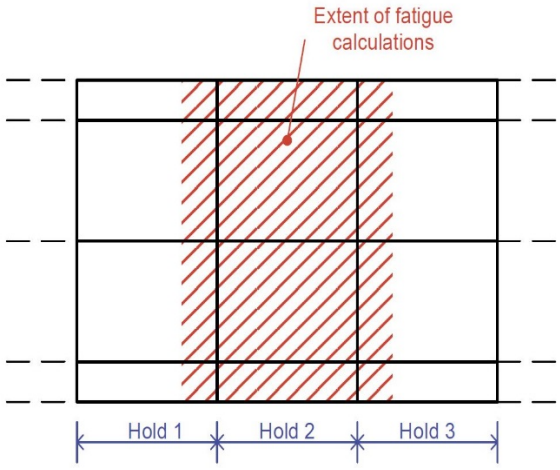

Figure 4.3: Typical fatigue extent within part-ship model (DNV, 2012)

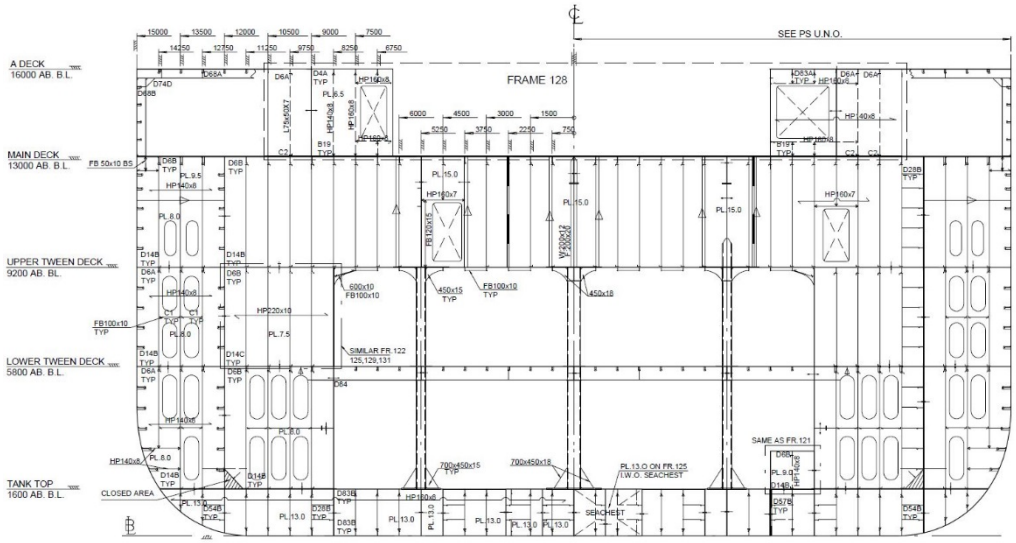

Figure 4.4: Frame 127 (drawing no. 823-200-055) [modified].

4.1.3 Stress Distribution

As shown in Figure 4.2, the main deck consists of many rectangular cut-outs that have a major impact on the stress distribution in in main deck. Their presence cause stress free zones as illustrated in Figure 4.5. They are also resources for geometric stresses that occur in the corners, which make them highly interesting with from a fatigue point of view. If they are to be evaluated, it is important that the stress distribution towards them is correct. The cut-outs that are within (/partly within) the interval 0.4L from AP and 0.65L from AP are (Figure 4.2):

- Laying hatch: Frame #54 - #64, midship
- Loading hatch: Frame #65 - #77, starboard side
- Moonpool: Frame #91 - #105, midship
- Flush hatch (small): Frame #103 - #107, port side.

To ensure the correct stress distribution towards the first two openings above it is reasonable to have a model that extends at least back to Frame #23. This is because the two deck openings in the aft carousel room area affect the stress distribution towards the two deck openings in the forward carousel room area, and should therefore be included in the model.

Regarding the last two openings (Moonpool and flush hatch) it will be sufficient to end the model at Frame #127. At this location the stress shadow from the moonpool opening is not present according to Figure 4.5.

The decision is also based upon the same principle about model extension with respect to stiffness variation in the hull girder (DNV, 2014a):"*In cases where the response within the region considered is dependent on the stiffness variation of the hull over a certain length, the finite element model is generally required to extend over minimum the same length of the hull*". However, in this context it is the effective material in main deck during bending of the hull girder.

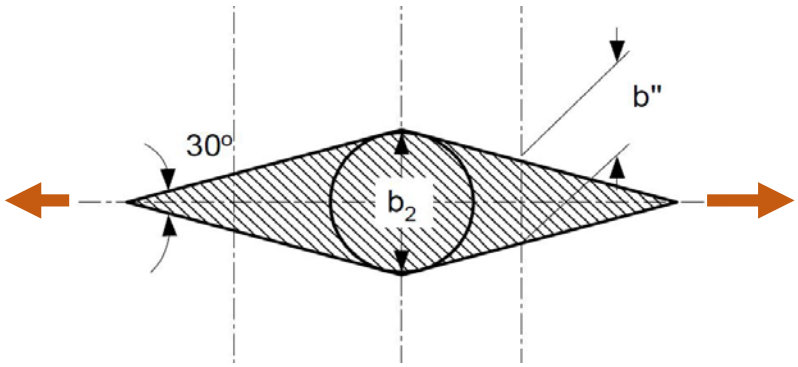

Figure 4.5: Deduction free opening (DNV, 2014c) [modified]

4.2 Modelling of Girders and Floors

Girder webs are modelled without cutouts in order to make the modelling less time consuming and with respect to the meshing later on. Consequently, the web thickness is reduced to a mean value according to eq. (20) (DNV, 2014a).

However, large cut-outs may cause secondary bending of the girder (DNV, 2014c). In such cases geometric modelling of the cut-out is advisable such that the effect is accounted for in the FEA result. When to consider this is determined by eq. (21) when r_{co} exceeds 2.0 (DNV, 2014a).

$$t_{mean} = \frac{h - h_{co}}{h r_{co}} t_w \tag{20}$$

$$r_{co} = 1 + \frac{l_{co}^2}{2.6(h - h_{co})^2} \tag{21}$$

Where

t_w = web thickness
l_{co} = length of cut-out
h_{co} = height of cut-out

h = girder web height

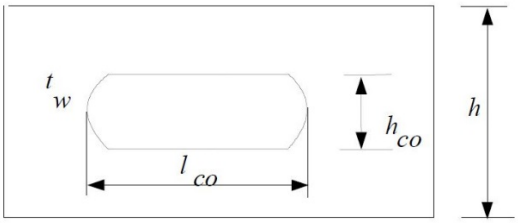

Beside cut-outs, the girder webs are often fitted with stiffeners as well. When the stiffeners are located in the longitudinal direction of the girder, they contribute to the bending strength (moment of inertia, I). In addition, longitudinal web stiffeners (on longitudinal girders/webs) contribute to the bending strength of the hull girder as well. Hence, web stiffeners in the girder direction are included in the model.

Further description of stiffeners and longitudinals regarding FE modelling is given in the next sub-chapter.

4.3 Modelling of Longitudinals and Stiffeners

When calculating the global stress distribution and the overall stiffness of the hull girder based on a global FE model, the common practice is to model the stiffened plates by means of orthotropic material (anisotropic), or a combination of plate elements and beam elements. In the former method the plate is given different elastic properties in two directions, orthogonal to each other, to represent the contribution from the dropped stiffeners (Moan, 2003). This requires that the designer compute the equivalent young modulus (E) in direction x and y, which is a relatively simple work. Alternatively, layered elements can be used.

For a hull structural design such as NB 823 where the design of the longitudinals (arrangement and dimension) varies a lot, the computation of the equivalent modulus requires a more work. To avoid this the plates are modelled with shell elements (see section 4.7), and the stiffeners and longitudinals are modelled with 2 node eccentric beam elements.

However, in the area where the hot spot stress is to be calculated, the longitudinal will be modelled as plated structure with shell elements. In such case attention should be paid when connecting a beam element to one node of a shell element, since the end of the beam elements may then be assumed as hinged in the calculation (DNV, 1999). This affects the load distribution and to minimize this effect the beam and shell elements are recommended to be overlapped (DNV, 1999).

The overlapping for longitudinals will basically be arranged two frames (2 x 2.8m) away from the hot spot region to ensure the correct stress distribution towards the hot spot.

Regarding the modelling of stiffeners and longitudinals with shell elements, the elements need to be arranged in the mid-plane of the structural components (DNV, 2014a) due to the fact that the thickness of a shell element is a property, not a "physical" size in the model (Moan, 2003). Consequently, the bulb flange cannot be modelled, hence replaced by an L-profile with the same section modulus and web height, as shown in Figure 4.6.

Not all stiffeners are included in the FE model. Many of the stiffeners do not contribute to the global strength of the hull structure, and locally their contribution are rather insignificantly.

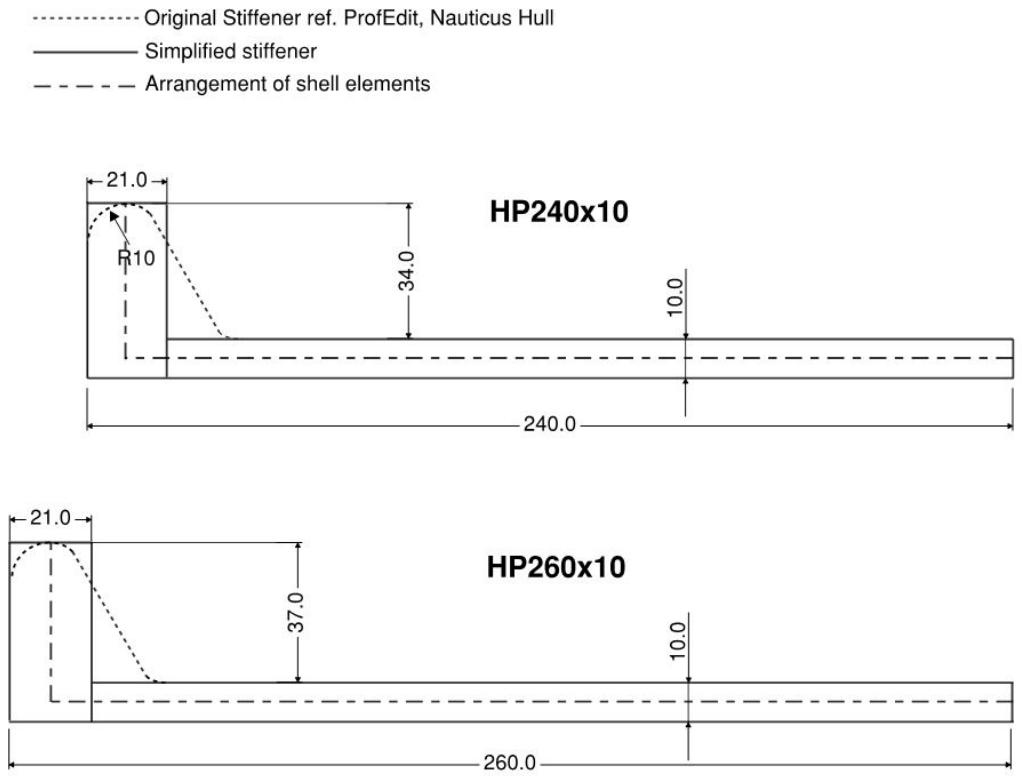

Figure 4.6: Simplified stiffener profile.

4.4 Boundary Conditions

When deciding how to apply the loads and make the boundary conditions the following three documents have been used to decide the most suited approach:

- DNV CN No. 30.7 – Fatigue Assessment of Ship Structures (DNV, 2014a);
- DNV RP C206 – Structural Design of Offshore Ships, Appendix A (DNV, 2012);
- DNV CN No. 31.3 – Strength Analysis of Hull Structures in Tankers (DNV, 1999).

There is one important property to have in mind when deciding the composition of the boundary condition: The bending moments represent all the global effects, whereas the internal/external pressure and the inertia loads represent the local load effects and should not induce any global effects. Hence, two sets of boundary conditions are to be established; one set for the global loads, and one set for the local loads. This involves a duplication of the FE model.

In general, the extent of the model has to be chosen such that effects due to the boundaries on the structural detail considered are sufficiently small and reasonable boundary conditions can be obtained. In addition, singularities need to be avoided.

The location of the boundaries for stress calculation due to global loads are already discussed in section 4.1.2, since there is an interaction between the boundary (extent) of the model and the boundary conditions.

4.4.1 Boundary conditions for global loads

The part ship model is considered as a freely supported beam as illustrated in Figure 4.7. Rigid links are then applied to the FE model in both ends and given the following properties: Fixed in all degrees of freedom, except rotation about y-axis, when applying the vertical moments. In addition, the aft boundary is free to translate in x direction. For the horizontal moment the boundaries are free to rotate about the global z axis instead of the y axis.

The moments are applied in both ends at the same location in the global yz-plane as the horizontal and vertical neutral axis of the hull girder cross section at #89, respectively. The rigid links are located at the same positions. According to section scantling, the position is 6.4 m above base line for the vertical moments and at center line (y=0) for the horizontal moment. This position may, however, be modified after analyzing the result file (SIN-file) in Cutres.

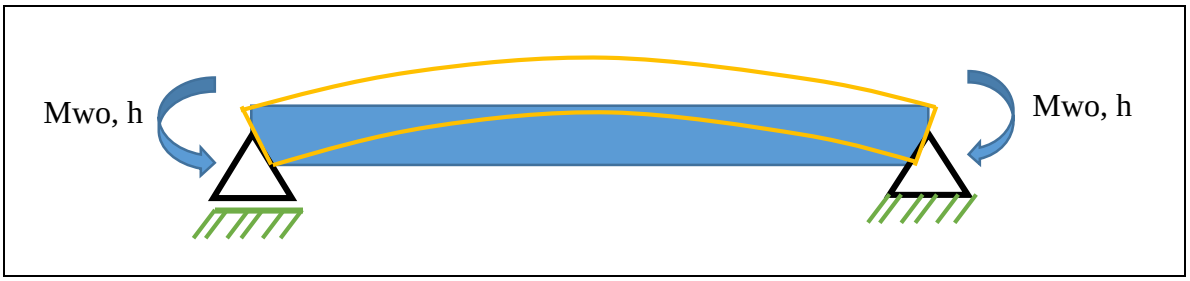

Figure 4.7: Boundary conditions and application of moments for global FE model.

By this approach the model provides the correct deflection pattern with respect to wave hogging and sagging condition. However, it should be noted that the method implies that the vertical and horizontal bending moments are defined uniformly over the length of the part ship model, which is not the case in the reality. One should therefore be careful when considering stresses outside the region that the rule moments are based on.

An alternative method is to model the part ship as a cantilever beam (DNV, 2012): Fixed in all degrees of freedom at one end, and free at the other, as shown in Figure 4.8. The bending moments are then applied at the free end.

Instead of being applied as a single moment point load, one can also apply a force pair acting in the opposite directions (DNV, 2012). They are applied at two points positioned vertically above each other where the lower is at the bottom of the hull girder cross section and the upper is at the top of the cross section. This is illustrated in Figure 4.8 and the two forces are determined by the following formula:

$$F = \frac{M}{h} \tag{22}$$

F = magnitude of force at the two positions
M = magnitude of bending moment
h = distance between the two forces

The moment magnitude can either be actual moment or a unit moment = 1 Nm. Doing the latter, one can obtain the actual stress amplitude by multiplying the derived unit stresses from the FEA with the current load magnitude.

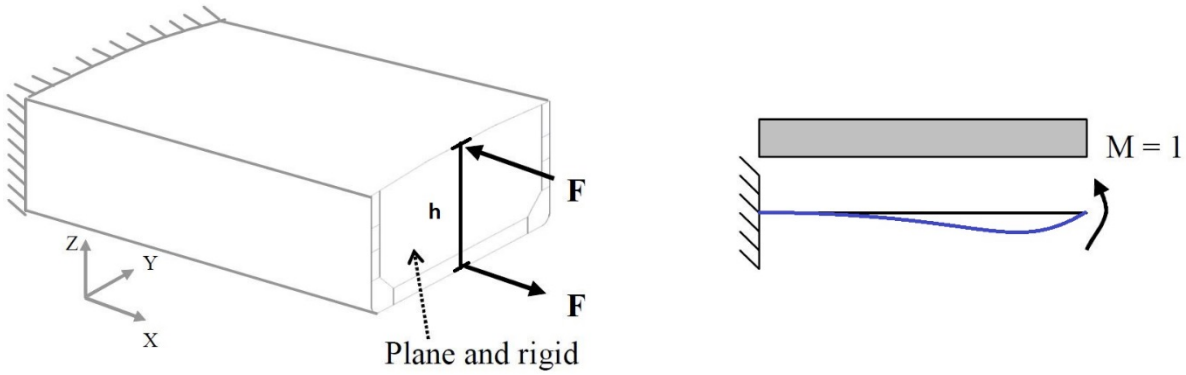

Figure 4.8: Applied vertical bending moment (DNV, 2012) [modified].

4.4.2 Boundary condition for local loads

The model is supported in the vertical direction by applying vertical boundary lines formed by the intersections between side and transverse bulkheads, inner side and transverse bulkheads, and longitudinal bulkhead and transverse bulkheads (DNV, 1999), as illustrated in Figure 4.9).

If the same boundary conditions as for the global loads are used, then the local loads also cause bending moments on the hull girder. This again will lead to global stresses that are already considered. Thus, the bulkheads

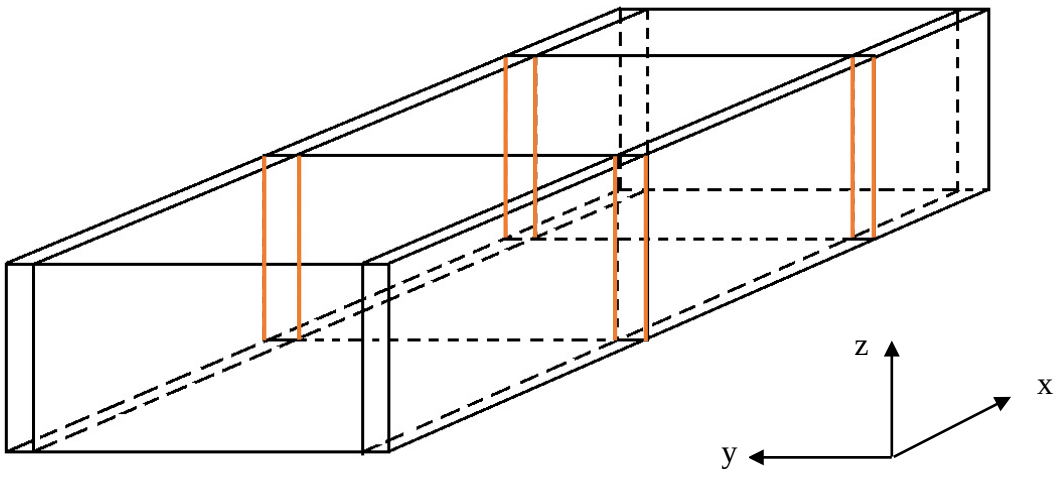

Figure 4.9: Illustration of vertical boundary lines (red) formed by the intersection between transverse and longitudinal bulkheads.

4.5 Application of External Dynamic Sea Pressure

The dynamic pressure is assumed constant when applied to the FE model, and is determined at the mid-position for each cargo hold (compartment) or tank (DNV, 2014a). This is conservative since the dynamic sea pressure depends on the wave amplitude which varies over the length as shown in Figure 4.10. However, according to (DNV, 2012), "the variation in absolute pressure level in the longitudinal direction is relatively small. Therefore, assuming a constant longitudinal pressure has no influence on the local bending. However, some conservatism will be introduced for the relative deflection and secondary bending stress". How conservative this is depends on the location where fatigue is calculated and the unit geometry.

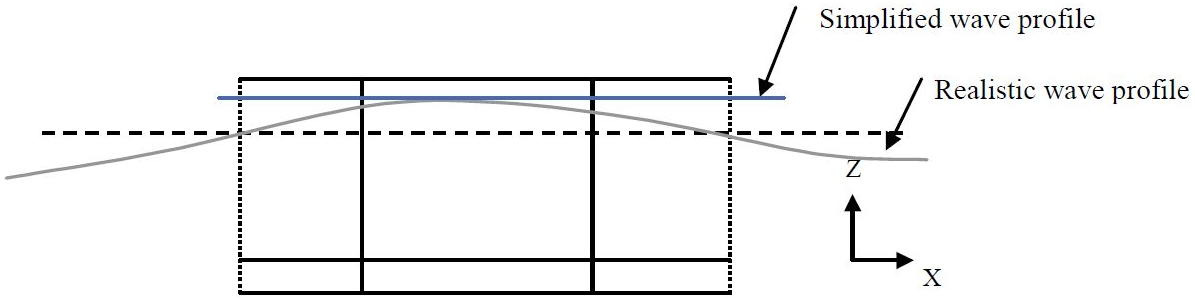

Figure 4.10: Simplified wave profile versus realistic wave profile (DNV, 2012).

4.6 Application of Internal Dynamic Loads and Inertia Loads

The ballast tank loads in the double bottom are applied to the shell plate. The load amplitude is determined at the mid-position for each tank – the same principle as presented in previous section.

Regarding the inertia loads from the cable drum, the loads are applied as line loads to the foundation in the tank top.

4.7 Elements and Meshing

The element portfolio of Sesam GeniE consists of shell elements which make the software well suited for curved structures, like ship structure. This is explained by the property that stress resultants acting on the middle surface of the shell have both bending (out-of-plane) and membrane (in-plane) parts (Moan, 2003). So, in cases where curved plates are exposed to

radial pressure, like the bilge exposed to external sea pressure, the shell element captures the stresses caused by the membrane action – which carry a major part of the load in this case - in addition to the stresses caused by bending of the plate.

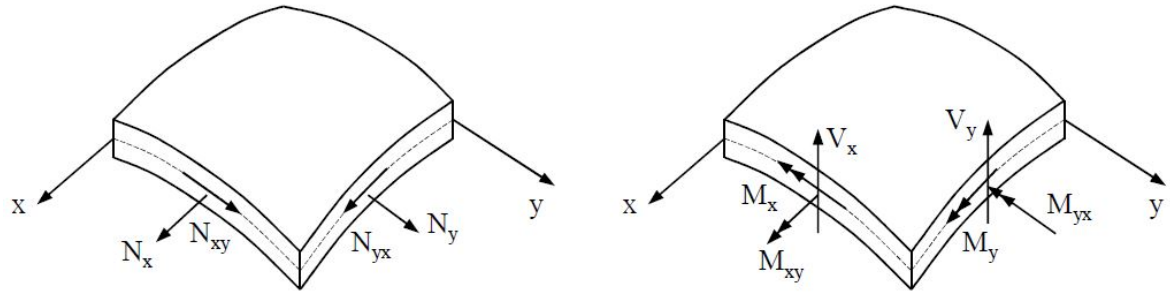

Figure 4.11: Membrane and bending conditions of a curved shell element (Moan, 2003).

Moreover, GeniE uses the isoparametric formulation which permits quadrilateral elements to have nonrectangular shapes and curved sides. This is an advantage w.r.t. modelling when the boundaries are curved and when going from coarse to fine mesh to capture the hot spot stress. However, there are also some disadvantages like lower convergence rate compared to quadrilateral elements of rectangular shape, and low accuracy depending on the level of distortion (Moan, 2003).

A second feature in GeniE with regards to irregular geometry and transition from coarse to finer mesh, is the use of triangular shell elements as shown in Figure 4.12 a). Triangular elements usually have fewer nodes than comparable rectangular elements, fewer degrees of freedom, and thus lower degree displacement functions (Moan, 2003). Thus, transition from coarse to fine mesh should in general be modelled with quadrilateral elements as shown in Figure 4.12 b). However, the latter may not always be right when considering flat thin shell elements (see section 4.7.1).

a) Triangular elements	b) Quadrilateral elements
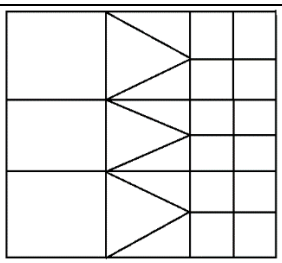	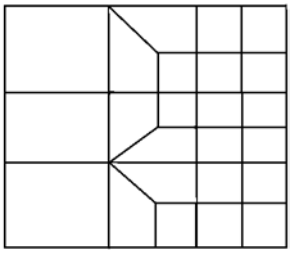

Figure 4.12: Transitions from coarse to fine mesh by use of a) triangular elements and b) quadrilateral elements.

The following element descriptions refers to (DNV, 2013) which is the Sestra's user manual. There are also some features that are found in other resources. Reference is then given directly.

4.7.1 Flat thin shell elements

The flat thin shell element family in Sestra consists of a 3 node Flat Triangular Shell element (FTRS) and a 4 node Flat Quadrilateral Shell element (FQUS). They both have 6 degrees of freedom in each node – three translation and three rotation, as shown in Figure 4.14 and Figure 4.15 for the triangular and quadrilateral element, respectively.

The deformation of flat thin shell elements are based upon the same assumption as for thin plates where the deformation is assumed to be according to Kirchhoff-Navier's hypothesis (Moan, 2003): "*A line that is straight and normal to the mid surface before loading is assumed to remain straight and normal to the mid surface after loading*", as shown in Figure 4.13 a) and b). This is the background for the assumption of zero transverse shear deformation.

a) Differential element of thin and thick plate before loading:

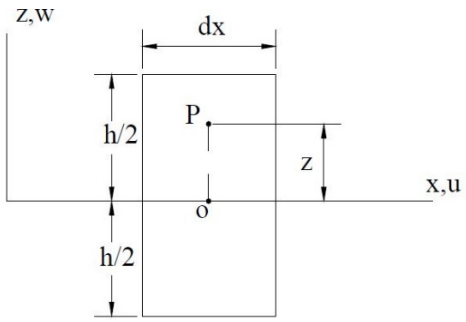

b) Deformation after loading according to Kirchhoff theory:

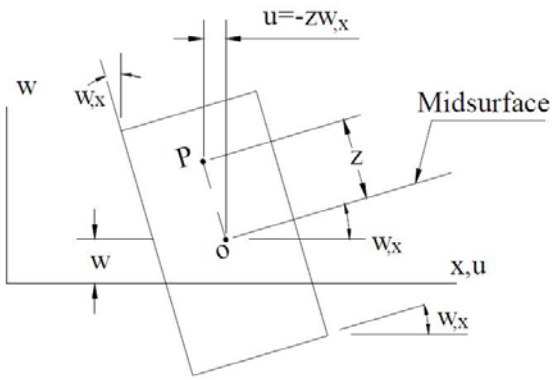

c) Deformation after loading according to Mindlin theory:

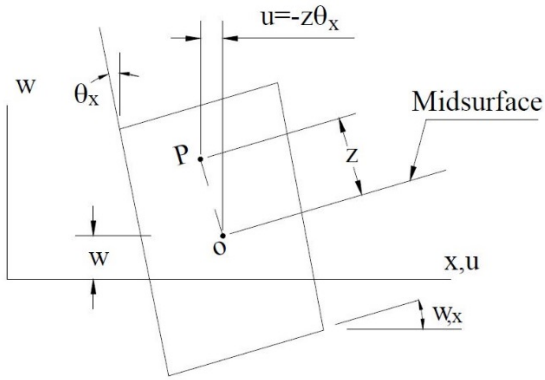

Figure 4.13: Deformation in thin plate (Kirchhoff's) and thick plate (Mindlin's) (Moan, 2003).

The thin shell elements are composed of independent membrane and plate-bending parts, and when describing the membrane part the elements utilize lower order membrane elements.

Besides number of nodes and degrees of freedom, there are also some differences between the two elements regarding performance. For curved surfaces the triangular element performs better than the quadrilateral, but when membrane action dominates the latter behaves better than the triangular element which behaves very stiff and thus not recommended to be utilized in such case.

The membrane stress and the bending stress are not coupled in shell element for plane structures, only the membrane part of the shell element will be activated in determining the membrane stresses.

The FQUS element may represent a complete linear field of in-plane stresses and hence pure in-plane bending of the element will be exactly represented, while the FTRS represent incomplete linear field of bending moments in the plate bending part.

As shown in Figure 4.14 and Figure 4.15, the stresses are computed and printed both on upper and lower element surface in the nodes and in the centroid of the elements. Consequently, there are 8 points for the triangular element and 10 points for the quadrilateral element.

It should be noted that there are two more flat thin shell elements, the 3 node FTAS (Flat Triangular Allman Shell) and 4 node FQAS (Flat Quadrilateral Allman Shell). They are the same elements as above, but with drilling. Such elements utilize the rotational dof around the axis perpendicular to the membrane plane in the membrane formulation. The plate-bending part is the same as for FTRS and FQUS.

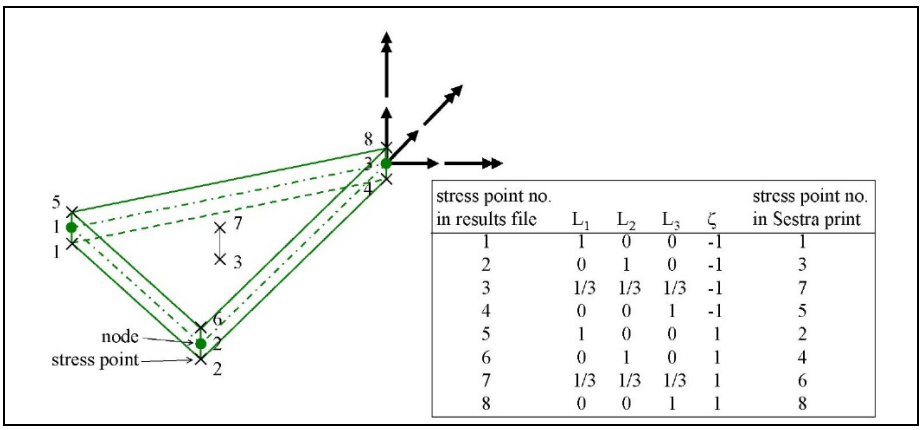

stress point no. in results file	L_1	L_2	L_3	ζ	stress point no. in Sestra print
1	1	0	0	-1	1
2	0	1	0	-1	3
3	1/3	1/3	1/3	-1	7
4	0	0	1	-1	5
5	1	0	0	1	2
6	0	1	0	1	4
7	1/3	1/3	1/3	1	6
8	0	0	1	1	8

Figure 4.14: Flat triangular shell elements FTRS and FTAS (drilling) with stress points (DNV, 2013).

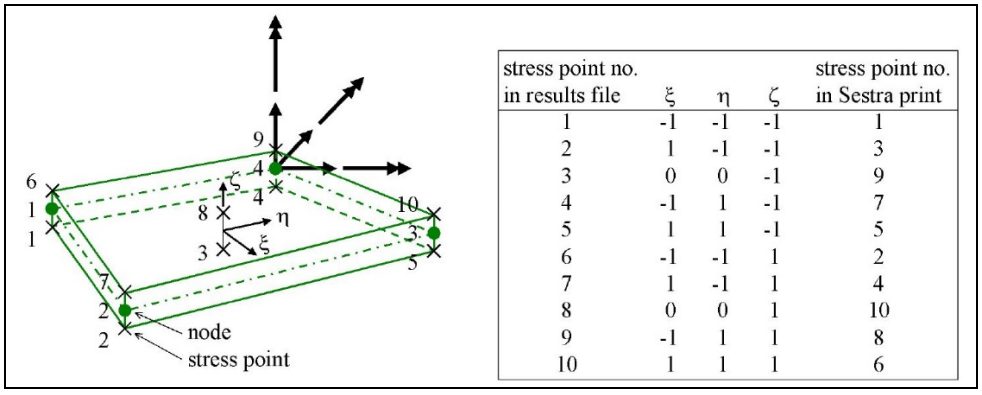

stress point no. in results file	ξ	η	ζ	stress point no. in Sestra print
1	-1	-1	-1	1
2	1	-1	-1	3
3	0	0	-1	9
4	-1	1	-1	7
5	1	1	-1	5
6	-1	-1	1	2
7	1	-1	1	4
8	0	0	1	10
9	-1	1	1	8
10	1	1	1	6

Figure 4.15: Flat quadrilateral shell elements FQUS and FQAS (drilling) with stress points (DNV, 2013).

4.7.2 Subparametric curved thick shell elements

The flat thin shell element family in Sestra consists of the 6 node *Subparametric Curved Triangular thick Shell element* (SCTS) and the 8 node *Subparametric Curved quadrilateral thick Shell element* (SCQS). Both elements have six degrees of freedom in each node, three translational and three rotational, which implies that the SCTS element has 36 dofs and the SCQS element has 48 dofs.

There are two more members of the family, a sandwich element (MCQS) and a layered element (LCQS). They are not described here since they are not utilized in this thesis work.

The deformation of thick shell elements is based on thick plate theory (Mindlin/Reissner) which enables the element to represent transverse shear deformation (Moan, 2003): "*A line that is straight and normal to the mid surface before loading is assumed to remain straight but not necessarily normal to the mid surface after loading*". See Figure 4.13 a) and c) on page 43.

Compared to thin plate, the thick plate formulation provides a better approximation of the shear forces and corresponding stresses, but when used for thin plates they may be less accurate (Moan, 2003).

The SCQS element is presented in Figure 4.16 on page 46. It may represent a complete linear field of membrane and shear forces and bending moments, but may also represent an incomplete quadratic field of the same forces and the moment. The linearization is obtained by a reduction of the integration order. The thickness may be different in all nodes due to the incomplete cubic variation of the thickness. For very thick shells with large thickness variation, a three dimensional stress situation come into being. In this case the membrane and bending components are not able to describe the situation leading to inaccurate stresses. Thus, the element should only be used for stiffness representation in such case.

The element has also problems when used for thin shells. In this situation locking effects occur and leading to poor a result.

The SCTS element is presented in Figure 4.18 on page 47. Like the quadrilateral element, the triangular element is able to represent a complete linear field of the membrane forces, bending moments and shear forces. However, initially the latter have a linear variation plus a quadratic variation, but due to the integration scheme used for the calculation of the stiffness matrix, the quadratic term is reduced to a linear term.

It should be noted that the SCTS element does not generally provide as good results as the SCQS elements and should therefore only be utilized when necessary reasons. However, when the triangular element is used in area

The stresses in the triangular element are calculated for the six Gaussian points given in Figure 4.18. The points are located with triangular area coordinates L1, L2 and L3 in the two Gaussian integration points in the thickness direction, as shown in Figure 4.18. In the eight node element the stresses are calculated at the eight points of the 2 by 2 by 2 Gaussian points shown in Figure 4.16.

4.7.3 Result points

The result point stresses are extrapolated to node positions on the surfaces of the elements. At the nodes, the stress is taken as the average of the nodal stresses from all adjoining elements sharing the node, as seen in Figure 4.17 (page 47) and Figure 4.19 (page 48) for the triangular and quadrilateral element, respectively. In the post processing software, Sesam Xtract, the stresses are shown for the top surface by default, but the user can manually switch to the bottom surface.

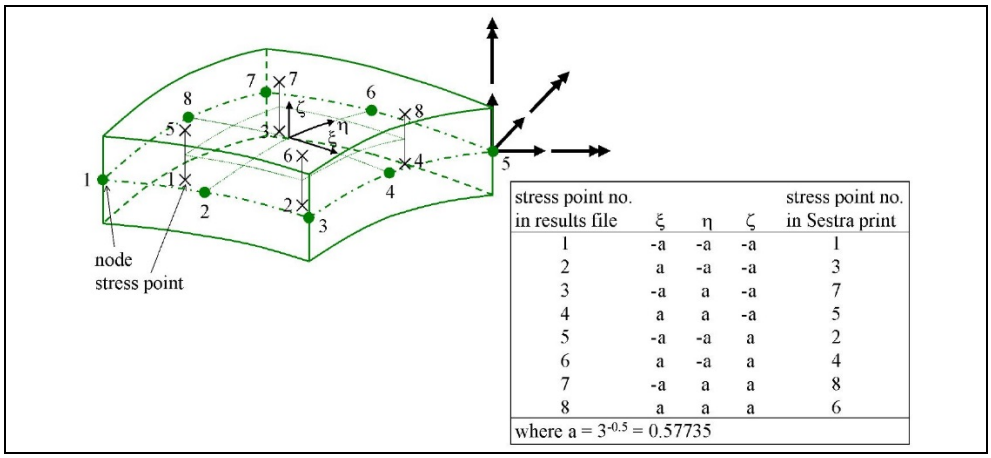

stress point no. in results file	ξ	η	ζ	stress point no. in Sestra print
1	-a	-a	-a	1
2	a	-a	-a	3
3	-a	a	-a	7
4	a	a	-a	5
5	-a	-a	a	2
6	a	-a	a	4
7	-a	a	a	8
8	a	a	a	6

where $a = 3^{-0.5} = 0.57735$

Figure 4.16: The 8 node quadrilateral thick shell element SCQS with stress points (DNV, 2013).

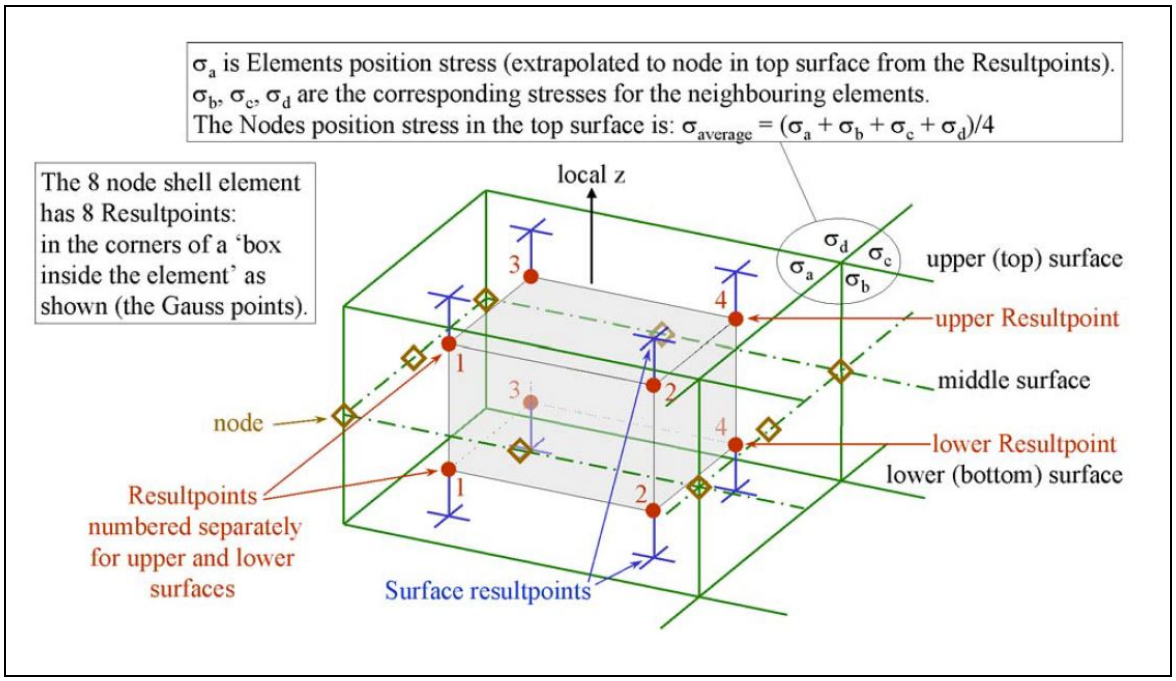

Figure 4.17: Result points for 8-node shell element (Xtract, 2014).

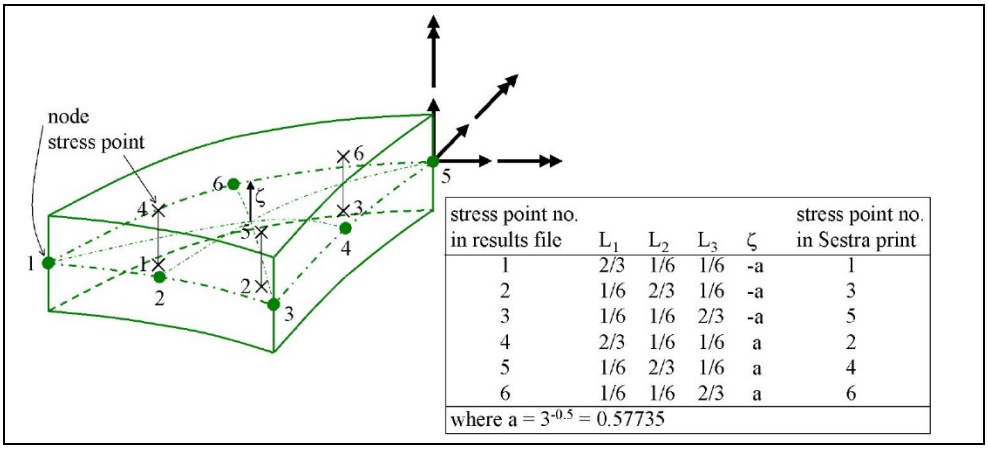

stress point no. in results file	L_1	L_2	L_3	ζ	stress point no. in Sestra print
1	2/3	1/6	1/6	-a	1
2	1/6	2/3	1/6	-a	3
3	1/6	1/6	2/3	-a	5
4	2/3	1/6	1/6	a	2
5	1/6	2/3	1/6	a	4
6	1/6	1/6	2/3	a	6
where $a = 3^{-0.5} = 0.57735$					

Figure 4.18: The 6 node triangular thick shell element SCTS with stress points (DNV, 2013).

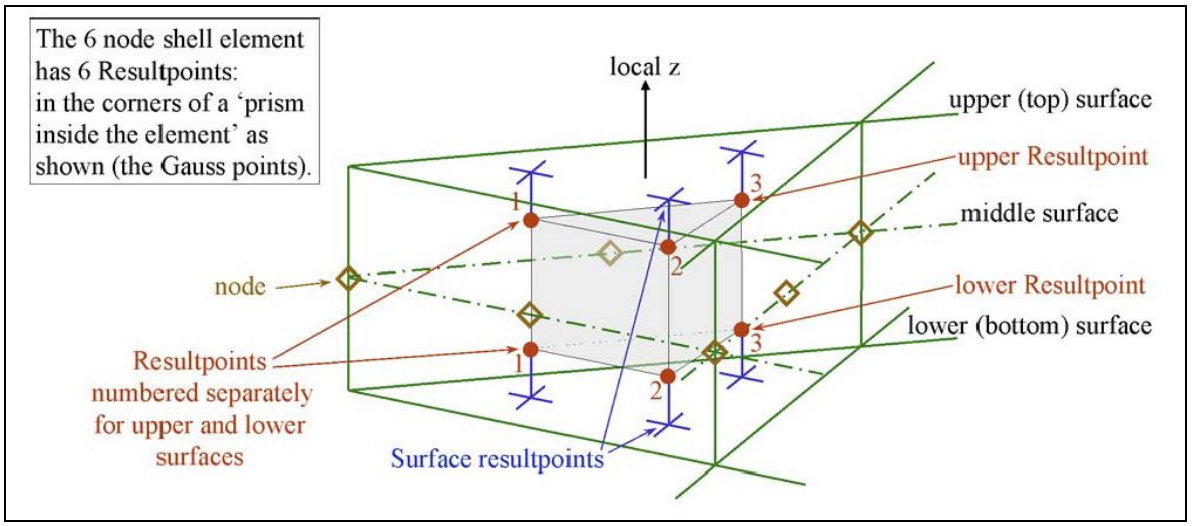

Figure 4.19: Resultpoints for 6 node shell element (SCTS) (Xtract, 2014)

4.7.4 Meshing – Element Size

According to (DNV, 2012), use of 6-node and 8-node shell elements is preferred when there is no restrictions by computer capacity. This is mainly based on the fact that 8-noded shells are less sensitive to element skewness than 4-noded shell, and have no "out of plane" restrictions. And regarding application of triangular elements, the 6-noded shells provide significantly better stiffness representation than that of 3-noded shells. Thus, the part-ship model will be modelled with 2nd order shell elements.

The element features are described in the previous sections.

When meshing the part-ship model, (DNV, 2012) recommends to arrange one element between the longitudinals and frames and one element over the girder height. Thus, the default meshing is set to 700x700 mm.

Regarding the mesh density at the hot spot region it is in general recommended to have elements with size t x t where t is the plate thickness (DNV, 2014a). This gives an efficient read out of element stresses and hot spot stress derivation. For 8-node shell element a mesh size from 0.5t to 2t can be used, but for 4 node shell elements with improved bending it is only recommended to use a mesh size from 0.5t to t. Larger mesh will lead to non-conservative results (DNV, 2014a).

4.8 Derivation of Hot Spot Stress

Since the notch effect is already included in SN curves it is only the hot spot / geometric stress that is of interest here. The classification note (DNV, 2014a) recommends that stress evaluation points are located at distances 0.5t and 1.5t away from the hot spot, where t is the plate thickness at the weld toe. These locations are also denoted as stress read out points (ROPs).

For modelling with shell elements without any weld the following two procedures are described by (DNV, 2014a):

- **Method#1**:*"A linear extrapolation of the stress to the intersection line from the read out points at t/2 and 3t/2 from the intersection line. The principal stress at the hot spot is calculated from the extrapolated component values (principal stress within an angle* $\pm 45^{o}$ *to the normal to the weld).*
- **Method#2**: *The hot spot stress is taken as the stress at the read out point t/2 away from the intersection line and multiplied by 1.12.*

The stress components on the plate surface should be evaluated along the paths and extrapolated to the hot spot. The stress components between adjacent elements are used for the extrapolation."

a) structural detail	b) model by shell elements
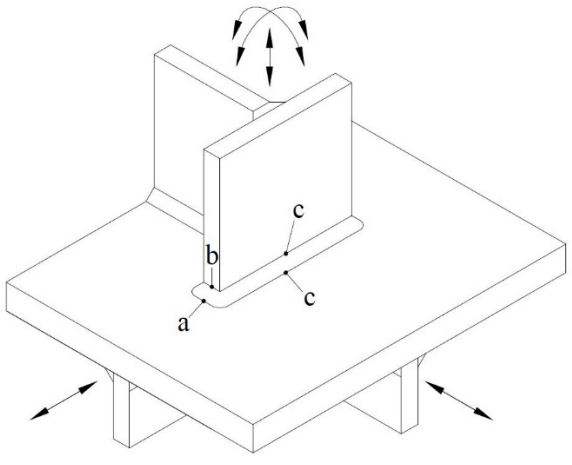	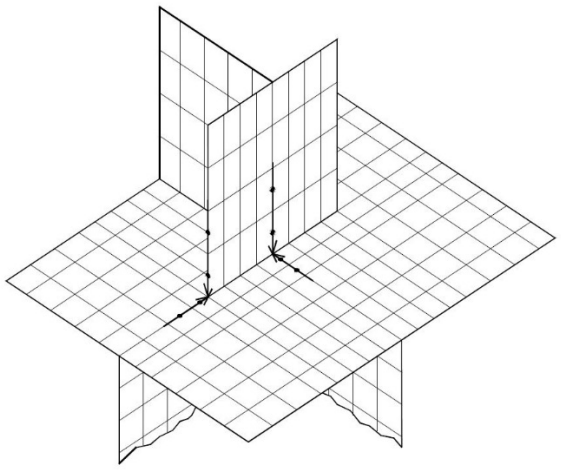

Figure 4.20: In a) different hot spot positions are presented. In b) the principle of stress extrapolation is shown for a 3D FE model to the weld toe (DNV, 2014a).

Sometimes, the element nodes/result points are not located t/2 and 3t/2 away from the intersection line of the hot spot. In such cases more effort is required in the post processing of stresses and valid procedures for establishing the stress values at t/2 and 3t/2 away from the hot spot are provided by the classification note. The procedures can be found Appendix A.

Some of the procedures for the SCQS element involves the Gauss integration points (Figure 4.17). These Gauss points are arbitrary placed in the isoparametric element and are expressed in terms of non-dimensional coordinates, (ξ,η), that are also denoted natural coordinates (Moan, 2003). The natural coordinates of the points are given in the table in Figure 4.16 on page 46.

4.9 Principal stress

According to (DNV, 2014a) the principal stress shall be used when determining the hot spot stresses. This type of stress is based on the membrane part of stress in the direction of local x and y axis, and the membrane part of shear stress in the direction of the local x/y-axes (see appendix C) (Xtract, 2014). There is no contribution from bending stress components.

The principal stress is divided in two components; P1, P2 and P3. These stress components are described by stress vectors that are shown as orthogonal intersecting lines, as shown in Figure 4.21. Negative (compressive) stresses are indicated by small cross-lines at both ends of the lines and the three stress components are as follows (Xtract, 2014):

- P1 is the highest principal stress in cases of shell, membrane and solid elements
- P2 is the second highest principal stress for solid elements, and the lowest principal stress in case of shell and membrane elements.
- P3 is the lowest principal stress in case of solid elements.

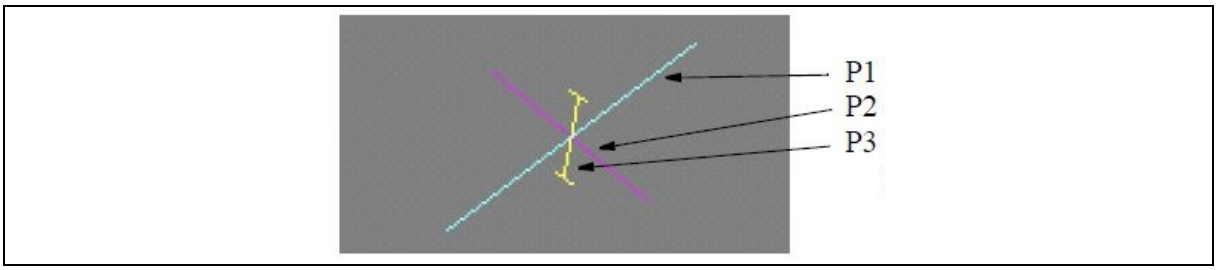

Figure 4.21: The three principal stress vectors shown as intersecting colored lines (Xtract, 2014).

.

5 Input to Fatigue Analysis

The following type of details are to be evaluated with respect to fatigue:

- Bottom longitudinal at end support, #89.
- Main deck longitudinal at end support, #89.
- Rounded corners of main deck openings between #53 and #107.

The exact location and the background for the choices are described in the following. What stress components the details are subject to, including the magnitude, are given as well.

Regarding the background, it should be mentioned that (DNV, 2014a) informs that in general, deck openings and longitudinals attached to transverse bulkheads (or other transversal members) are in general structural elements being of possible interest for fatigue evaluation. This statement can also be found in Table 2.3 on page 12, where possible details for oil tankers are presented.

The material properties used in the FEA is given in Table 5.1.

Table 5.1: Material properties FE model

Yield stress, σ_{yield}:	355 N/mm2
E-modulus, E:	210 000 N/mm2
Poisson number, ν:	0.3
Steel density, σ_{steel}:	7850 kg/m3

5.1 Longitudinal in bottom

It is decided to analyze the longitudinal at the end support at the transverse bulkhead at #89, at the aft side of the bulkhead. The specific detail is the weld connection between the longitudinal and the bulkhead plate. The design is presented in Figure 5.1 and the location is given in Table 5.2 on page 52. Tabulated K-factors are also provided since the detail is a standardized design.

The decision is based on the fact that the longitudinal is subject to stresses caused by the three load components hull girder bending, double bottom bending and local stiffener bending. In addition, relative deflection between boundaries is expected to cause stresses as well. However, structural details in bottom may be subject to the mean stress effect which leads to a

reduction of the stress range as described in section 2.11.3 on page 17. Thus, the question is not necessarily how long the fatigue life of the detail is, but also if this effect is of such magnitude that the detail can be regarded as not relevant with respect to fatigue.

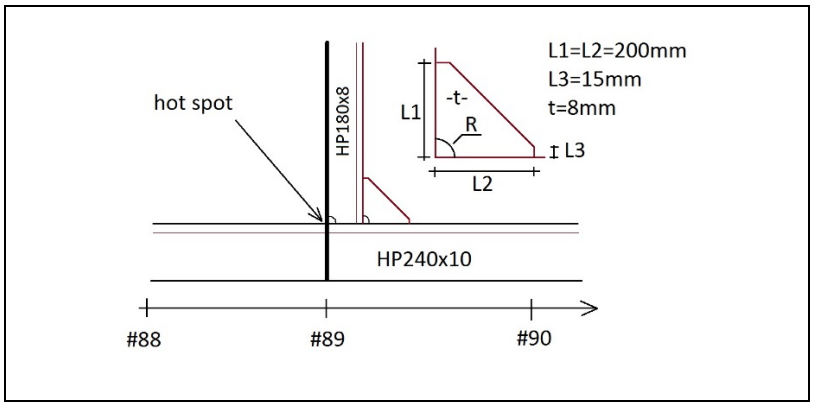

Figure 5.1: Detail D83B according to structural detail drawing no. 823-200-048_A.

Table 5.2: Location (global coordinate system) for the hot spot on the bottom longitudinal, including tabulated K-factors (SCFs).

Profile:	HP240x10	
Environment:	Void tank	
x (distance from AP), #89	= 64.5	m
y (horizontal distance from center line)	= 6.75	m
z (distance above keel/base line)	= 0.24	m
Web frame spacing	= 2.8	m
Effective span length	= 2.7	m
$K_{g,\ axial}$ (DNV, 2014a)	= 1.6	-
$K_{g,\ bending}$ (DNV, 2014a)	= 1.73	-

5.2 Longitudinal in main deck

Likewise the longitudinal in bottom, the longitudinal in main deck is also going to be evaluated at an end support at #89, on the aft side of the bulkhead. The specific detail is the weld connection between the longitudinal and the bracket toe. The design and failure mode are presented in Figure 5.2 and the location is given in Table 5.3 on page 53.

Mainly, the detail is subject to stresses caused by hull girder bending, but it may also be subject stresses due to relative deflection, which is the background for choosing the current position. The statement is based on the fact that the double bottom in the forward carousel

room compartment is supported by a pillar (in the middle) which is supported by the main deck girders. Consequently, the main deck girders will be enabled when the double bottom in the middle of the forward carousel room deflects. Hence, the relative deflection between transverse bulkhead and transverse girders will cause stresses in the longitudinals in main deck. How large the stresses caused by the relative deflections are, is unknown. It may be that they are insignificant.

a) End support:	b) Failure mode:
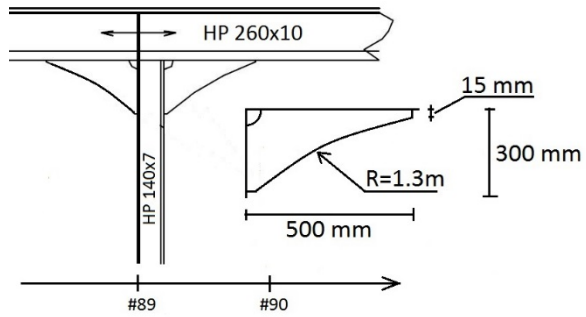	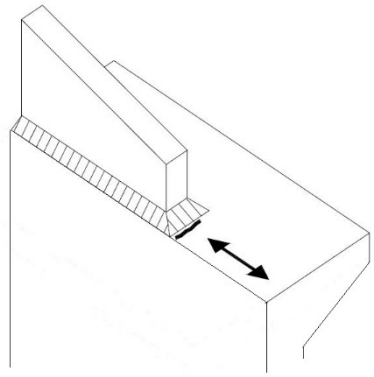

Figure 5.2: A) shows the end support detail A-A for longitudinals in main deck that are crossing the transverse bulkhead at #89 (Drawing No. 823-200-053), and b) shows the location of the fatigue failure mode (DNV, 2014a) [modified].

Table 5.3: Location (global coordinate system) of hot spot for the longitudinal in main deck.

Profile:	HP260x10	
Environment:	Void tank	
x (distance from AP), #89	= 64.5	m
y (horizontal distance from center line)	= 6.75	m
z (distance above keel/base line)	= 12.74	m
Web frame spacing	= 2.8	m
Effective span length	= 2.7	m
$K_{g,\ axial}$ (DNV, 2014a)	N/A	-
$K_{g,\ bending}$ (DNV, 2014a)	N/A	-

5.3 Hatch openings in main deck

The openings in main deck to be analyzed are shown in Figure 5.3 on page 54. They are selected since they according to (DNV, 2014a) have relatively large SCFs compared to attachment to longitudinals. In the current design the SCFs are around 3.0, as prsented in

Table 5.4 on page 54. In addition, the openings are arranged “asymmetric” as seen in. Two of them - the two located in the forward carousel compartment - are relatively close to each other which may lead to additional stress raise due to the interaction between them. However, this location is outside the region where the wave induced vertical moment is at its maximum.

How big the SCF is, depends on the ratio between the length and breadth of the cut out, in addition to the ratio between the radius of the rounded corners and the breadth of the cut out.

Based on empirical data (see Appendix C) provided by (DNV, 2014a), the tabulated SCFs for the loading hatch opening and the flush hatch opening are found to be 3.0 and 3.2, respectively, as given in Table 5.4. Empirical data for insert plates at the corners is not provided, thus not included in the table.

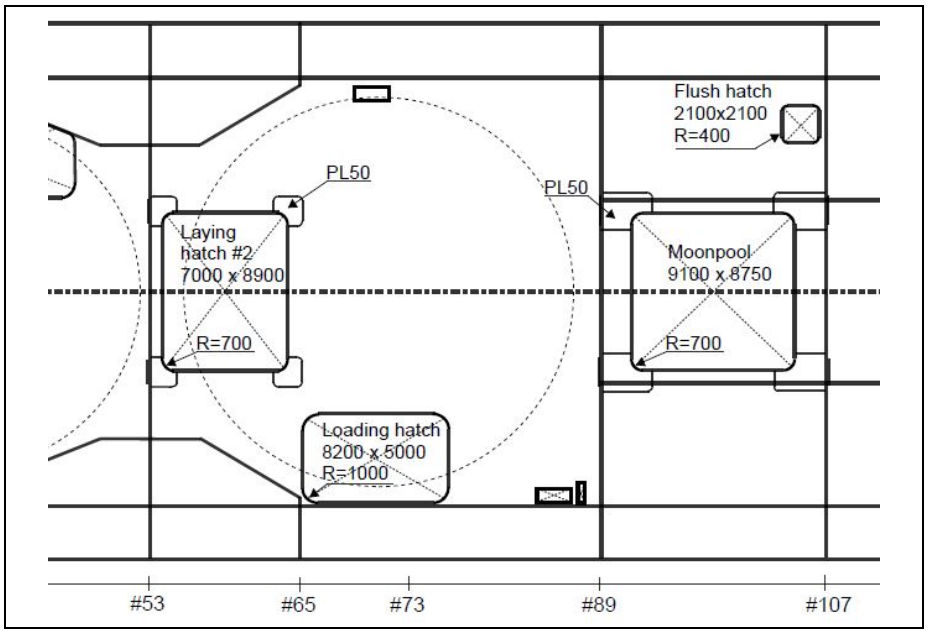

Figure 5.3: Main deck openings to be evaluated in the fatigue screening (drawing 823-200-011) [re-drawn].

Table 5.4: Stress concentration factors for cut outs in main deck (DNV, 2014a).

Deck openings:	a [m]	b [m]	r [m]	SCF
Loading hatch:	8.20	5.00	1.00	3.00
Flush hatch:	2.10	2.10	0.40	3.20
Moonpool:	9.10	8.75	0.70	N/A
Laying hatch:	7.00	8.90	0.70	N/A

The corner location of the hot spot, in other words where the fatigue crack is expected to occur, is shown by the red line in Figure 5.4, and applies for all four corners. The location is according to (DNV, 2014d). There is no weld in the hot spot area for the current design. Hence, the SN-curve III (base material) in the classification note is to be applied.

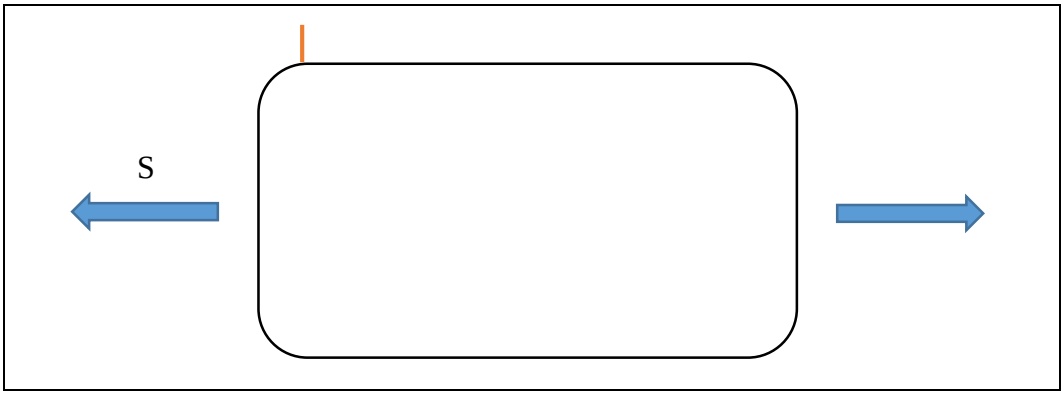

Figure 5.4: Fatigue crack (red line) in rounded corners of rectangular cut-outs. The failure mode applies for all four corners.

5.4 Loads and Acceleration

The global rule loads are calculated for the three loading conditions ballast, loaded and cable-laying, and are presented in

Table 5.5. Since the mean stress effect is to be evaluated, the Stillwater bending moment is also calculated.

The internal dynamic loads from the ballast tanks in the double bottom are given in Table 5.6. The rule accelerations giving the basis for calculating the inertia loads from the cable drum are given in Table 5.7, and the dynamic and static external pressures are presented in Table 5.8 and Table 5.9, respectively.

Table 5.5: Loading conditions including global loads for NB 823

	Ballast	Loaded	Cable-laying
$M_{wo,h}$ (10^{-8} prop. level)	628 989 kNm	628 989 kNm	628 989 kNm
$M_{wo,h}$ (10^{-4} prop. level)	327 248 kNm	327 248 kNm	327 248 kNm
$M_{wo,s}$ (10^{-8} prop. level)	-723 174 kNm	-723 174 kNm	-723 174 kNm
$M_{wo,s}$ (10^{-4} prop. level)	-376 250 kNm	-376 250 kNm	-376 250 kNm
M_H (10^{-8} prop. level), x=64.5m (#89)	322 636 kNm	334 388 kNm	314 783 kNm
M_H (10^{-4} prop. level), x=64.5m (#89)	167 860 kNm	173 974 kNm	163 774 kNm
$M_{sw,h}$ (rule), midship:	521 515 kNm	521 515 kNm	521 515 kNm
$M_{sw,h}$ (design), midship:	925 000 kNm	925 000 kNm	925 000 kNm
$M_{sw,s}$ (rule), midship:	-427 330 kNm	-427 330 kNm	-427 330 kNm
Draught T_{act}:	7.885 m	8.500 m	7.474 m
Block coefficient (assumed const.)	0.71	0.71	0.71
Speed, V:	14 kn	14 kn	0 kn
Metacentric height (GM):	1.6 m	3.27 m	2.1 m
Roll radius of gyration, k_r:	11.7 m	11.7 m	11.7 m
Vertical acceleration midship	4.20 m/s2	4.20 m/s2	3.41 m/s2

Table 5.6: Rule loads at 10^{-4} prob. level for dynamic ballast load (DNV, 2014a).

	a_v [m/s^2]	a_t [m/s^2]	a_l [m/s^2]	P [kN/m2]
Ballast tank no. 55 and 56	3.56	3.55	0.94	3.91
Ballast tank no. 59 and 60	4.07	3.55	0.94	4.47
Ballast tank no. 50	3.81	3.55	0.94	4.18
Ballast tank no. 51	4.07	3.55	0.94	4.47

Table 5.7: Rule accelerations [m/s2] cable drum (DNV, 2014c).

Location on tank top (z = 2.0 m):	Load condition			Cable-laying		
	a_v	a_t	a_l	a_v	a_t	a_l
#56 center line	4.20	3.93	1.13	3.41	3.72	1.13
#71, 10.75 m from center line	4.20	3.93	1.13	3.41	3.72	1.13
#86, center line	4.20	3.93	1.13	3.41	3.72	1.13
Center of drum (#71, center line)	4.20	3.93	1.13	3.41	3.86	0.92

Table 5.8: External dynamic sea pressure (DNV, 2014a).

	External (sea pressure) [kN/m2]		
Location (x, y, z): \ Load condition:	Ballast	Loaded	Cable-lay.
Longitudinal bottom (64.5m, 6.75m, 0.0m):	25.4	24.7	25.9
Mid position of cargo hold (52.6m, 0.0m, 0.0m):	25.4	24.7	25.9

Table 5.9: Static local loads - external and internal pressure [kN/m2] (CN-30.7, 2014).

	External pressure			Internal	
Load condition:	Ballast	Load	Operation	Ballast	Carousel
Longitudinal bottom:	79.30	85.47	75.15	20.11	10 500
Longitudinal main deck:	N/A	N/A	N/A	20.11	10 500
Main deck openings:	N/A	N/A	N/A	N/A	N/A

5.5 Screening

When the first analysis of the FE model is executed, all details are screened to see if further attention should be given to each detail, or if some of them can be omitted due to low stress range. The part-ship is then modelled with 8-node shell element (SCQS) with size 700 x 700 mm, while the details to be checked are modelled with a finer mesh with size t x t where t is the:

- Plate thickness at the weld toe for longitudinals at end supports.
- Plate thickness of the deck plate for rounded cut-out corners.

Regarding derivation of hotspots, the stress will be based on the Principal stress in accordance with the classification note. For longitudinals at end supports the hot spot is taken (for simplicity) as the stress at the read out point t/2 away from the intersection line and multiplied by 1.12 (DNV, 2014a), while for the cut-out corners it is taken as the greatest stress magnitude observed in the hot spot zone.

Finally, the stress components are combined, given a long-term stress range value and entered to the SN curves in accordance with the method described in section 2.

Table 5.10: Overview of load components to be applied for the different details.

Detail:	Loads		
	$M_{wo,\ s(h)}$	External	Internal
Bottom Longitudinal	x	x	x
Main deck longitudinal	x	x	x
Loading Hatch, aft corner PS	x		
Loading hatch, fwd. corner PS	x		
Moonpool, aft corner PS, butt weld	x		
Flush Hatch	x		

5.6 Comparison study of D81X and DA-A

An alternative bracket design for longitudinals that are crossing transverse bulkheads in main deck, is detail D81 presented in Figure 5.5. It is used when the longitudinals are subject to high relative deflections (VARD, 2015), like A-A, which is the present detail in the current design (see Figure 5.2 on page 53).

In this thesis work the two details will be compared to see which of them that represents the lowest SCF at the bracket toe gives the lowest SCF for bending and axial loading. The result can also be used as K-factors in future fatigue analyzes where simple stress calculation (Beam theory) is going to be applied instead of FEM.

According to Figure 5.5 there are two types of D81: X and Y. The former is used when the height of the profile is 260 mm and the other is used when the height is 280 mm. So in this study type X will be used since the current longitudinal stiffener is a HP 260x10 (H=260 mm).

The details will be termed *D81X* and *DA-A* in the proceeding.

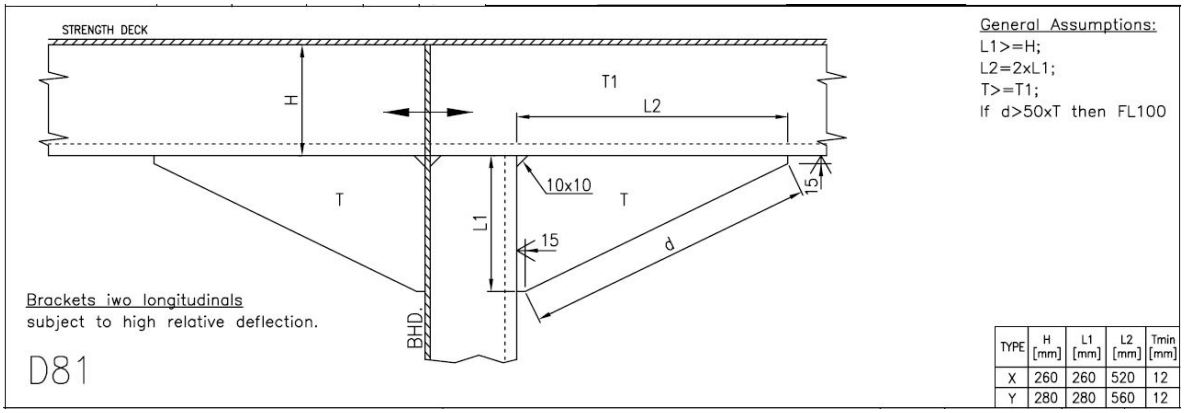

Figure 5.5: End support detail D81 for longitudinals in main deck that are subject to high relative deflections (drawing no. 823-200-048_revA).

When comparing the two bracket designs, they have be applied to a base model such that the only difference between them is the bracket itself, and not the other parts, loads and boundary conditions. The model is shown in figure below.

a) bending:

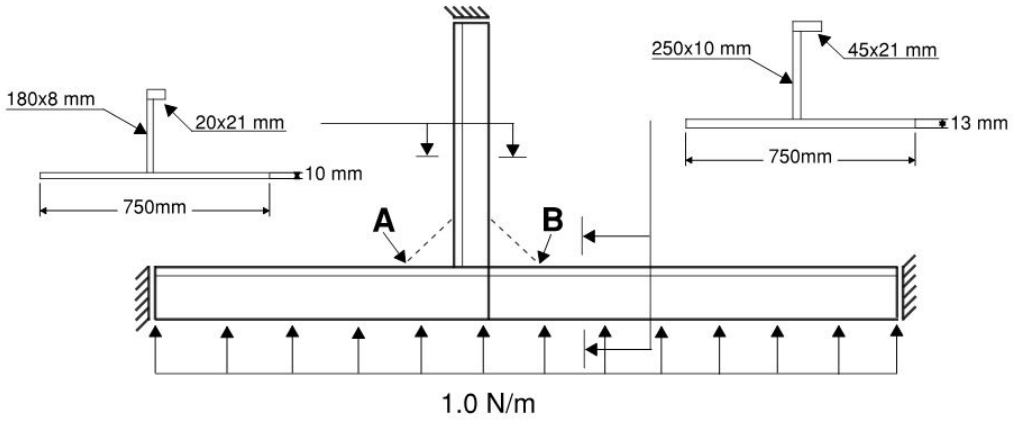

b) axial loading:

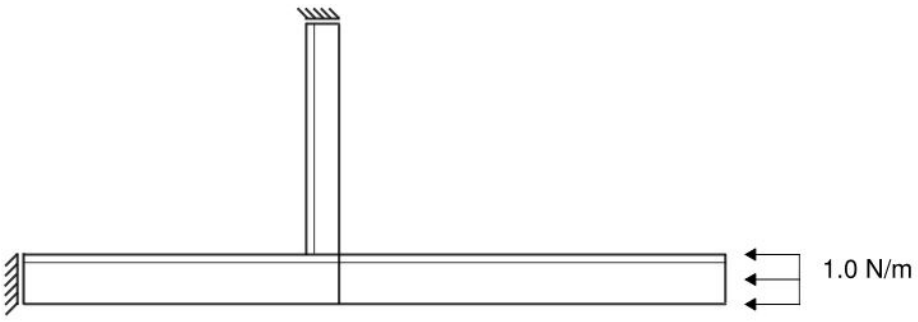

Figure 5.6: Basic geometry and the loads of the model.

6 Results

The results from the finite element analysis (FEA) are presented in the following. In the first section, the global stresses are given to provide a basis for verification of the model, i.e. that the model provides valid results. Secondly, the screening result is presented. Here, details are evaluated to see which of them that can be omitted from a further investigation. The weld connection between a longitudinal in main deck at the end support (bracket) turns out to be the most critical one, and is taken for further analysis. The analysis is then based on the operation profile given in Table 8.1.

6.1 Global stresses due to vertical wave moments

Before going into details, the output of the FEA needs to be controlled to make sure that the FE model, including the applied loads and the boundary conditions, provides correct results. In such case the displacement, stress distribution and the stress level in the hull girder needs to be verified/controlled.

The global mesh, longitudinals stress distribution and hull girder deformation when global bending moments are applied, are presented in Appendix F. The stress distribution in main deck and bottom is presented in Figure 6.1 on page 62.

Figure 6.2 on page 63 and Figure 6.3 on page 64 show the stresses along the hull girder cross section in main deck and bottom at #89, port side.

a) Main deck #53 to #107, z =13.0 m:

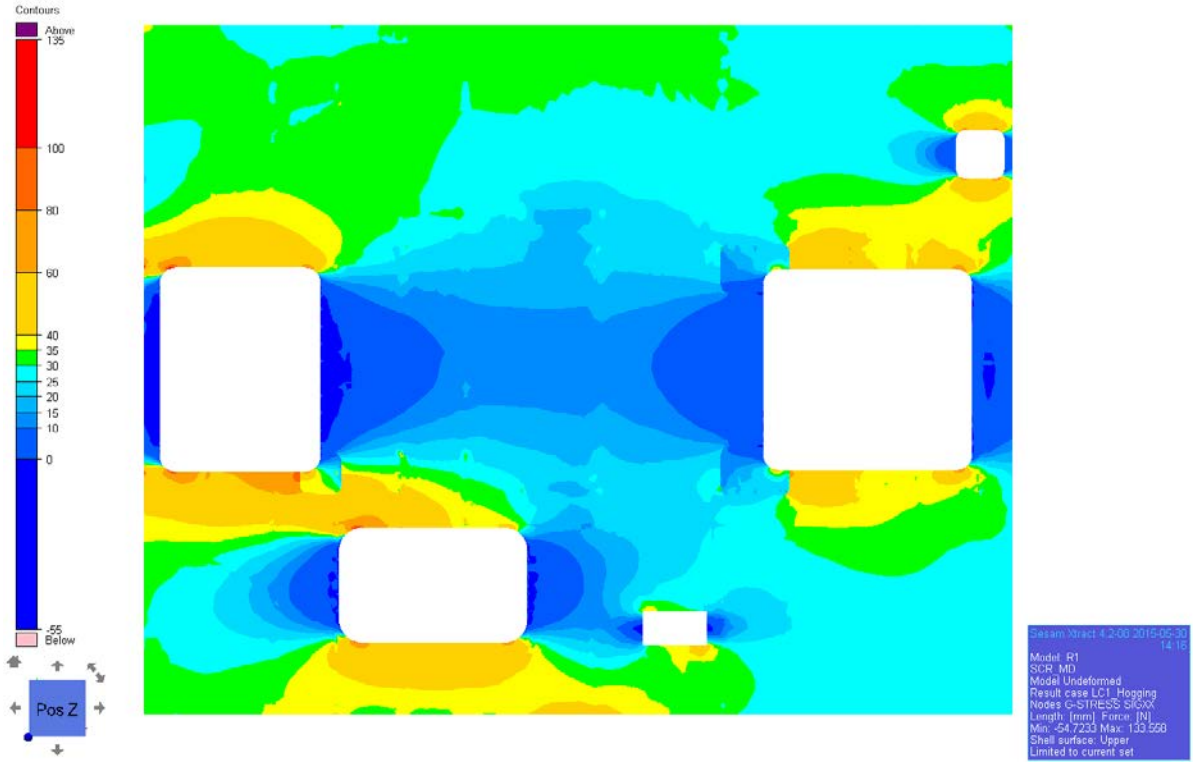

b) Bottom #53 to #107, z =0.0 m:

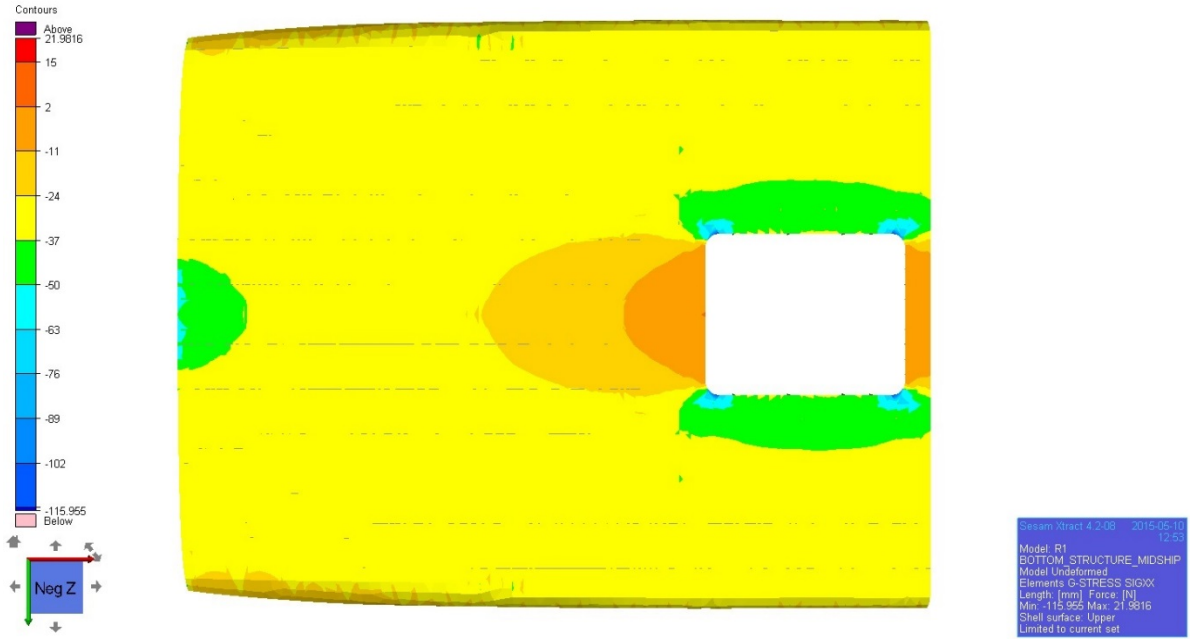

Figure 6.1: Distribution of longitudinal stresses [N/mm^2] (hogging condition) from frame 53 to frame 107, and y=-15 m to y=15 m. The elements are 2nd order and the size is 750x700mm.

a) Hogging condition – $M_{wo,\,h}$ = 327 248 kNm:

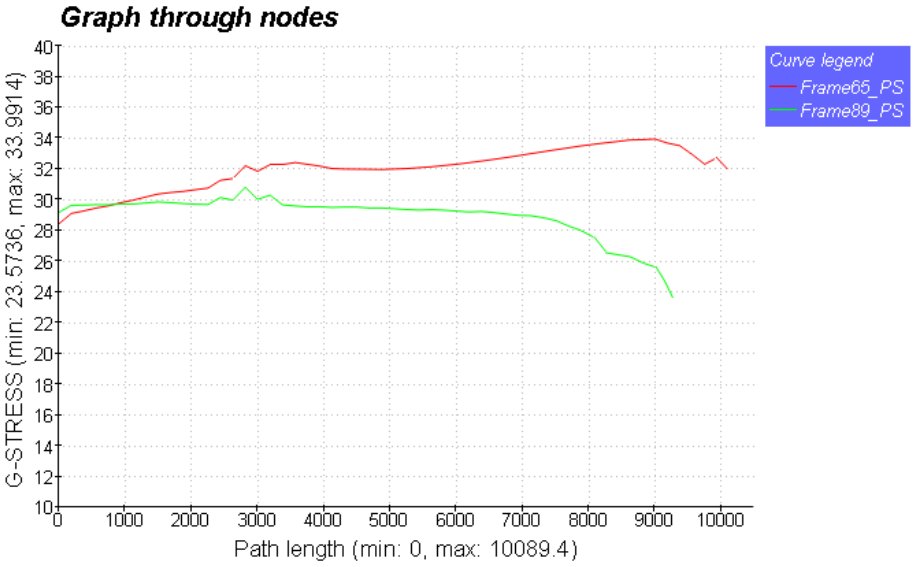

b) Sagging condition - $M_{wo,\,s}$ = -376 250 kNm:

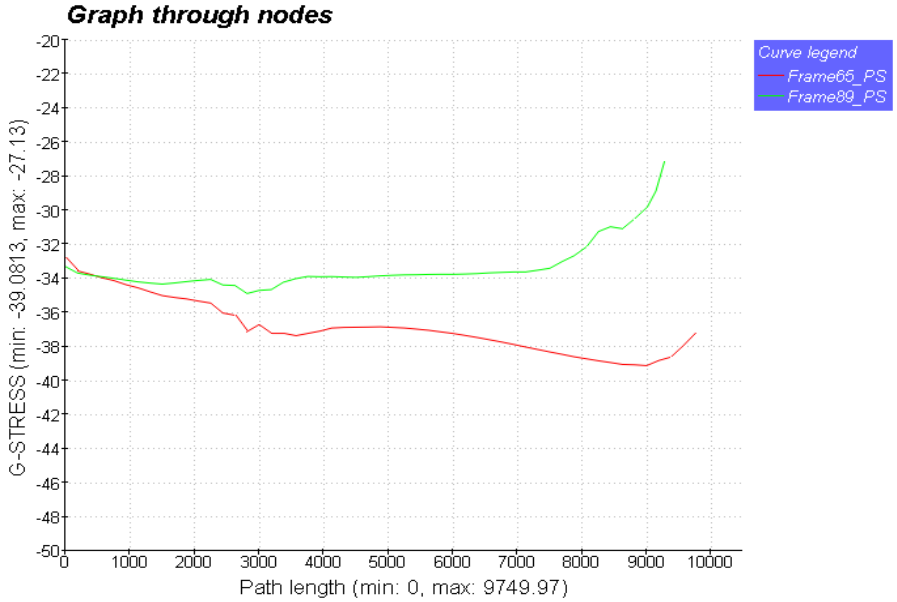

Figure 6.2: Longitudinal stresses [N/mm^2] in main deck at #89, portside of moonpool. The x-axis represents the distance [mm] from ship side (y=15 m) towards the center line.

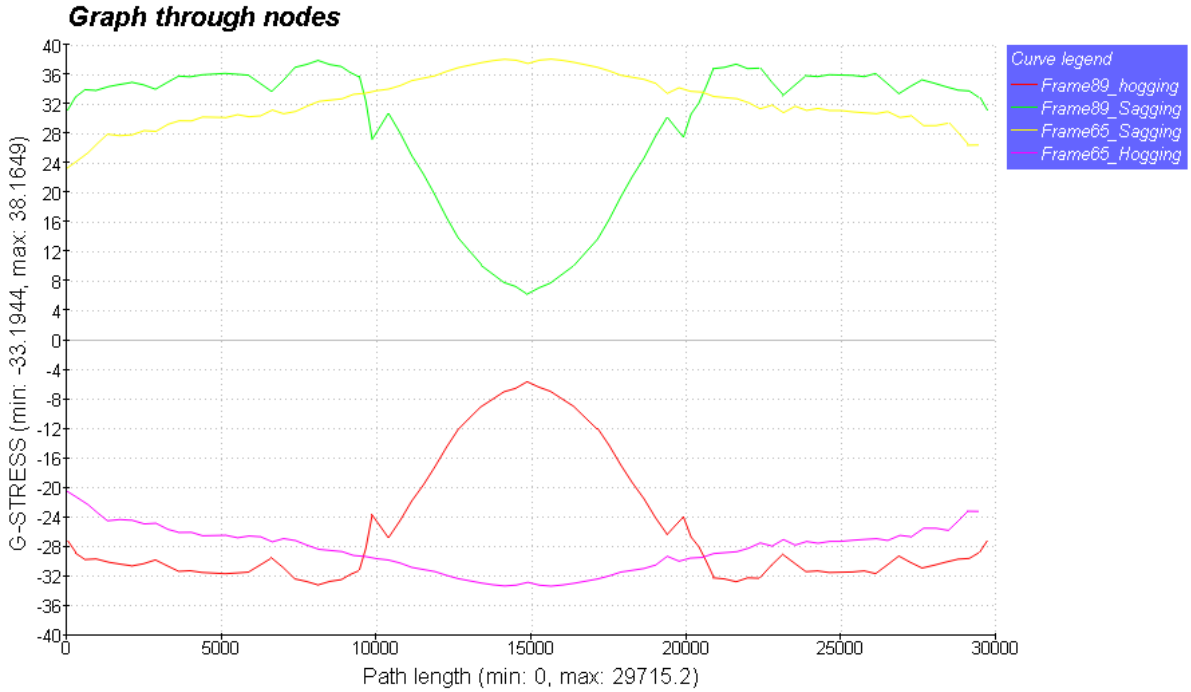

Figure 6.3: Longitudinal stresses [N/mm^2] in bottom at frame 65 and frame 89 in hogging and sagging condition. The x-axis represents the distance [mm] from SB side (y= -15 m) to PS (y=15m).

6.2 Screening

Table 6.1: Overview of the details evaluated in the screening process.

ID:	Detail:
Det#1	Bottom Longitudinal
Det#2	Main deck longitudinal
Det#3	Loading Hatch, aft corner PS
Det#4	Loading hatch, fwd. corner PS
Det#5	Moonpool, aft corner PS, butt weld
Det#6	Flush Hatch

A screening of the details is performed with the purpose to check if there is some details that appears to be critical with respect to fatigue, and if there are someone that can be omitted without going any further.

The HS stresses and the combination of them are given in Table 6.2 on page 66. The long term stress range parameters are given in Table 6.3, and the fatigue damage calculation is given in Table 6.4.

The result shows that neither of the calculated linear cumulative usage factors exceed the limit η=1.0 for 20 years' service life and that Det#2 has the largest fatigue damage D=0.27. Since the fatigue capacity of the hull is a matter of fatigue capacity of each structural detail, it is natural to go further with the most critical detail.

The screening is based on ballast condition and a time fraction at sea P=1.0. According to Table 5.6 on page 56, the external dynamic sea pressure is almost equal in all three loading cases, thus the analysis is only based on the ballast loading condition with respect to local loads. In addition,

Regarding further work, the object is to check the effect different mesh densities have on the result, and to apply the time fractions in each loading condition. In addition, a comparison study between the bracket designs D81X (drawing no. 823-200-048) and D A-A (drawing no. 823-200-023) since both of them are used as end supports for longitudinals in main deck.

Table 6.2: Stress components w.r.t. screening.

Detail:	Global stress components [N/mm^2]			Local stress components [N/mm^2]			
	Hogging	Sagging	$\Delta\sigma_G$	External	Internal	correlation	$\Delta\sigma_L$
Det#1	-36.60	43.40	80.0	-64.00	2.30	0.559	125.49
Det#2	56.94	-64.46	121.40	6.5	-1.01	0.470	6.09
Det#3	119.50	-137.10	256.6				
Det#4	60.15	-68.15	128.3				
Det#5	68.15	-56.40	106.2				
Det#6	49.80	-109.75	208.3				

Table 6.3: Long term stress range parameters.

Load condition:	h, main deck:	h, bottom:	v_0 (sec.)	Return period:	T_d [years]	Weibull scale, q:
Ballast	1.061	1.022	8.512	0.00277	20	12.40

Table 6.4: Calculated long-term stress distribution and fatigue damage calculation w.r.t. screening.

Detail	$\Delta\sigma_0$	f_m	f_e	f_{HTS}	$\Delta\sigma$	SN curve	D (20yrs)	Fatigue life [yrs.]
Det#1	187.48	0.70	0.80	1.00	97.15	I	0.22	93
Det#2	137.00	1.00	0.80	1.00	100.04	I	0.27	73
Det#3	256.60	1.00	0.80	0.91	186.80	III	0.25	81
Det#4	128.30	1.00	0.80	0.91	93.40	III	0.02	872
Det#5	106.20	1.00	0.80	0.91	77.31	I	0.09	219
Det#6	208.30	1.00	0.80	0.91	151.64	III	0.09	230

6.3 Hot spot stress at longitudinal end support in main deck

The hot spot stresses due to global moments are presented in Table 6.5, and the hotspot stresses due to local loads are presented in Table 6.6. The tables show the stresses obtained by hotspot derivation Method#1 and Method#2. Further, a contour plot of the Principal stress including the vectors are shown in Figure 6.4 and in Figure 6.5 when the material is tension and compression, respectively. The final stress range including the three reduction factors f_e, f_m and f_{HTS} are presented in Table 6.7.

Regarding the horizontal stresses, it is seen that the difference between the three loading cases are relatively small. The maximum stress (11.36 MPa) is about 6% higher than the minimum

one (10.69 MPa), when considering the result for Method#2. In addition, it is seen that the stress levels caused by horizontal bending moment is about $1/5^{th}$ and $1/6^{th}$ of the stress magnitude due to vertical moment in hogging and sagging, respectively. In other words, the vertical bending moments are the major drivers and the difference between the horizontal stresses are considered insignificant. Thus, the proceeding calculation is based upon the horizontal stress obtained in loaded condition, i.e.11.06 MPa for Method#1 and 11.36 MPa for Method#2. This is also to reduce the calculation effort.

Table 6.5: Result HS stress [N/mm^2] due to hull girder bending and resulting global stress range. Method#1 and Method#2 are both presented to see if they give different results.

8-noded shell, element size t x t	*HS derivation methods:*	
	Method#1	*Method#2*
M_{wo} hogging:	55.17	56.94
M_{wo} sagging:	-63.44	-64.46
M_{hg} (Ballast):	10.80	10.95
M_{hg} (Loaded):	11.06	11.36
M_{hg} (Cable-laying):	10.54	10.69
$\Delta\sigma_G$ ($M_{h,\ loaded}$) (ρ_{vh}=0.1):	122.53	126.34

Table 6.6: Result HS stresses [N/mm^2] due to relative deflection caused by local loads and boundaries fixed in vertical direction.

8-noded shell, element size t x t	*HS derivation methods:*	
	Method#1	*Method#2*
External pressure, Ballast:	6.54	6.50
External pressure, Loaded:	13.02	12.94
External pressure, Cable-laying:	6.66	6.62
Internal pressure, Ballast tanks (no. 55,56, 59, 60):	-1.00	-1.01
Internal Inertia loads drum, Loaded:	-1.93	-1.92
Internal inertia loads drum, Cable-Laying:	-3.14	-3.12
Stress range, ballast (ρ_p=0.389):	12.58	12.48
Stress range, loaded (ρ_p=0.402):	11.74	11.65
Stress range, cable-laying (ρ_p=0.380):	12.41	12.31

Table 6.7: Stress range including the reduction factors f_e, f_m and f_{HTS}.

	Load condition:	Δσ (a=b=0.6):	f_e:	$f_{m:}$	$f_{HTS:}$	$\Delta\sigma_0$:
Method#1	Ballast	130.08	0.8	1.0	1.0	104.07
	Loaded	129.58	0.8	1.0	1.0	103.66
	Cable laying	129.98	0.8	1.0	1.0	103.98
Method#2	Ballast	133.83	0.8	1.0	1.0	107.06
	Loaded	133.33	0.8	1.0	1.0	106.66
	Cable laying	133.72	0.8	1.0	1.0	106.98

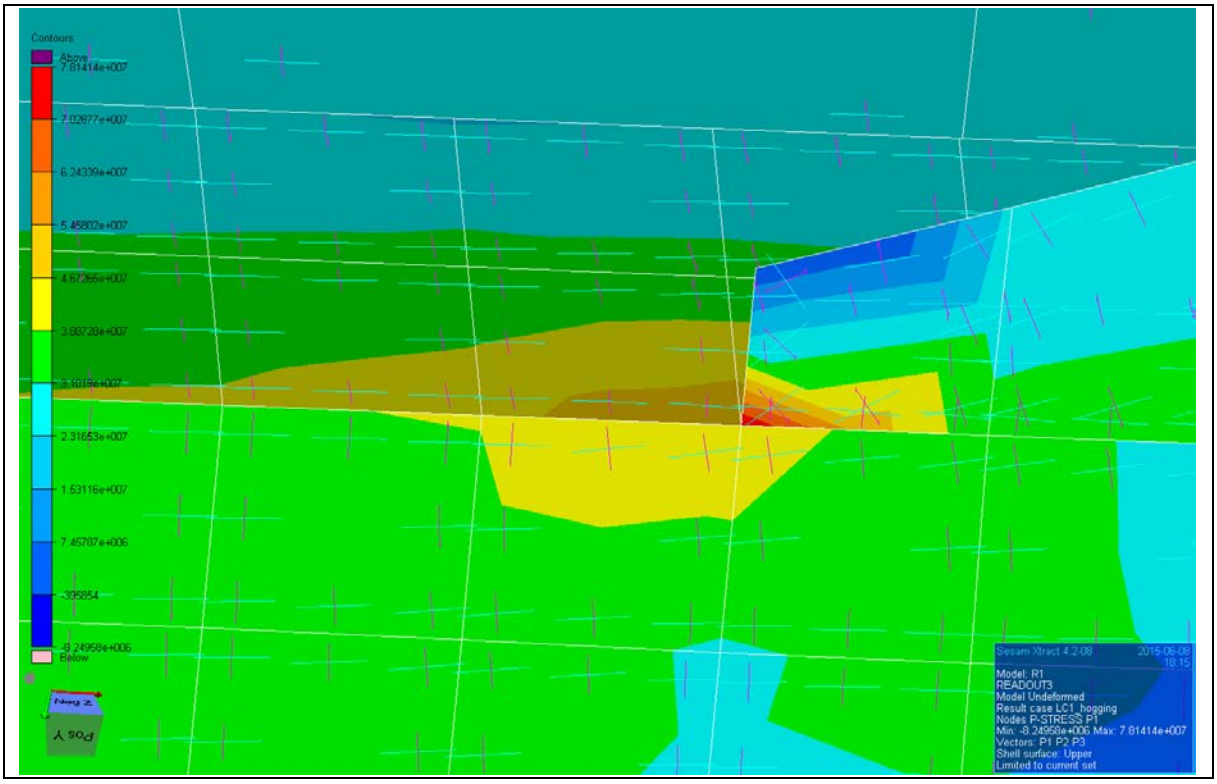

Figure 6.4: Principal stress when the material is in tension at the hot spot (bracket toe), and contour for P1 shown. Mesh size t x t.

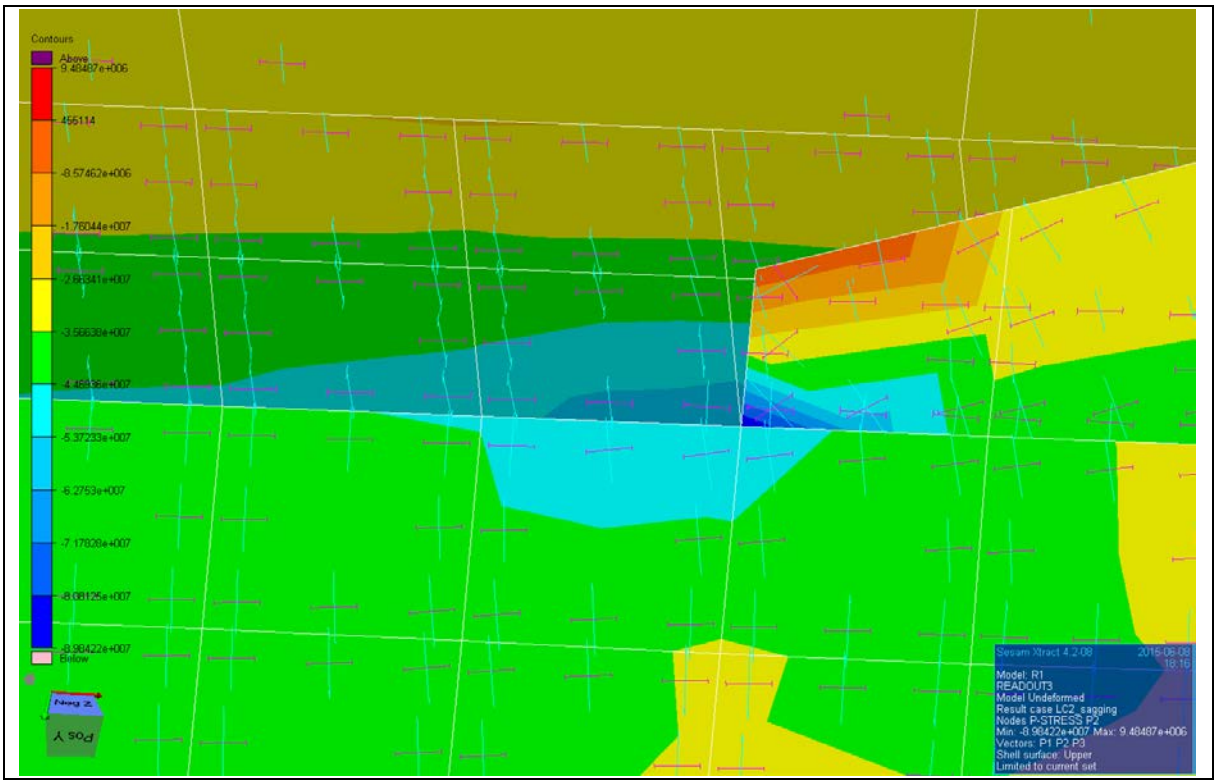

Figure 6.5: Principal stress when the material is in compression at the hot spot (bracket toe), and contour for P2 shown. Mesh size: t x t.

6.4 Long-term Stress Range and Fatigue Damage Accumulation

The Weibull parameters for the postulated long-term stress range distribution is shown in Table 6.8 and the fatigue damage calculation is presented in Table 6.9.

The fatigue damage is based on the stress ranges obtained by Method#2 to be on the conservative side.

When applying the fraction of time at sea in each loading condition, according to Table 3.1 on page 26, the total fatigue damage, D_{tot} is calculated to be 0.237 (84 years). If the time fractions are not considered and instead assuming a time fraction at sea equal to 1.0, and the most critical loading condition (Cable-laying/Ballast), the fatigue damage, D is calculated to be 0.36 which corresponds to 56 years.

When calculating the fatigue damage, an excel-file constructed by DNV GL is used. The document is not for external distribution. However, a print screen of the calculation sheet can be found among the attached file that are submitted together with the report in Daim.

Table 6.8: Long-term distribution data for the stress ranges

Load condition:	Weibull shape, h:	v_0 (sec.)	Return period:	T_d [years]	Weibull scale, q:
Ballast	1.061	8.512	0.00277	20	12.40

Table 6.9: Fatigue damage accumulation, method#2.

	Class (SN curve)	D	Correspond. Fatigue life (years)	P_n	D * P_n
Ballast	C air (I)	0.36	56	0.09	0.032
Loaded	C air (I)	0.35	57	0.09	0.032
Cable-laying	C air (I)	0.36	56	0.48	0.173
			P_{tot} ; D_{tot}:	0.66	0.237

6.5 K-factors for detail D81X and DA-A

The calculated K-factors in bending and axial loading, including hot spot stress and nominal stress, are presented in Table 6.10 and Table 6.11 on page 71.

The K-factors are obtained by dividing the derived hotspot stress with the derived nominal stress. When calculating the nominal stresses one may use beam theory, but in this case they are found by cubic extrapolation from three result points far away from the hot spot. The reason behind this is that the boundary conditions depend on the interaction with the surrounding structure and the bracket, which is not considered when using beam theory.

Figure 6.6 and Figure 6.7 show the FE models of the two bracket designs.

Figure 6.8 and Figure 6.9 on page 73 represent the stress distribution in front of the hotspot is for different element sizes for the two bracket designs.

Results for application of 4-noded shells in the model is not carried out due to errors with the meshing. This should, however, not be a problem since utilization of 8-noded shell elements provides more accurate results than 4-noded shells in regions with high steep stress gradients (DNV, 2014a).

Table 6.10: Calculated K-factor in bending for D81X and DA-A. Element: 8-noded shell.

				Method#1		Method#2	
Detail:	Mesh size:	Point:	Nominal [N/m^2]	HS: [N/m^2]	$K_{g,\ bending}$	HS: [N/m^2]	$K_{g,\ bending}$
DA-A	0.5t	A	3553	5451	1.53	5723	1.61
		B	3073	4670	1.52	4911	1.60
	1.0t	A	3553	5330	1.50	5635	1.59
		B	3073	4615	1.50	4863	1.58
D81X	0.5t	A	3444	5500	1.60	5769	1.68
		B	2945	4777	1.62	5009	1.70
	1.0t	A	3444	5379	1.56	5681	1.68
		B	2945	4653	1.58	4900	1.65

Table 6.11: Calculated K-factor in axial loading for D81X and DA-A. Element: 8-noded shell.

				Method#1		Method#2	
Detail:	Mesh size:	Point:	Nominal [N/m^2]	HS: [N/m^2]	$K_{g,\ axial}$	HS: [N/m^2]	$K_{g,\ axial}$
DA-A	0.5t	A	105.0	143.6	1.37	154.0	1.47
		B	105.0	144.5	1.38	155.8	1.48
	1.0t	A	105.0	142.1	1.35	152.8	1.46
		B	105.0	144.7	1.38	155.6	1.48
D81X	0.5t	A	105.0	146.8	1.40	157.2	1.50
		B	105.0	150.4	1.43	161.4	1.54
	1.0t	A	105.0	144.3	1.37	155.3	1.48
		B	105.0	148.3	1.41	159.2	1.52

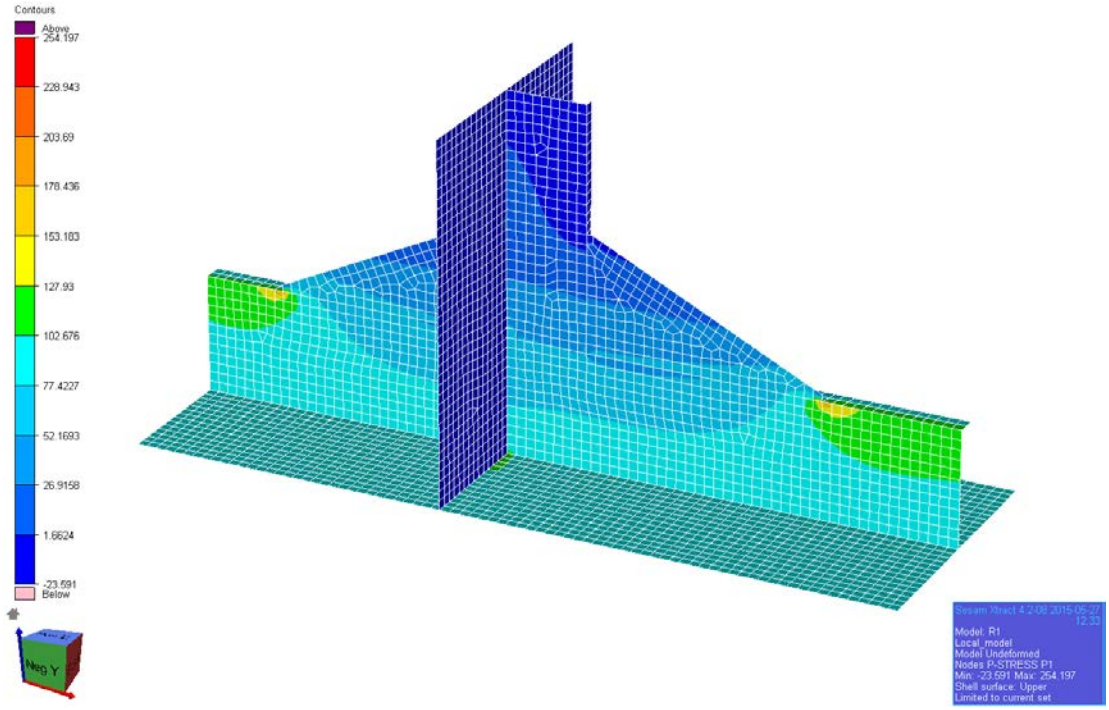

Figure 6.6: FE model of D81X subject to axial loading, mesh txt Principal stress and 8-node shell element. Contour of SIGXX shown.

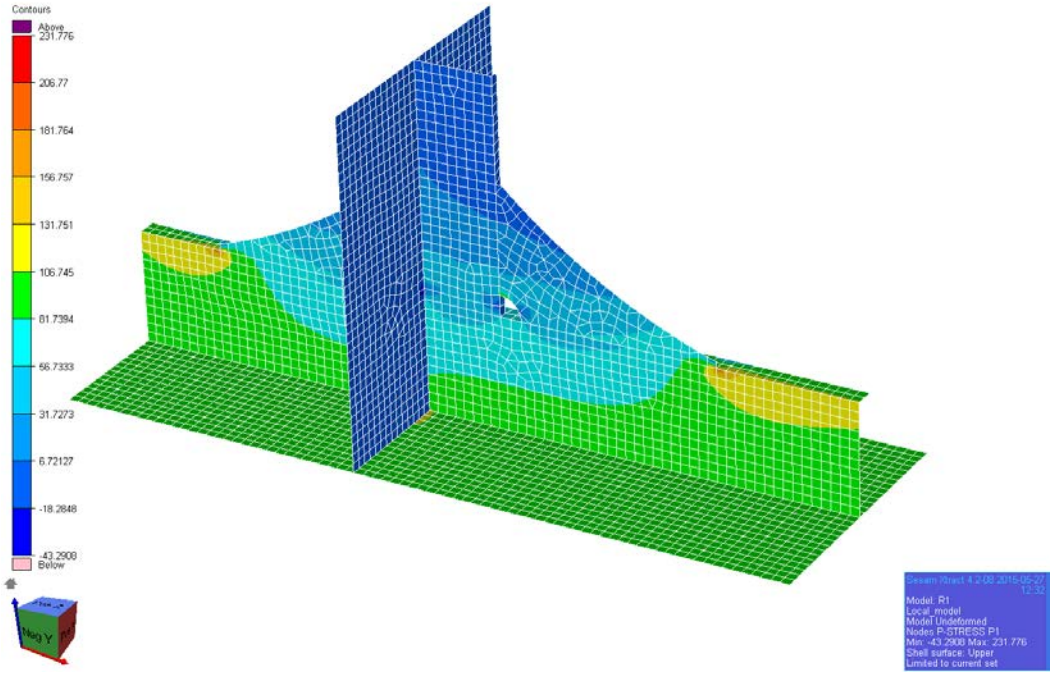

Figure 6.7: FE model of DA-A subject to axial loading, mesh txt Principal stress and 8node shell element. Contour for SIGXX shown.

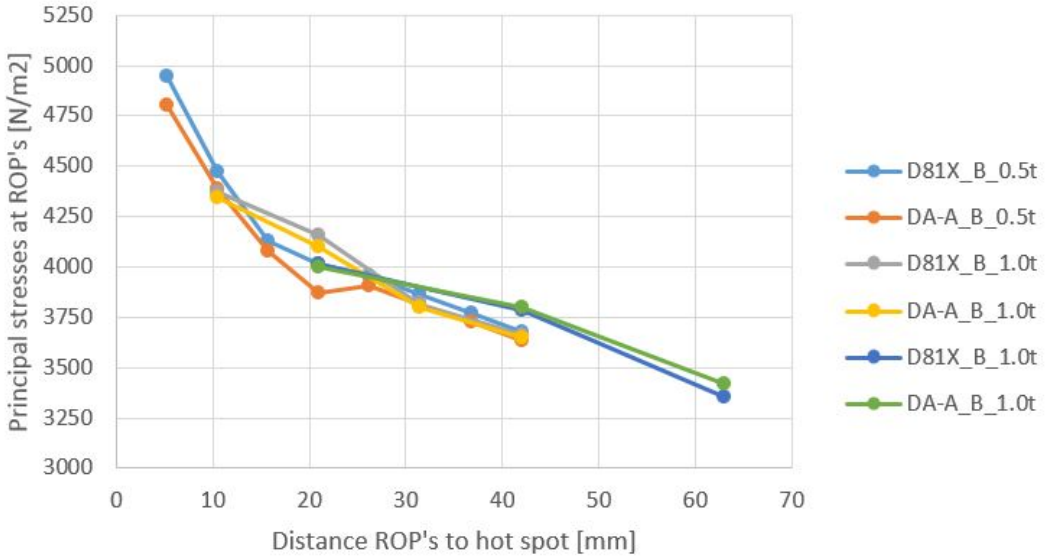

Figure 6.8: Stress distributions in front of hot spot from FE models subject to bending load. Location: Point B.

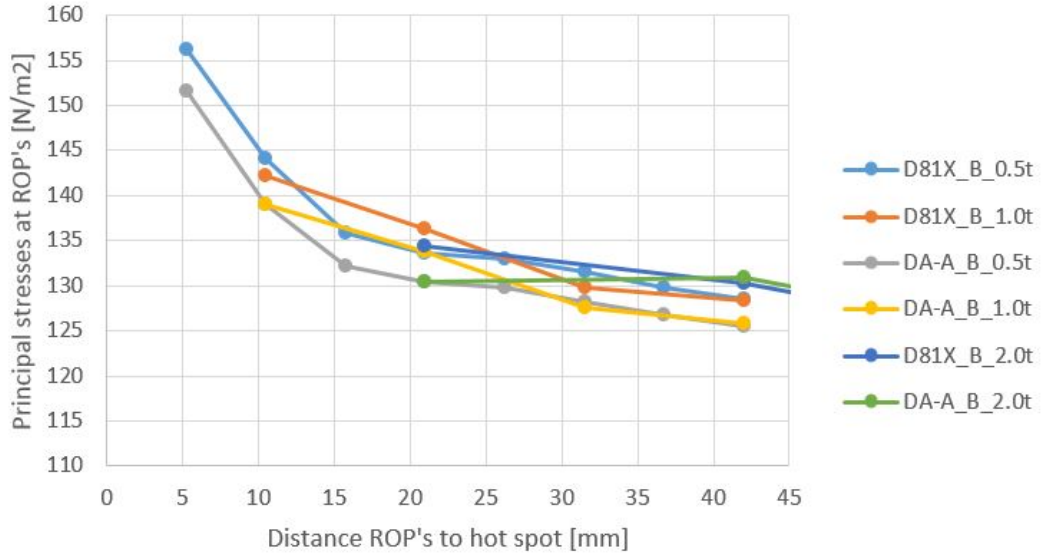

Figure 6.9: Stress distributions in front of hot spot from FE models subject to axial force. Location: Point B.

7 Discussion of Result

7.1 Loads

According to Mürer (Mürer, 1995), the acceleration parameter a_0 in the rule loads, should be specially considered for stationary operations in the North Sea since the loads are based on the North Atlantic and the world wide sea conditions. This implies that the dynamic sea pressure loads (rule) used in the FE analysis, when analyzing loading conditions during marine operations in the North Sea, may deviate from the correct ones. Experience have shown that application of direct wave load calculation by strip-theory computer programs, has often resulted in higher wave loads, especially for ships with low block coefficient.

For the design evaluated herein, with C_b=0.71, this implies that the vertical hull girder stress obtained in this thesis may be underestimated. Furthermore, it is said that during the recent years - 80s - 90s in this context – the softwares have been refined to take into account non-linear and 3-dimensional effects, and the results seem to come out closer to the ship rule values (Mürer, 1995).

7.2 Boundary conditions

The result shows (see Appendix F) that the model is rotating about the transverse axis at the boundaries, when applying the vertical wave moments. In addition, the greatest vertical deflection is located at the half length of the model. The same behavior also applies when the model is subject to horizontal moment, but then rotation about the vertical axis and displacement in transverse direction. This implies that the boundaries provide the correct behavior of the hull girder when the wave moments are applied.

Regarding the location of the boundaries with respect to vertical load application, a sensitive analysis is performed. The aim is to check if un-correct location of the rigid links affect the stresses in a considerable way. The FE model is then analyzed for three different location (6.4, 5.9 and 6.9 m above base line) of the rigid links, and the general stress, SIGXX is used as comparative parameter. The stress read out point is located in main deck at the intersection between the longitudinal 6.75 m from center line (y=6.75m) and the bulkhead plate at #89. The result shows a small difference between the results, which implies that inaccurate position of the rigid links can be regarded as uncritical for the stress result.

Table 7.1: stress result for different position of the boundary conditons (rigid links).

Location of Rigid link:	z = 5.9 m	z = 6.4 m	z = 6.9 m
SIGXX, upper surface [N/mm2]:	29.67	29.50	29.43

7.3 Global stress level at #89

When considering the longitudinal stresses in main deck along the cross section at #89 in Figure 6.2, it is seen that the nominal stress is about 29.5 MPa when the hogging moment is applied. In Nauticus Section Scantlings the stress in main deck at #89 is calculated to be 30.21 MPa, as shown in Table 7.2 below. That is 2.4 % higher than the stress level calculated in GeniE. Both models have been controlled, and all dimensions regarding plates and stiffener scantlings are the same.

Another way to control the FE model, is to open the result-file in Sesam Cutres. This software calculate the moment force at a specified frame, based on the stress result at the same frame. In that way, the user can check if the applied moment forces can be found at the current frame. However, errors occurred during the running and only the horizontal neutral axis is found. This turned out to be 6.41 m at #89. In Section Scantlings the neutral axis is calculated to be 6.61 m above base line. Hence, it can be concluded that the FE model provides correct results.

Table 7.2: Longitudinal stresses in main deck and bottom at #89, calcualted by FEM and Section Scantlings (beam theory).

	Hogging moment:		Sagging moment	
Hogging	Main deck	Bottom	Main deck	Bottom
FE model:	29.50	32.00	34.00	36.00
Section Scantling:	30.21	31.28	34.73	35.96
Difference (FE model=100%):	2.41	-2.25	2.15	0.00

7.4 Global stress distribution and main deck openings.

When looking at the stress distribution in Figure 6.1 on page 62, the result shows that the longitudinal stresses in main deck vary significantly due to the openings that cause “stress-free” zones, in addition to stress raise towards the corners. However, when considering the aft

corners of the moonpool opening it is observed that the stress raise is less prominent. This is due to the insert plates that evidently reduce the stress concentration factor that would be present if the insert plate was not applied. Table 7.3 shows the SCF for the aft portside corner of the moon pool based on the result obtained by the FEA, and a tabulated value (DNV, 2014a) for the opening when no insert plate is introduced.

The stress contour in Figure 6.1 also shows that the narrow area between the laying hatch and the loading hatch (see Figure 4.2 on page 31) is subject to higher stress amplitude than port side of the laying hatch. When considering the aft portside corner of the loading hatch, the SCF is determined to be 3.67, which is 22 % higher than the tabulated one, as shown in Table 7.3. The nominal stress is then based on the nominal stress in main deck at #65, given in Figure 6.2 on page 63, and the hotspot stress is taken from the result in Table 6.2 on page 66. This implies that additional stress raise is caused when two cut outs are close to each other, i.e. located in each other's stress raise zones.

Table 7.3: Stress concentration factors for moonpool corner and loading hatch corner.

		Nominal stress	Hotspot stress	SCF
Moonpool corner, aft PS:	Current design	29.50	49.45	1.68
	No insert plate	N/A	N/A	4.00
Loading hatch corner, aft PS:	Current design:	32.00	117.31	3.67
	Tabulated:	N/A	N/A	3.00

7.5 SCF for end support detail in main deck

Figure 7.1 on page 79 shows the stresses along the bulb and plate for the longitudinal in main deck, in hogging. As seen in the figure, the nominal stress at the hotspot (x = 0 mm) is higher than the stress in main deck. According to beam theory it should be the opposite, since the hot spot is nearest to the horizontal neutral axis of the hull girder cross section.

The overlapping between the beam element and shell elements is also checked to see if it has an effect on the hot spot stress. In Figure 7.1 the overlap is 700 mm. As seen in the figure there is a significant jump in the stress level at around x = 7180 mm. This is where the beam element of the longitudinal ends, while the longitudinal built up by shell elements ends at x=7880 mm.

In Figure 7.2 the overlapping is increased from 0.7 m to 2.8 m. The overlapping is now from the transvers girder at #77 to the transverse girder at #81. In the figure this corresponds to x=7880 and x=5080, respectively. The result shows that this has no impact on the nominal stress at the hot spot. The only change is a re-location of the singularity, which is now located at x=5080.

In Table 7.4, the stress concentration factor at the hot spot is calculated, based on the hotspot stress given in Table 6.5 on page 67 and the nominal stress equal 35 MPa, in accordance with Figure 7.1. In addition, the SCFs obtained in the comparison study for both bending and axial loading are also included. These are for mesh size t x t which is the same mesh density used in the fatigue analysis of the longitudinal in main deck.

The table shows that the calculated SCFs when the detail is subject to global stresses in hogging are equal to the K-factors for bending. This is not as expected, since the detail is subject to axial loading when global bending moment is applied. According to (DNV, 2014a) the axial K-factor shall be applied when calculating the hot spot stress due to global loading, so this result is not as expected.

This indicates that the longitudinal may be subject to relative deflection between the boundaries when hogging moment is applied to the FE model, and thus bending of longitudinal.

Table 7.4: SCF for D81X based on stresses in hogging condition.

	Nominal:	Method#1		Method#2	
		HS stress:	SCF:	HS stress:	SCF:
Kg (hogging cond.)	35	55.17	1.58	56.94	1.63
Kg, axial	N/A	N/A	1.41	N/A	1.52
Kg, bending	N/A	N/A	1.58	N/A	1.65

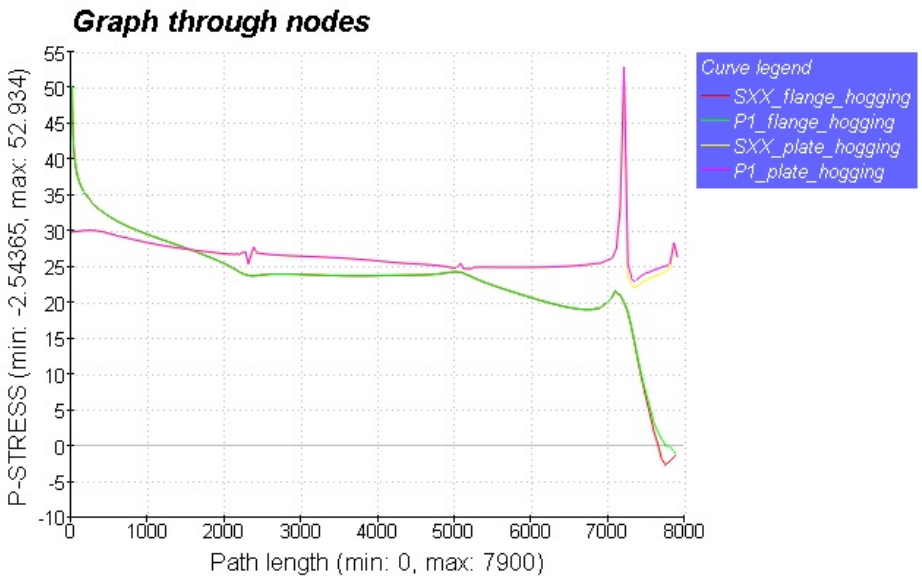

Figure 7.1: Graphical presentation of the stress distribution along the longitudinal bulb-flange and plate-flange from 0.5t (10.5mm) from HS to 7880 mm from HS (#77).

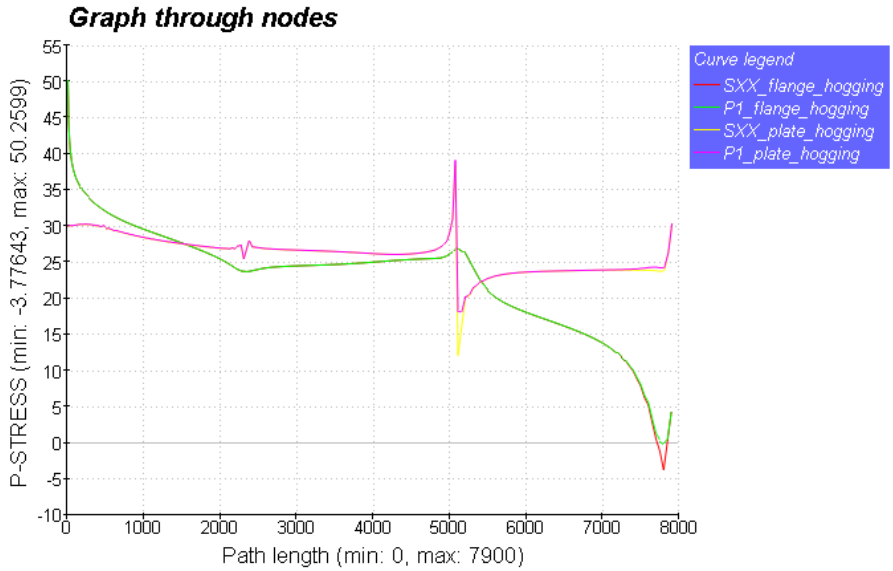

Figure 7.2: Graphical presentation of the stress distribution along the longitudinal bulb-flange and plate-flange from 0.5t (10.5mm) from HS to 7.88 m from HS (#77).

7.6 Comparison of D81X and DA-A

The result shows that Method#2 for derivation of hot spot stress gives larger SCFs compared to Method#1.

Regarding the different SCF value between Method#1 and Method#2 may, among other factors, lie in the fact that the stress read out points are not exactly located at 10.50 mm (0.5t) from the hotspot intersection line in accordance with the method description. Instead, the location deviates slightly from the "correct" one. The largest error found is at point A for element size txt (21x21 mm) where the real "0.5t location" is 10.0 mm from the hot spot, which is a deviation of 4.8 %. How large effect this has on the result is unknown.

7.7 Mesh density in rounded corners of deck opening

In the screening work, the mesh size is taken as t x t, where t is the plate thickness at the hot spot. This is based on mesh recommendations (DNV, 2014a) addressed to welded connections between structural members and attachments, as shown in Figure 4.20 on page 49 and Figure 2.2 on page 5. However, no recommendations are found regarding cut outs.

The hotspot stress at Det#3 is calculated for different mesh densities to check what consequence the element size has on the stress magnitude. In this study 8-node shell element is used and the mesh size vary from 0.5t to 2t, where t is the plate thickness (24 mm) of the main deck in the current area.

To assess the hotspot stress, the principal stress is used and its vectors in Figure 7.3 shows that the vector of the maximum stress (blue line) follow the edge curve.

The result in Table 7.5 shows that the stresses are more or less the same. However, it should be noted that all three element sizes are very small compared to the radius of the corner (1.0 m).

Table 7.5: Hotspot stress at rounded (radius=1.0m) cut-out corner for different mesh densities.

Element size (t = 24mm):	0.5t x 0.5t	t x t	2t x 2t
Hotspot stress at cut-out corner [N/mm^2]:	117.36	117.31	117.15
$\frac{\text{element size}}{\text{Corner radius (1000mm)}}$:	0.012	0.024	0.048

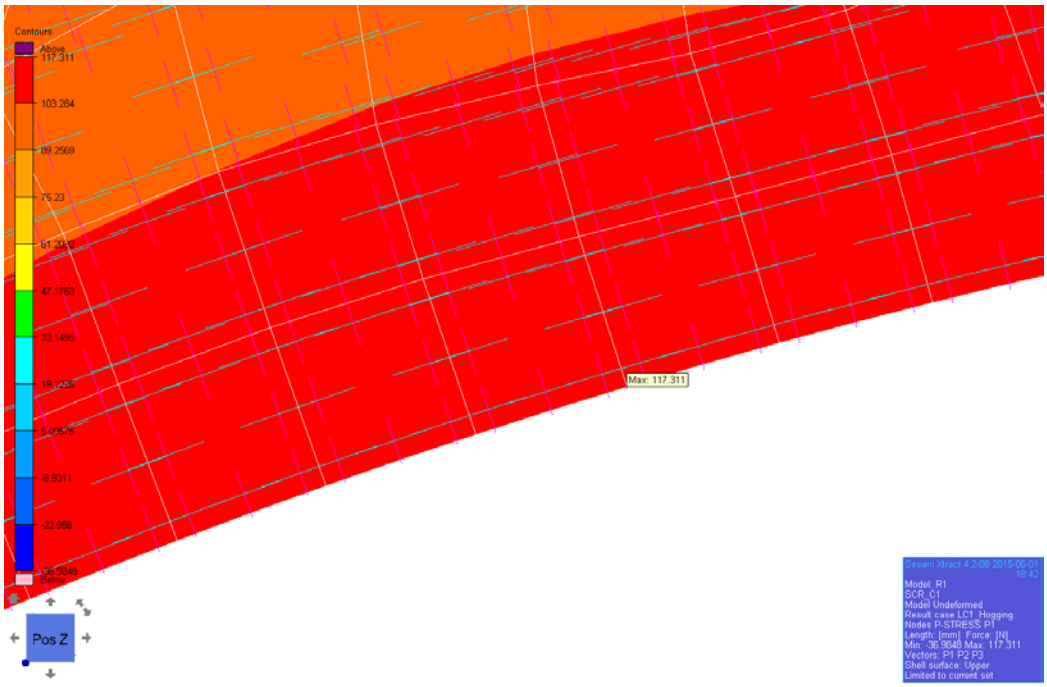

Figure 7.3: Principal stress P1 contoured and vectors for P1 and P2 shown.

8 Conclusion

A fatigue assessment of an OSCV with rule length L=134.3 m is performed according to DNV Classification Notes No. 30.7 - Fatigue Assessment of Ship Structures, in addition to a general investigation of the operational profile to be used when determining the input for the analysis.

The result shows that fatigue is not critical for longitudinals in main deck and bottom at typical end supports, nor for rectangular main deck openings with rounded corners.

Among these structural elements, the longitudinals in main deck turn out to be the most "critical" objects and the fatigue life of the specific one calculated herein, is calculated to be 84 years. Long-term worldwide operation is then assumed, and the sailing frequency is taken as 66 percent of the operational life, according to the concluded operational profile.

8.1 Operational profile

The conclusion of the operational study is given in Table 8.1 and is based on the historical data in Table 3.1 on page 26 and the discussion in section 3.2 on page 22.

Table 8.1: Fraction of time at sea in frequently used loading conditions for OSCV in general.

Status:		Loading condition:	
Field:	0.48	Cable-laying:	0.32
		Loaded:	0.16
Transit:	0.18	Loaded:	0.09
		Ballast:	0.09
SUM:	0.66		0.66

There are also some features that are concluded on with respect to how the OSCVs operates:

- Regarding the environmental reduction factor (section 2.11.3 on page 17) that distinguish between North Atlantic environment and worldwide operation, application of the latter turns out to be the most correct one with respect to OSCVs in general.
- It is difficult to determine the long-term operational environment for OSCVs in the design phase. When the service life is at its end the ships' log may deviate significantly from the assumed operational profile.

- The time fraction at sea may vary from vessel to vessel. Some OSCVs may experience a lot of time at mobilization (preparing for next mission), while others are taking general missions in the long-term that do not require re-/additional outfitting.
- The OSCVs are generally exposed to benign sea when operating. During heavy sea, the ship type aborts the mission temporary while waiting on better weather.
- The loading conditions may be modified during the operational life and lead to new properties with respect to draught and GM. Consequently the long-term stress range is changed regarding the local loads. Whether the change is significant, or the opposite, is not concluded on.

8.2 Fatigue assessment

The following items are considered in the fatigue evaluation:

- The weld connection between a longitudinal in bottom and the end support;
- The weld connection between a longitudinal in main deck and the bracket toe of an end support;
- Rectangular main deck openings with rounded corners (some also with insert plates, see Figure 5.3 on page 54).

The result shows that the most critical item with respect to fatigue, even though it is not critical, is the longitudinal in main deck, as shown in Table 6.4 on page 66. Based on 20 years' service life, long-term worldwide operation (f_e =0.8) and the time fractions presented in Table 8.1 on previous page, the fatigue life is determined to be 84 years. If North Atlantic environment (f_e =1.0) is assumed instead of worldwide operation, the fatigue life will be reduced to 37 years. If one take it even further, and in addition assume a fraction of life at sea equal to 0.85, the fatigue life is about 27 years

The study also showed that the stress range of the bottom longitudinal is subject to a mean stress in compression. Consequently, the stress range is reduced by up to 30%. If this phenomenon is not present, the bottom longitudinal would be a lot more critical than the main deck longitudinal since its initial stress range is larger than the initial stress range of the main deck longitudinal.

9 Design Recommendations in a Fatigue Perspective

The insert plates in the rounded corners of the rectangular deck openings are reducing significantly the stress raises that would be present if the insert plates were not there. Thus, such details are recommended in the corner of the deck openings when a low stress concentration factor is found necessary.

The end support of the longitudinal in bottom at #89 is a single sided bracket. According to (DNV, 2012), this is not recommended. Instead, double bracket design should be used. This gives less eccentric load transfer of the shear force into the transverse bulkhead (or web frame) than a single sided bracket design, and with lower stress concentration. However, this may be insignificant considering the result obtained in this thesis work.

When determining the main deck arrangement, it should be kept in mind that cut-outs relatively close to each other, cause additional stress raise beyond the initial hot spot stress. The initial hot spot stress in this context is the hotspot stress that is present when the cut-outs are not close to each other. This is based on an observation during the discussion in section 7.4 on page 76.

Ice Belt – a fatigue design advantage

Even though details in the ship side have not been considered in this thesis work it is worth mentioning that ice belt may be an advantage with respect to fatigue design. According to RP-C206 fatigue may be the governing factor of the thickness of the shell plating at the waterline area. Often, the critical detail is the fillet weld between the longitudinal and the shell plate. Experience show, however, that if the plate thickness is greater than 1/46 of the stiffener span, the fatigue contribution due to lateral pressure is considered to be minor (DNV, 2012), hence application of Baltic ice notation may be an advantage in a fatigue design perspective.

10 Further Work

The result showed that the rule wave induced hull girder moments are the major load components behind the hot spot stress in the main deck longitudinal at the bracket toe of an end support. Whether the hull girder bending moments are accurate, or not, for the VARD 3-serie design, is unsure, as discussed in section 7.1. This issue should be investigated and wave loading by direct calculation should be considered.

A second recommendation for further work is the study of the operational profile for OSCVs. The operational profile used in the fatigue evaluation herein is only based on one operating OSCV. It is therefore recommended that more samples are gathered to ensure that the profile is representative for the average OSCV.

Thirdly, it is recommended to perform a fatigue analysis of a welded connection between a longitudinal and an end support in the ship side and investigate the interface between the hull structure and the top side. In this context, the top side is the tower of the vertical layer system (VLS tower) and the offshore crane, which are shown in Figure 10.1 below.

According to (DNV, 2012) the interface needs to be carefully considered since in many cases, fulfillment of both the Ultimate Limit State (ULS) and Fatigue Limit State (FLS) criteria will require that the hull structure be strengthened beyond that of normal ship designs.

Last thought about further work is to investigate the consequences an application of the MODU-code has on the ship structure, with respect to fatigue.

Figure 10.1: Top side of current design.

Almar-Næss, A. (1985). *Fatigue handbook: offshore steel structures*. Trondheim - NTH: Tapir, Norwegian University of Science and Technology.

Berge, S. (2006). *Fatigue Design of Welded Structures*. Marine Technology Centre Trondheim, Norway: Norwegian university of Science and Technology.

DNV. (1999). *Classification Notes No.31.3 - Strength Analysis of Structures in Tankers*. Høvik, https://exchange.dnv.com/servicedocuments/dnv: Det Norske Veritas AS.

DNV. (2010). DNV-RP-C205 - Environmental Conditions and Environmental Loads *Recommended Practice* (Vol. C205). Høvik / https://exchange.dnv.com/servicedocuments/dnv: Det Norske Veritas.

DNV. (2012). RP-C206 - Fatigue Methodology of offshore Ships *Recommended Practice* (Vol. RP-C206, pp. 94). Høvik, https://exchange.dnv.com/servicedocuments/dnv: Det Norske Veritas, .

DNV. (2013). *Sesam User Manual*. Høvik / http://dnvs.force.com/: DNV GL Software.

DNV. (2014a). *DNV Classification Notes No.30.7 - Fatigue Assessment of Ship Structures*. https://exchange.dnv.com/publishing/CN/: DNV.

DNV. (2014b). DNV Recommended Practice C102 - Structural Design of Offshore Ships *Recommended Practice* (Vol. DNV-OS-C102). Høvik, Norway, https://exchange.dnv.com/servicedocuments/dnv: Det Norske Veritas AS.

DNV. (2014c). *DNV Rules 2014 Pt.3 Ch.1*. https://exchange.dnv.com/servicedocuments/dnv.

DNV. (2014d). Recommended Practice C203 - Fatigue Design of offshore Steel Structures *DNV Service documents, Recomended practice*. Høvik, Norway / https://exchange.dnv.com/servicedocuments/dnv: Det Norske Veritas AS.

DOF. (2015). The Dof Fleet 2015. In D. ASA (Ed.), (pp. 80). www.dof.no: DOF Corporate Communication Department.

Dokkum, K. v. (2011). *Ship knowledge: ship design, construction and operation*. Enkhuizen: DOKMAR.

Espen Venge, D. M. A. (2015) *Operational Profile for Offshore Service Construction Vessels/Interviewer: M. V. Steffensen*. DOF Management AS, Bergen.

Group, D. (2015). Web page. Retrieved April 17, 2015

Hovem, L. A. (1993). Loads and Load combinations for Fatigue Calculations - Background for the Wave Load Section for the DNVC Classification Note: Fatigue Assessment of Ships (S. a. Offshore, Trans.). Høvik: Det Norske Veritas Classification AS.

IMO. (2009). Prevention of Air Pollution from Ships (M. E. P. Committee, Trans.). In M. E. P. Committee (Ed.), *INO GHG Study* (2. ed., pp. 181). http://www.imo.org/OurWork/Environment/PollutionPrevention/AirPollution/Pages/Greenhouse-Gas-Study-2009.aspx: International Maritime Organization.

Larsen, K. (2015). TMR4225 - Marine Operations by Statoil *Course material*. Trondheim: Statoil.

Magasin, M. (2014). Ship reviews. Retrieved September, 2014

Moan, T. (2003). *TMR 4190 - Finite Element Modelling and Analysis of Marine Structures*. Trondheim: Norwegian University of Science and Technology, Department of Marine Technology.

Mürer, C. (1995). *DNV Hull Structural Rules - Development, Background, Motives*. HØVIK: Det Norske Veritas AS.

VARD. (2015). VARD Design AS. In L. E. Nygård (Ed.). Ålesund.

Xtract. (2014). Sesam user manual, Xtract (Version 4.2) [DNV software Report]. http://dnvs.force.com/: DNV GL.

Appendix A - Classification Notes No. 30.7

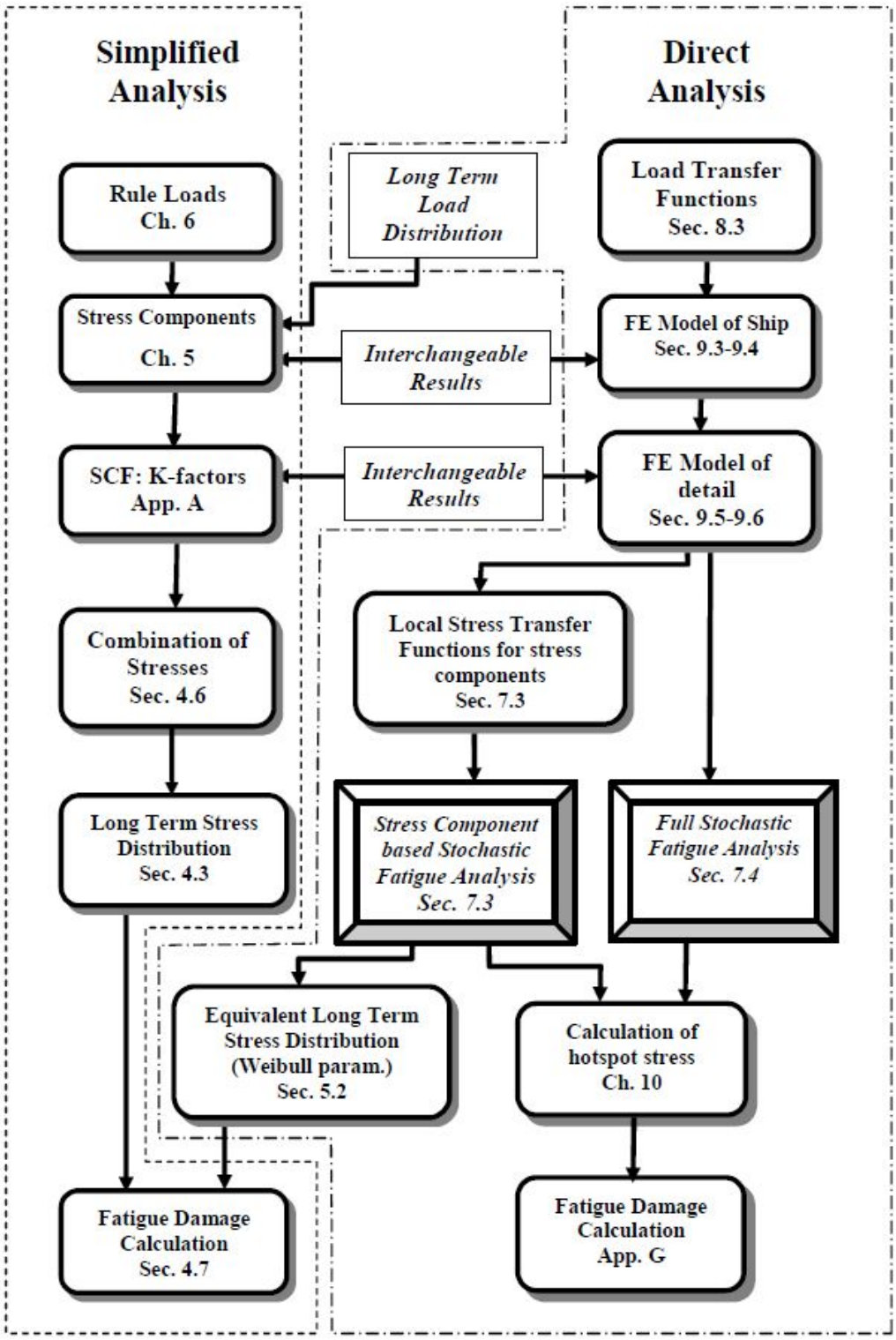

Figure A.1: Flow diagram over possible fatigue analysis procedures (DNV, 2014a).

Appendix B - Marsden Square and Scatter Diagrams

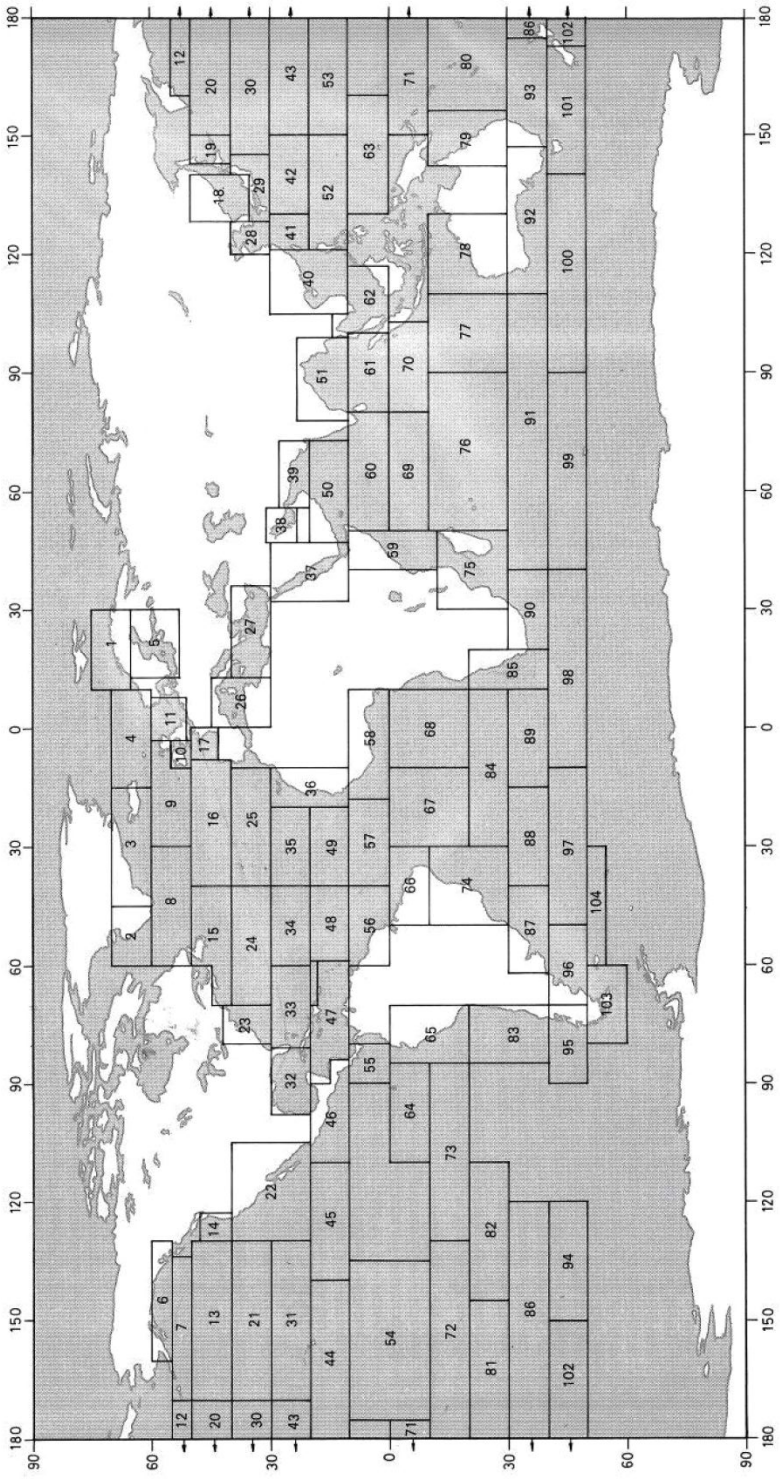

Figure A.1: Marsden Squares – Nautic zones for estimation of long-term wave distribution parameters (DNV, 2010).

Tz(s)	3.5	4.5	5.5	6.5	7.5	8.5	9.5	10.5	11.5	12.5	13.5	14.5	15.5	16.5	17.5	18.5	Sum
Hs (m)																	
0.5	1.3	133.7	865.6	1 186.0	634.2	186.3	36.9	5.6	0.7	0.1	0	0	0	0	0	0	3 050
1.5	0	29.3	986.0	4 976.0	7 738.0	5 569.7	2 375.7	703.5	160.7	30.5	5.1	0.8	0.1	0	0	0	22 575
2.5	0	2.2	197.5	2 158.8	6 230.0	7 449.5	4 860.4	2 066.0	644.5	160.2	33.7	6.3	1.1	0.2	0	0	23 810
3.5	0	0.2	34.9	695.5	3 226.5	5 675.0	5 099.1	2 838.0	1 114.4	337.7	84.3	18.2	3.5	0.6	0.1	0	19 128
4.5	0	0	6.0	196.1	1 354.3	3 288.5	3 857.5	2 685.5	1 275.2	455.1	130.9	31.9	6.9	1.3	0.2	0	13 289
5.5	0	0	1.0	51.0	498.4	1 602.9	2 372.7	2 008.3	1 126.0	463.6	150.9	41.0	9.7	2.1	0.4	0.1	8 328
6.5	0	0	0.2	12.6	167.0	690.3	1 257.9	1 268.6	825.9	386.8	140.8	42.2	10.9	2.5	0.5	0.1	4 806
7.5	0	0	0	3.0	52.1	270.1	594.4	703.2	524.9	276.7	111.7	36.7	10.2	2.5	0.6	0.1	2 586
8.5	0	0	0	0.7	15.4	97.9	255.9	350.6	296.9	174.6	77.6	27.7	8.4	2.2	0.5	0.1	1 309
9.5	0	0	0	0.2	4.3	33.2	101.9	159.9	152.2	99.2	48.3	18.7	6.1	1.7	0.4	0.1	626
10.5	0	0	0	0	1.2	10.7	37.9	67.5	71.7	51.5	27.3	11.4	4.0	1.2	0.3	0.1	285
11.5	0	0	0	0	0.3	3.3	13.3	26.6	31.4	24.7	14.2	6.4	2.4	0.7	0.2	0.1	124
12.5	0	0	0	0	0.1	1.0	4.4	9.9	12.8	11.0	6.8	3.3	1.3	0.4	0.1	0	51
13.5	0	0	0	0	0	0.3	1.4	3.5	5.0	4.6	3.1	1.6	0.7	0.2	0.1	0	21
14.5	0	0	0	0	0	0.1	0.4	1.2	1.8	1.8	1.3	0.7	0.3	0.1	0	0	8
15.5	0	0	0	0	0	0	0.1	0.4	0.6	0.7	0.5	0.3	0.1	0.1	0	0	3
16.5	0	0	0	0	0	0	0	0.1	0.2	0.2	0.2	0.1	0.1	0	0	0	1
Sum	1	165	2 091	9 280	19 922	24 879	20 870	12 898	6 245	2 479	837	247	66	16	3	1	100 000

Figure A.2: Scatter diagram for North Atlantic – zone no. 8, 9, 15 and 16 in the Marsden Squares map (DNV, 2014a) which is shown in previous figure.

Tz(s)	3.5	4.5	5.5	6.5	7.5	8.5	9.5	10.5	11.5	12.5	13.5	14.5	15.5	16.5	17.5	Sum
Hs (m)																
1.0	311	2 734	6 402	7 132	5 071	2 711	1 202	470	169	57	19	6	2	1	0	26 287
2.0	20	764	4 453	8 841	9 045	6 020	3 000	1 225	435	140	42	12	3	1	0	34 001
3.0	0	57	902	3 474	5 549	4 973	3 004	1 377	518	169	50	14	4	1	0	20 092
4.0	0	4	150	1 007	2 401	2 881	2 156	1 154	485	171	53	15	4	1	0	10 482
5.0	0	0	25	258	859	1 338	1 230	776	372	146	49	15	4	1	0	5 073
6.0	0	0	4	63	277	540	597	440	240	105	39	13	4	1	0	2 323
7.0	0	0	1	15	84	198	258	219	136	66	27	10	3	1	0	1 018
8.0	0	0	0	4	25	69	103	99	69	37	17	6	2	1	0	432
9.0	0	0	0	1	7	23	39	42	32	19	9	4	1	1	0	178
10.0	0	0	0	0	2	7	14	16	14	9	5	2	1	0	0	70
11.0	0	0	0	0	1	2	5	6	6	4	2	1	1	0	0	28
12.0	0	0	0	0	0	1	2	2	2	2	1	1	0	0	0	11
13.0	0	0	0	0	0	0	1	1	1	1	0	0	0	0	0	4
14.0	0	0	0	0	0	0	0	0	1	0	0	0	0	0	0	1
Sum	331	3 559	11 937	20 795	23 321	18 763	11 611	5 827	2 480	926	313	99	29	9	0	100 000

Figure A.3: Scatter diagram for worldwide trade (DNV, 2014a).

Appendix C - Stress Components and Stress Derivation

a) normal stress

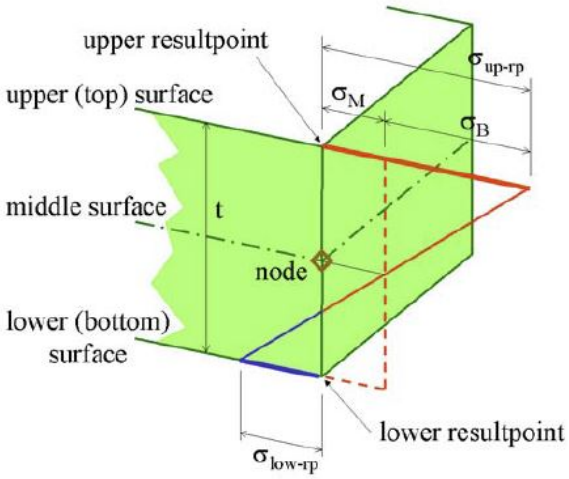

σ represents σ_x and σ_y

G-STRESS:

σ_{up-rp} is stress in upper resultpoint

σ_{low-rp} is stress in lower resultpoint

D-STRESS:

$\sigma_M = (\sigma_{up-rp}+\sigma_{low-rp})/2$ is membrane stress

$\sigma_B = (\sigma_{up-rp}-\sigma_{low-rp})/2$ is bending stress

b) membrane shear

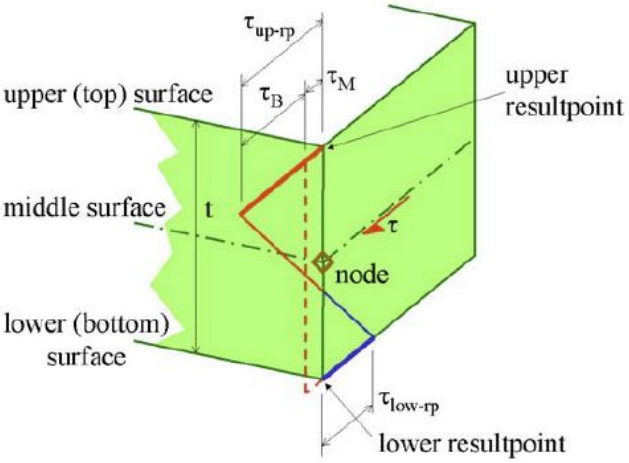

τ represents τ_{xy}

G-STRESS:

τ_{up-rp} is shear in upper resultpoint

τ_{low-rp} is shear in lower resultpoint

D-STRESS:

$\tau_M = (\tau_{up-rp}+\tau_{low-rp})/2$ is membrane shear

$\tau_B = (\tau_{up-rp}-\tau_{low-rp})/2$ is twisting shear

Figure C.1: D-STRESS for 4 node shell elements (Xtract, 2014).

a) normal stress

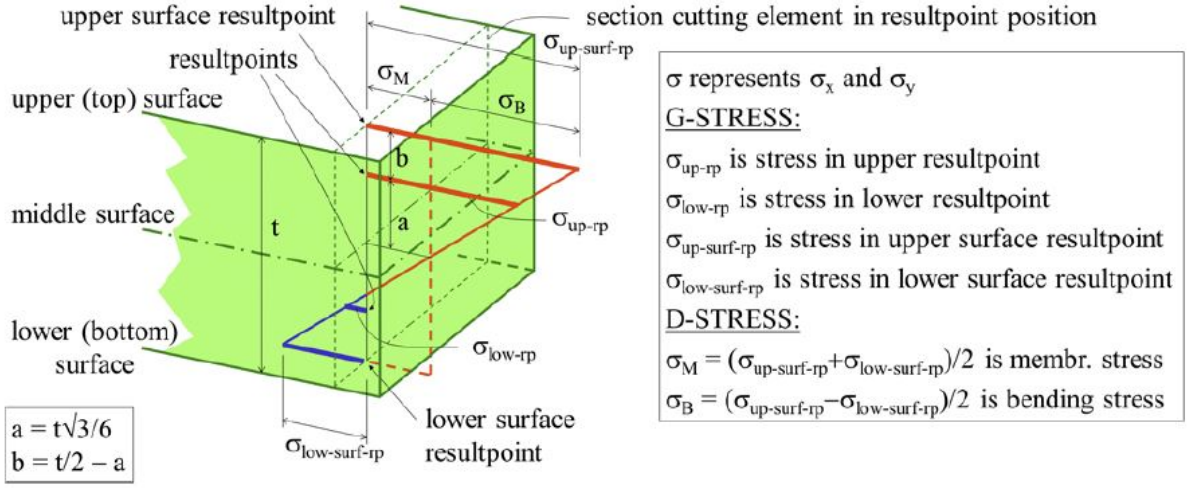

b) membrane shear

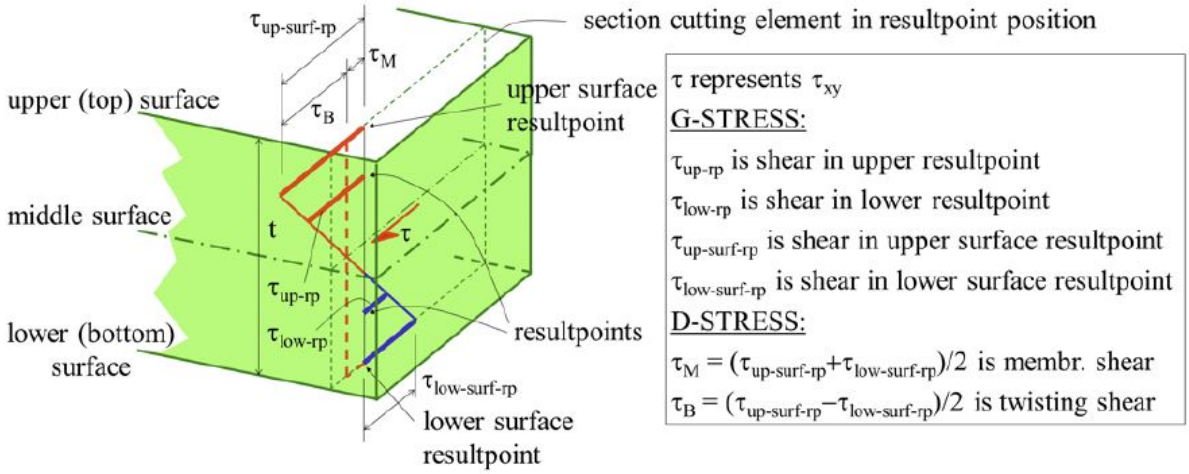

Figure C.2: D-STRESS for 8 node shell elements (Xtract, 2014).

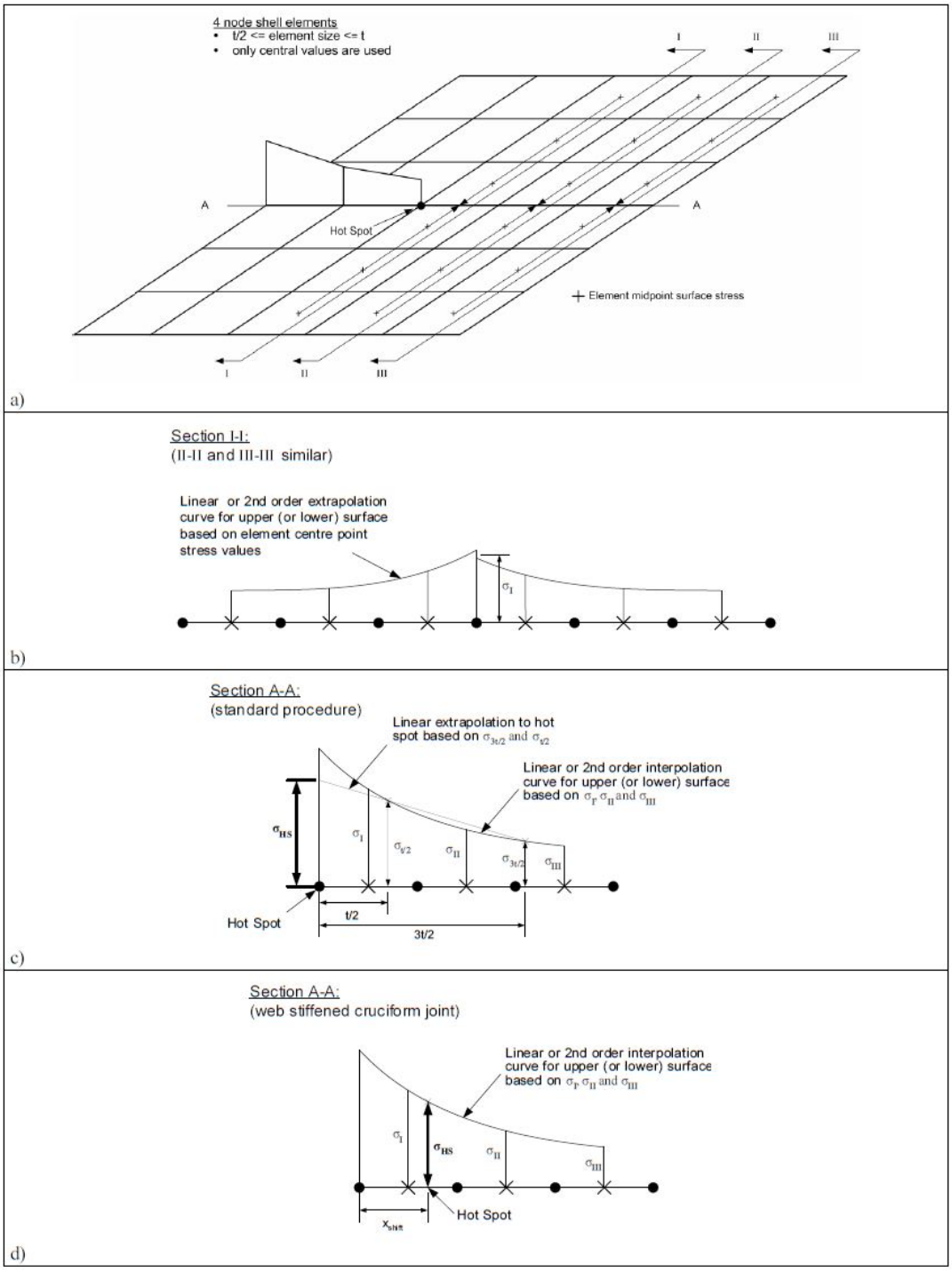

Figure C.3: Determination of stress read out points and hot spot stress for 4-node shell elements with t/2≤ element size ≤ t (DNV, 2014a).

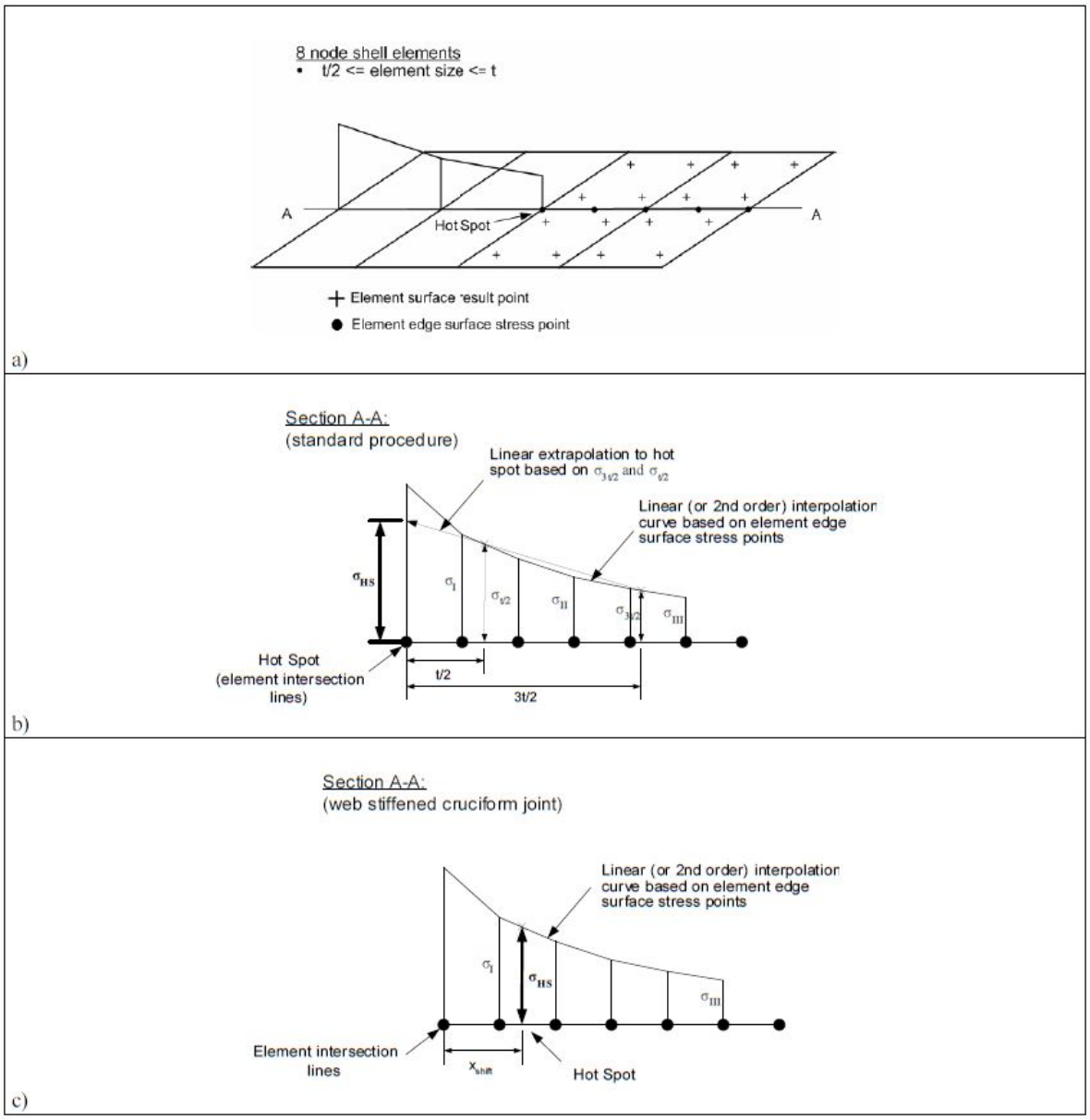

Figure C.4: Determination of stress read out points and hot spot stress for 8-node shell elements with t/2≤ element size ≤ t (DNV, 2014a).

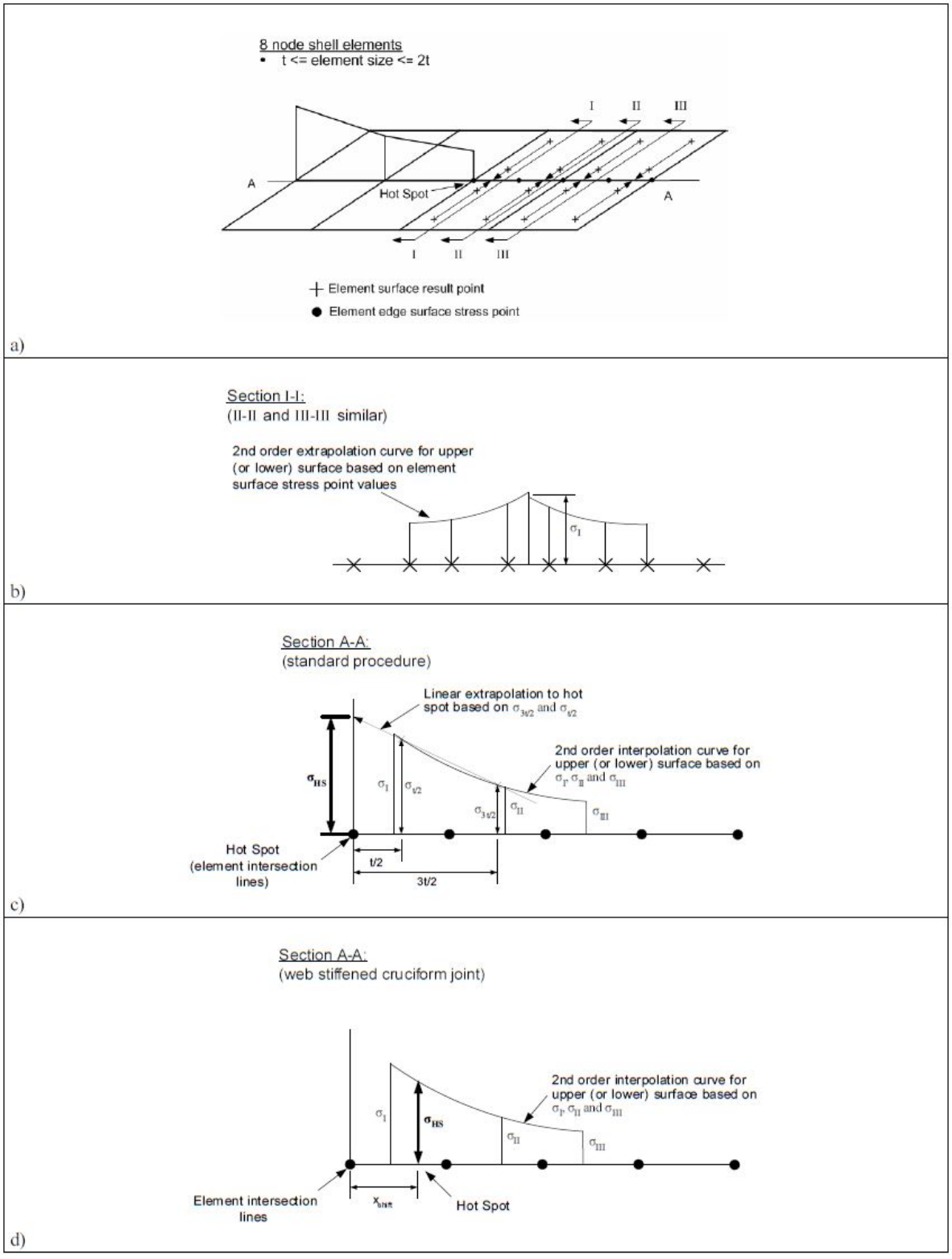

Figure C.5: Determination of stress read out points and hot spot stress for 8-node shell elements ≤t element size ≤2t (DNV, 2014a).

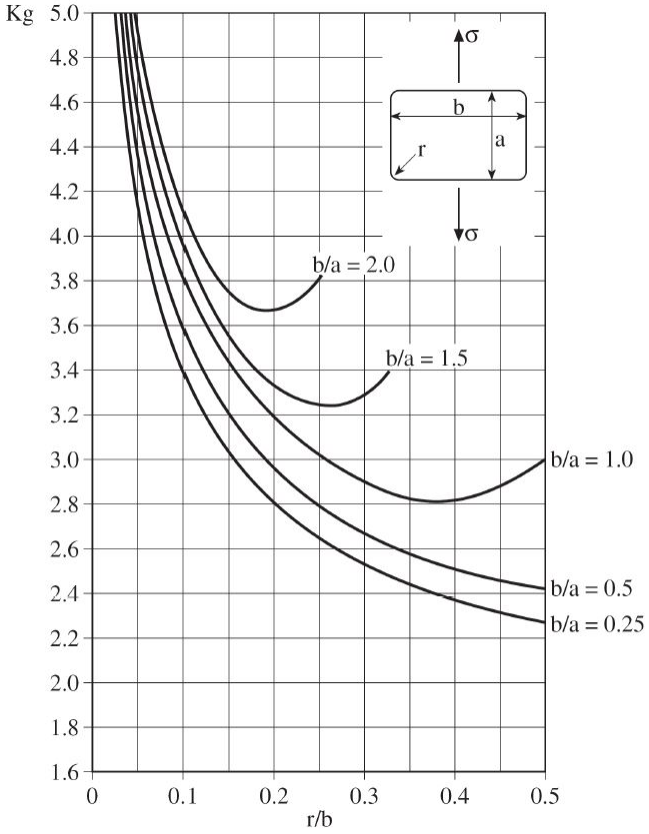

Figure C-6: Stress concentration factors for rounded rectangular holes (DNV, 2014a).

Appendix D – BCs and Load Application for FE model

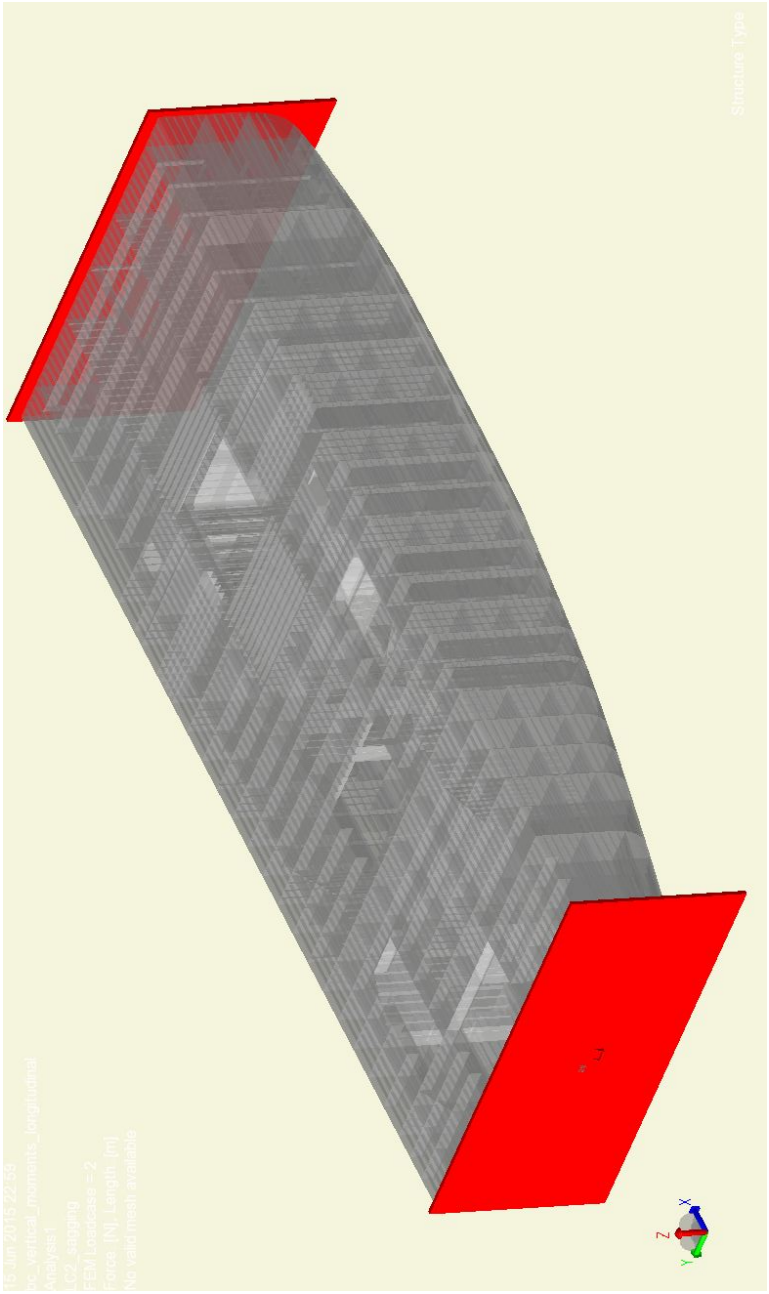

Figure D.1: Boundary condition for global loads. The red “plates” are the rigid links at the ends of the model. They are free to rotate about y-axis, and fixed in the other five dofs when vertical moments are applied. When horizontal moments are applied, the rigid links are free to rotate about z-axis, instead of the y-axis. The aft rigid link is, however, free to translate in x-direction for both cases.

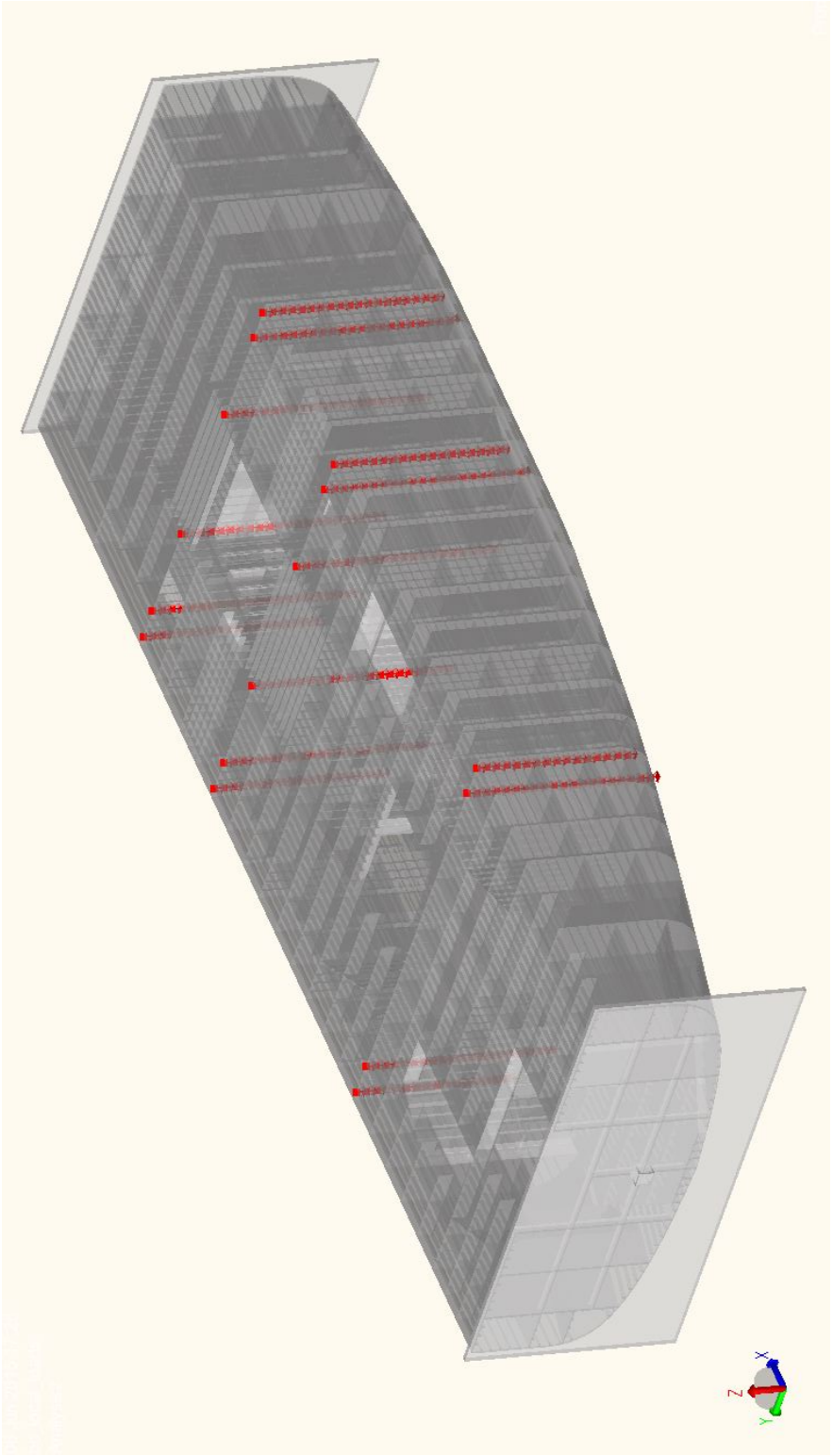

Figure D.2: Boundary conditions for application of local loads. The red lines are the vertical boundary lines formed by the intersection between longitudinal and transversal bulkheads, and they are only fixed in z direction. The grey “plates” in the ends are the rigid links, and they are fixed in all six dofs.

a) Vertical moment:

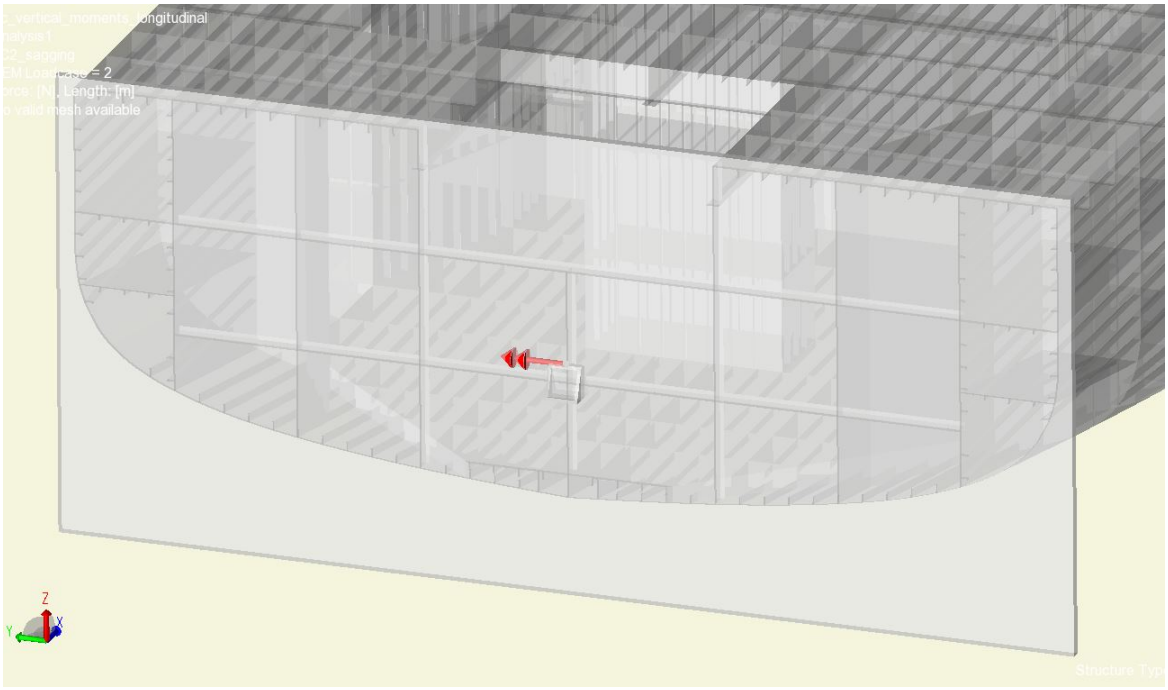

b) Horizontal moment:

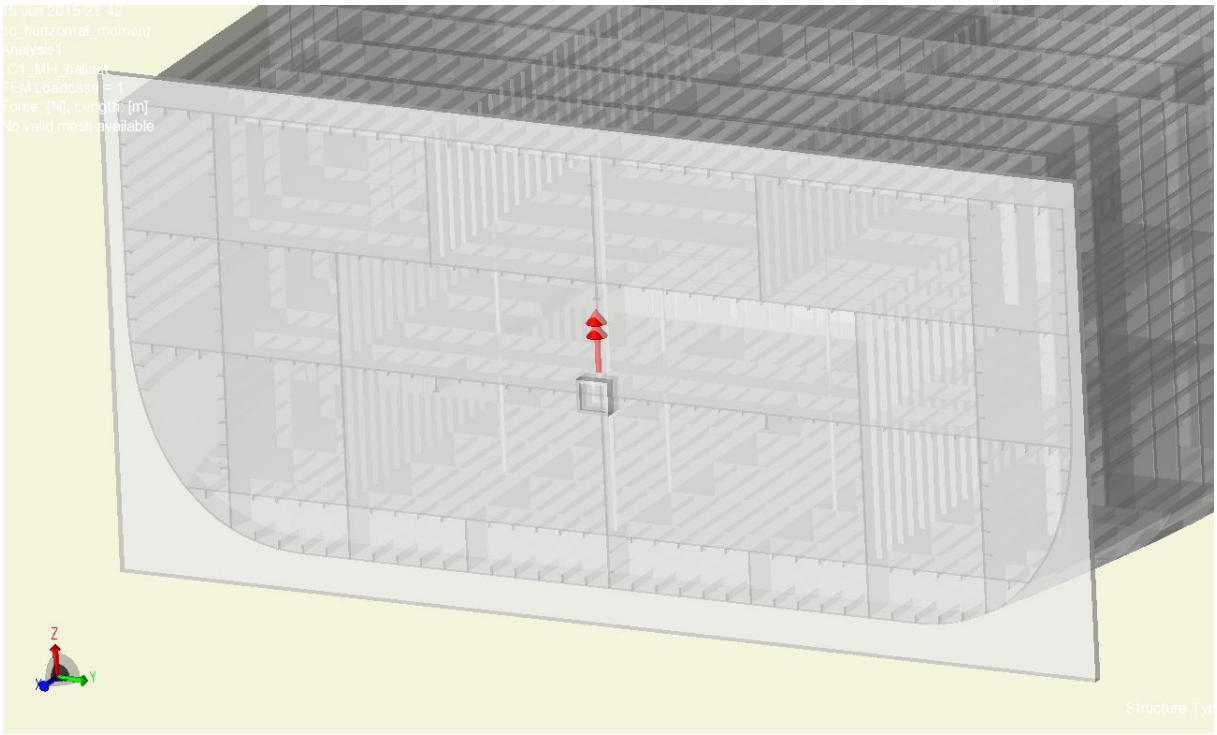

Figure D.3: Application of a) vertical wave bending moment and b) horizontal wave bending moment. The two point loads are applied at the same location as the rigid links.

a) External pressure:

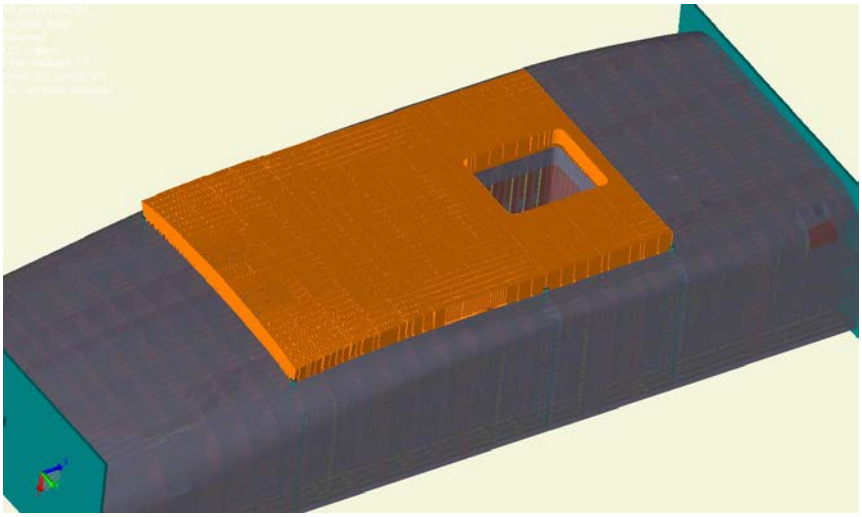

b) Ballast tanks:

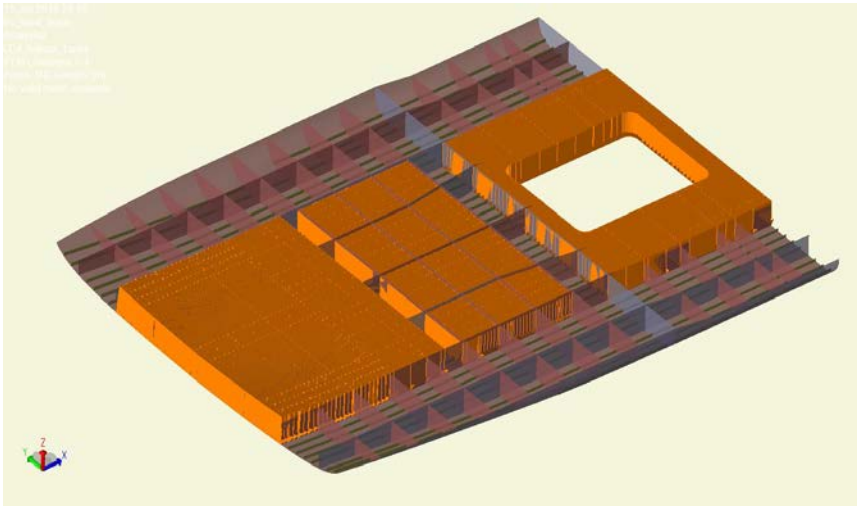

c) Inertia loads from cable drum:

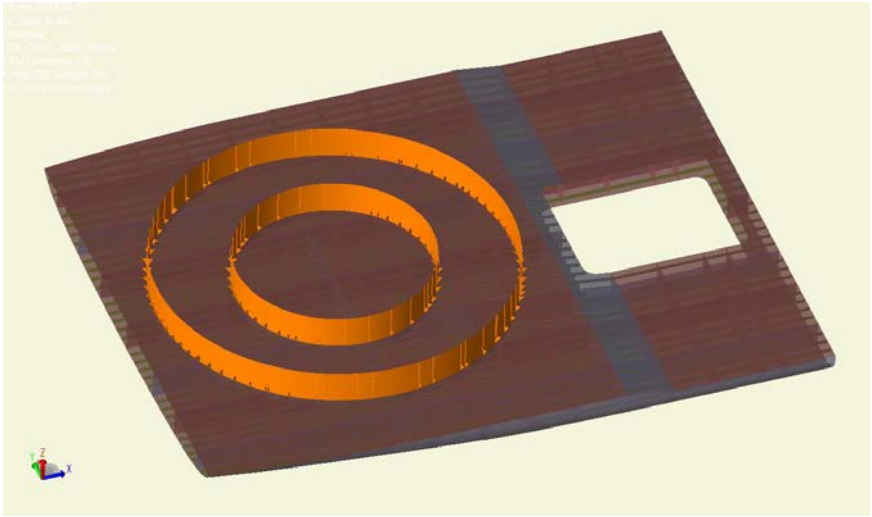

Figure D.4: Application of a) external pressure, b) internal pressure in ballast tanks and c) inertia loads (vertical acceleration) from cable drum.

Appendix E – Input

Wave induced vertical hull girder moment

The moment distributor, k_{wm}:

$$C_v = \frac{\sqrt{L}}{50} = \frac{\sqrt{134.3}}{50} = 0.23 \text{ (maximum } 0.2) \rightarrow C_v = 0.2$$

$$C_{AV} = \frac{C_v V}{\sqrt{L}} = \frac{0.2*14}{\sqrt{134.3}} = 0.242 < 0.32 \rightarrow k_{wm} = 1.0$$

Wave sagging amplitude:

$$M_{wo,s} = -0.11*0.52*1.0*8.617*134.3^2*30*(0.71+0.7) = -376\ 250 \text{ kNm}$$

Wave hogging amplitude:

$$M_{wo,h} = 0.19*0.52*1.0*8.617*134.3^2*30*0.71 = -327\ 248 \text{ kNm}$$

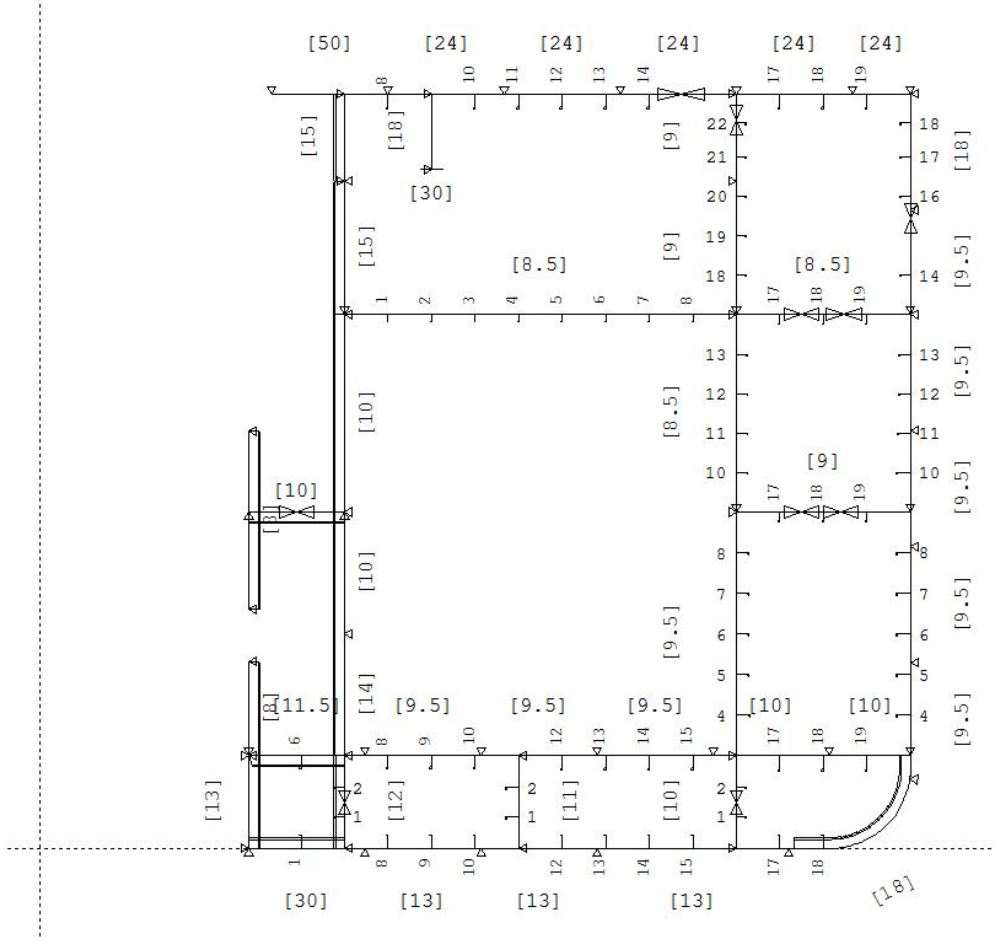

8 Cross-Sectional Data

		EFFECTIVE Cut-outs subtracted	GROSS Cut-outs disreg.
Cross sectional area of the longitudinal elements	(cm2) :	23200.5	29555.1
Position of the centroid: Ycg	(mm) :	0	0
Position of the centroid: Zcg	(mm) :	6613	6680
Moment of inertia about the horz. neutral axis, Ih	(m4) :	69.191	77.081
Moment of inertia about the vert. neutral axis, Iv	(m4) :	269.942	306.377
Product of inertia about the neutral axes, Ihv	(m4) :	0.000	0.000
SECTION MODULUS, BOTTOM (z = 0 mm)	(m3) :	10.462	11.539
SECTION MODULUS, DECK LINE (z = 13000 mm)	(m3) :	10.833	12.196
SECTION MODULUS, AT SIDE (y = 15000 mm)	(m3) :	17.996	20.425
First moment of the area above the neutral axis, S	(cm3) :	6640234.9	6942995.6
I/S	(cm) :	1042	1110

DESCRIPTION:

Gross — Results based on the given scantlings.

Effective — Results based on the effective cross-sectional area, as follows:
Possible cut-outs are subtracted (plates only).
The area of plates and stiffeners are multiplied by the given bending efficiency for the related panel.

Figure E.1: #89 in Nauticus Hull Section Scantlings.

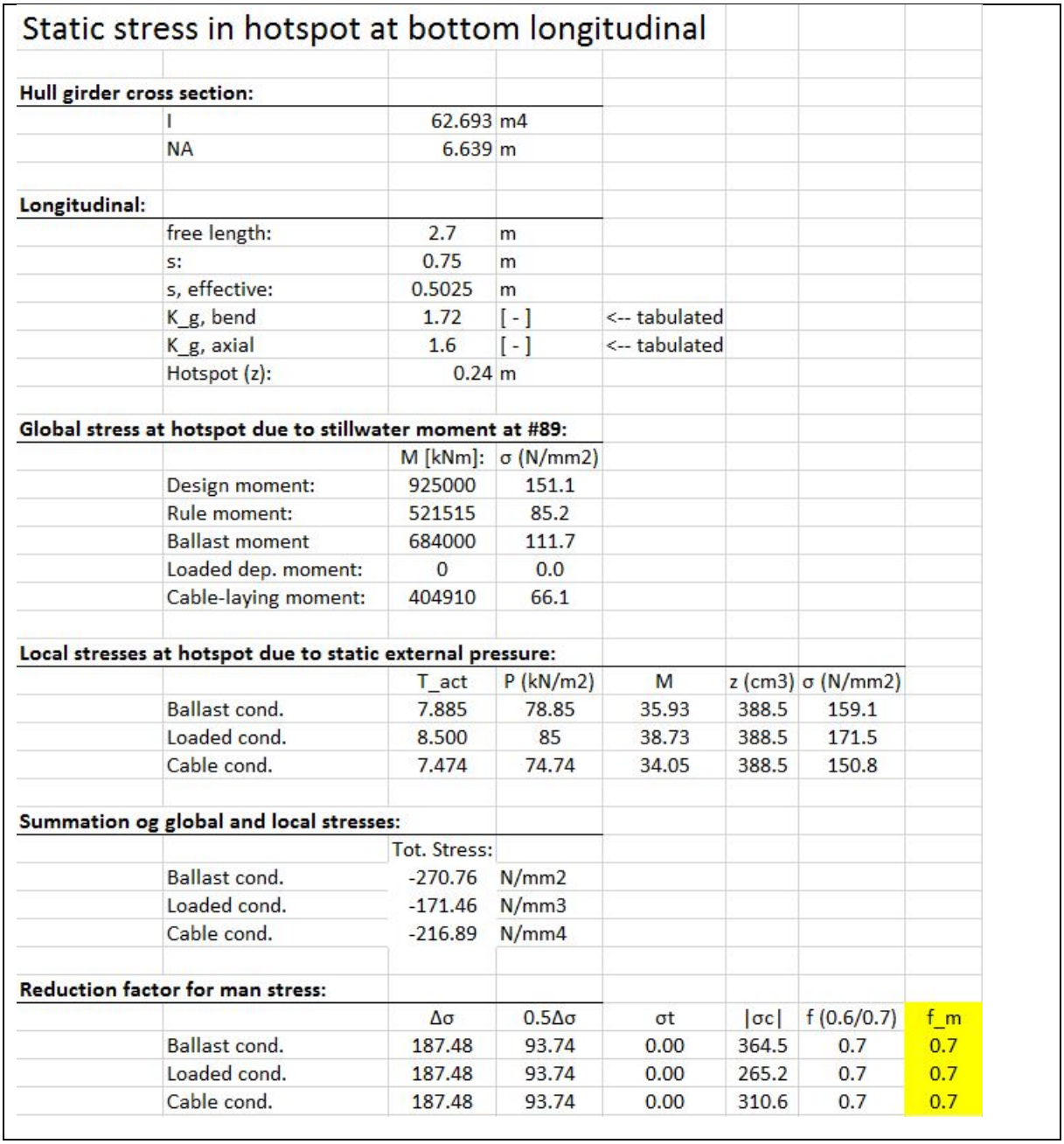

Static stress in hotspot at bottom longitudinal

Hull girder cross section:							
	I	62.693	m4				
	NA	6.639	m				
Longitudinal:							
	free length:	2.7	m				
	s:	0.75	m				
	s, effective:	0.5025	m				
	K_g, bend	1.72	[-]	<-- tabulated			
	K_g, axial	1.6	[-]	<-- tabulated			
	Hotspot (z):	0.24	m				
Global stress at hotspot due to stillwater moment at #89:							
		M [kNm]:	σ (N/mm2)				
	Design moment:	925000	151.1				
	Rule moment:	521515	85.2				
	Ballast moment	684000	111.7				
	Loaded dep. moment:	0	0.0				
	Cable-laying moment:	404910	66.1				
Local stresses at hotspot due to static external pressure:							
		T_act	P (kN/m2)	M	z (cm3)	σ (N/mm2)	
	Ballast cond.	7.885	78.85	35.93	388.5	159.1	
	Loaded cond.	8.500	85	38.73	388.5	171.5	
	Cable cond.	7.474	74.74	34.05	388.5	150.8	
Summation og global and local stresses:							
		Tot. Stress:					
	Ballast cond.	-270.76	N/mm2				
	Loaded cond.	-171.46	N/mm3				
	Cable cond.	-216.89	N/mm4				
Reduction factor for man stress:							
		Δσ	0.5Δσ	σt	|σc|	f (0.6/0.7)	f_m
	Ballast cond.	187.48	93.74	0.00	364.5	0.7	0.7
	Loaded cond.	187.48	93.74	0.00	265.2	0.7	0.7
	Cable cond.	187.48	93.74	0.00	310.6	0.7	0.7

Figure E.2: Calculation of the reduction factor due to mean stress effect. f=0.7 is used since the detail in bottom is welded connection. Calculation of static stresses is also included.

			X		Frame
Shear force (min)	-2029.2	t	65.00	m	93.71
Shear force (max)	2506.3	t	15.50	m	23.00
Max. rel. shear force	88.9	%	13.00	m	19.43
Sagging moment	-0.2	tm	137.41	m	205.35
Hogging moment	68400.1	tm	47.84	m	69.21
Max. rel. bending moment	79.9	%	21.25	m	31.21

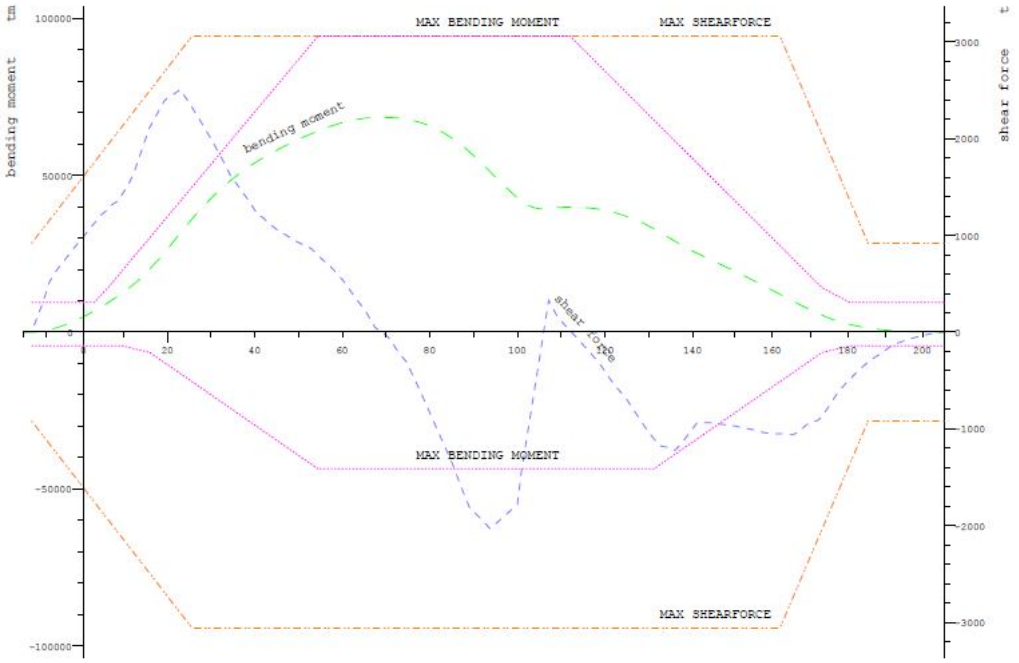

Figure E.3: Static global forces in ballast condition.

			X		Frame
Shear force (min)	-1739.0	t	46.60	m	67.43
Shear force (max)	2890.3	t	54.60	m	78.86
Max. rel. shear force	94.5	%	54.60	m	78.86
Sagging moment	-4032.1	tm	49.60	m	71.71
Hogging moment	46175.8	tm	84.31	m	121.30
Max. rel. bending moment	70.3	%	109.24	m	158.40

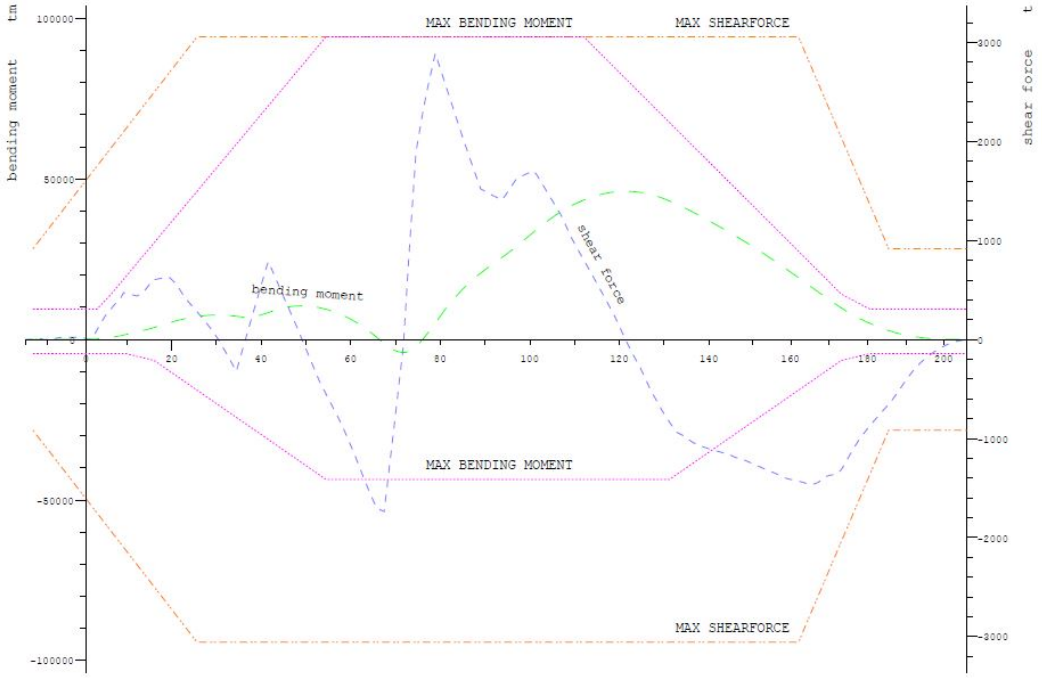

Figure E.4: Static global forces in loaded condition.

			X		Frame
Shear force (min)	-1225.0	t	109.00	m	158.00
Shear force (max)	1090.7	t	13.00	m	19.43
Max. rel. shear force	48.2	%	-0.60	m	-1.00
Sagging moment	-				
Hogging moment	40491.1	tm	50.00	m	72.29
Max. rel. bending moment	53.8	%	99.68	m	143.25

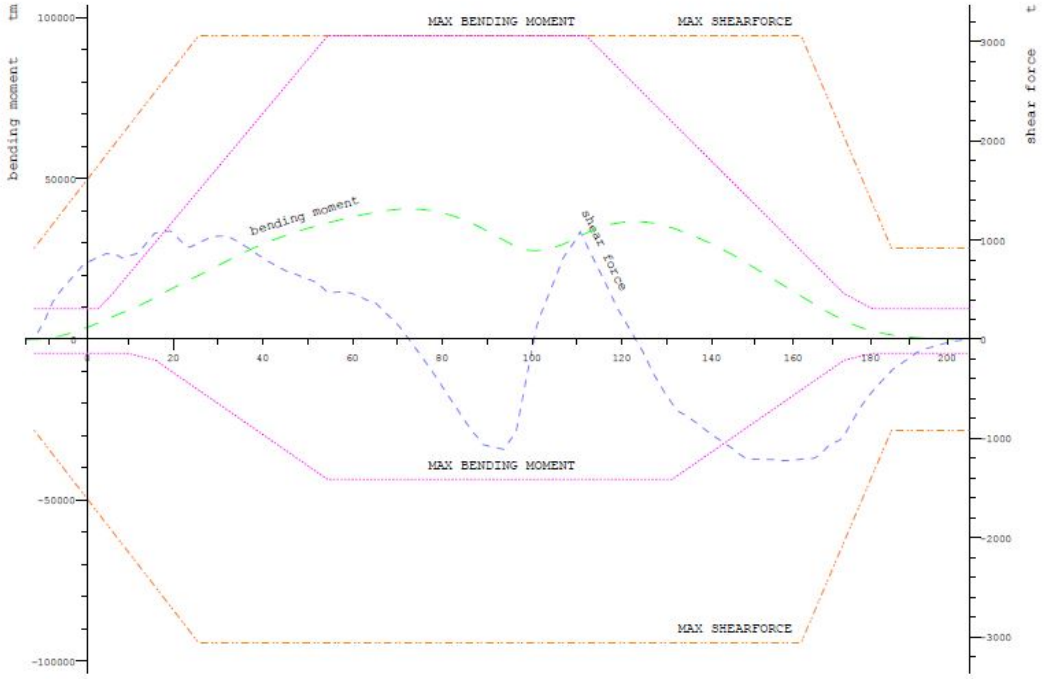

Figure E.5: Static global forces in cable-laying condition.

Appendix F – Result FEA

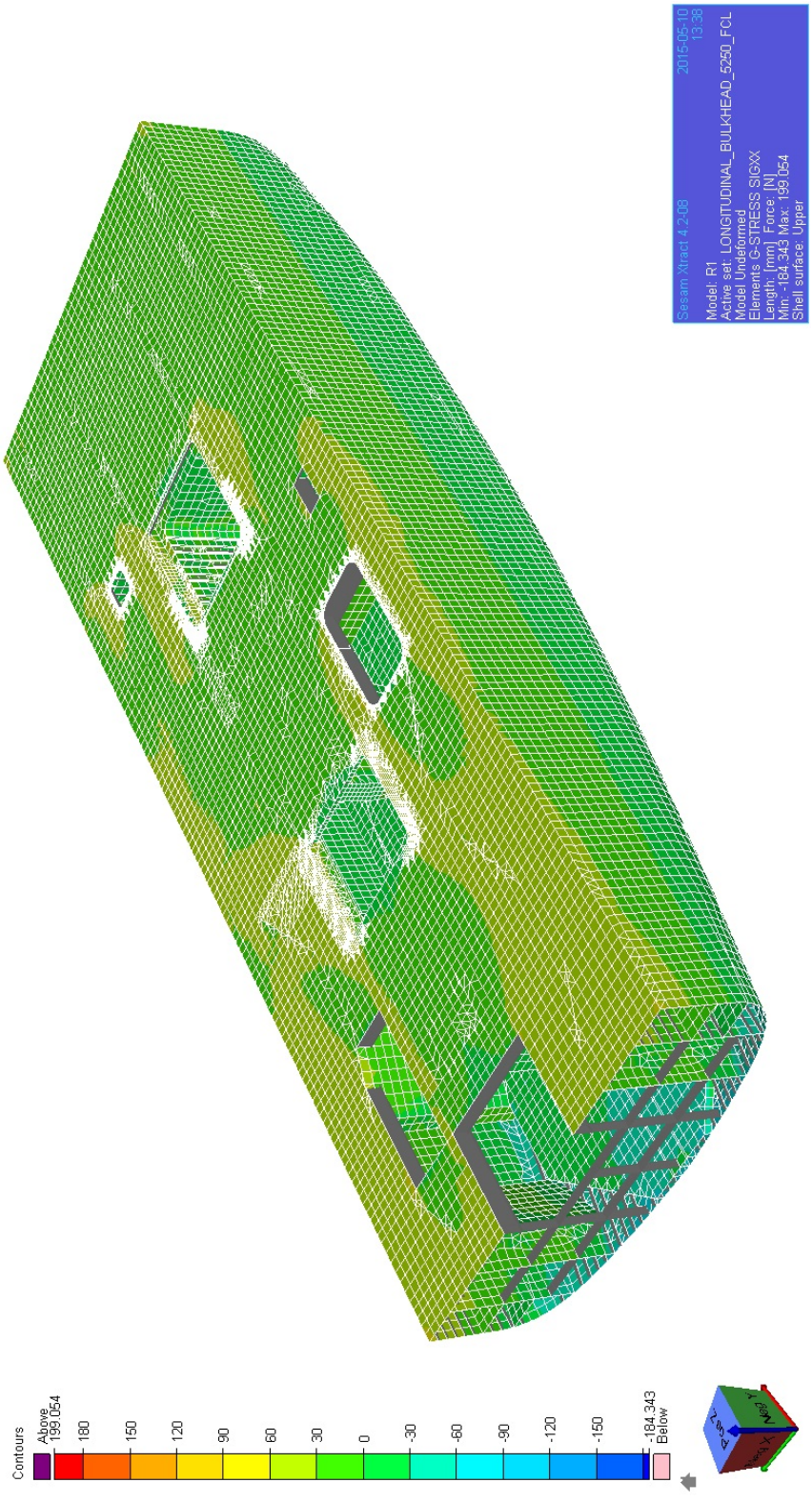

Figure F.1: Global mesh density (700 x 700 mm) for 8 node shell elements. Contour of general stress SIGXX, is shown.

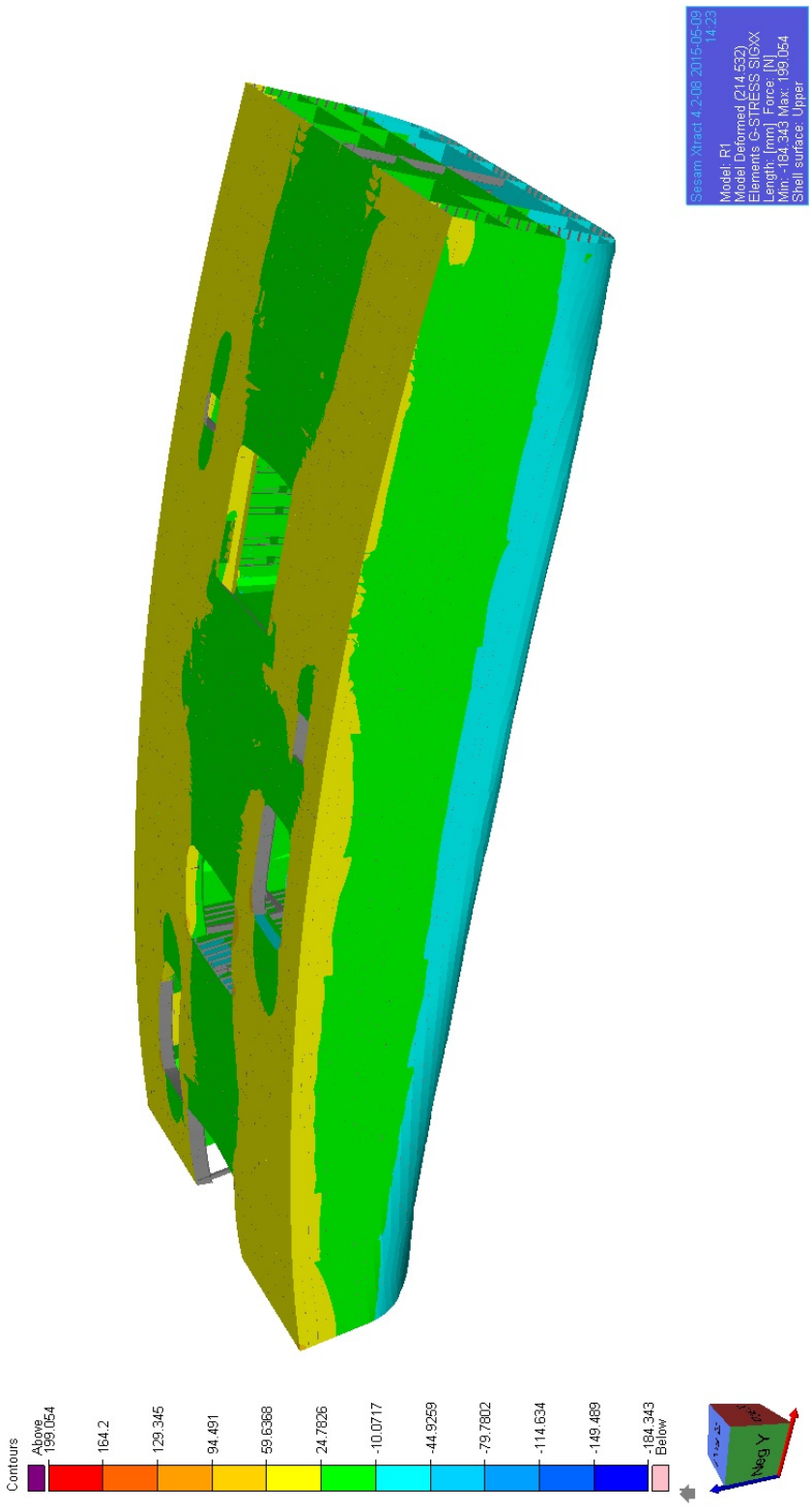

Figure F.2: Contour of the longitudinal stresses, SIGXX, in hogging condition, including hull deformation.

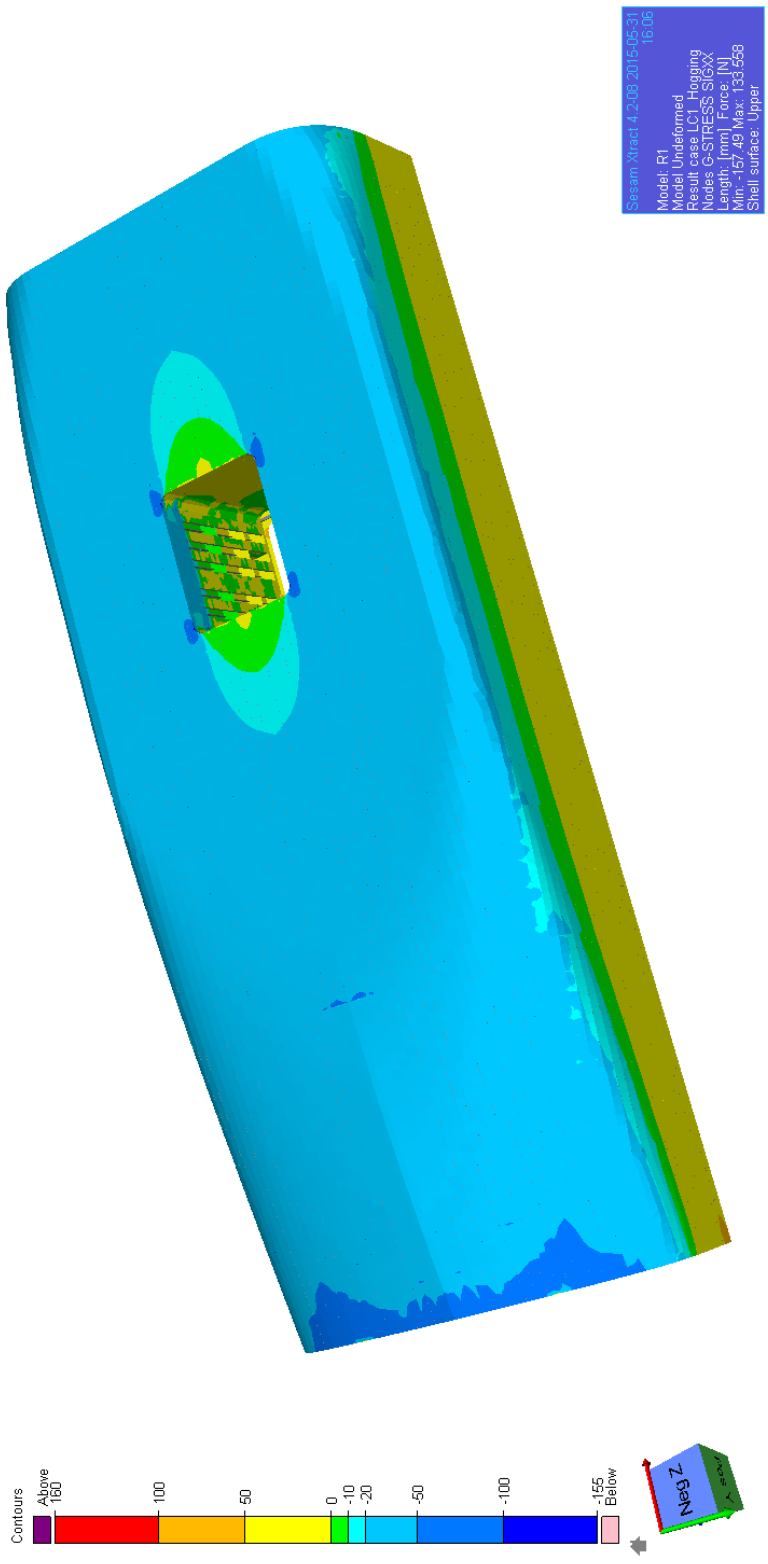

Figure F.3: Contour of the longitudinal stress, SIGXX, in the bottom.

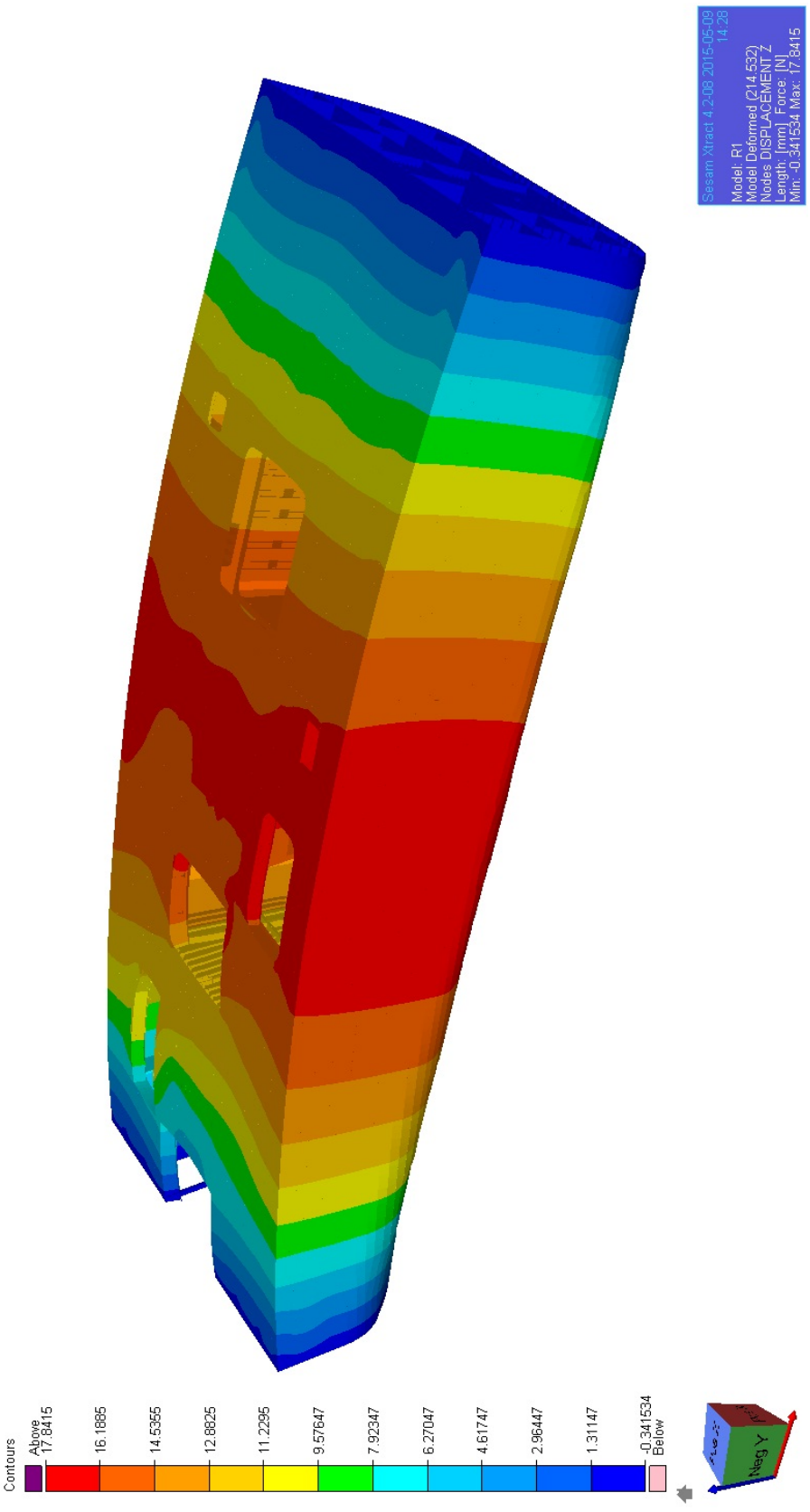

Figure F.4: Contour of vertical hull girder displacement in hogging condition, including deformation of the hull.

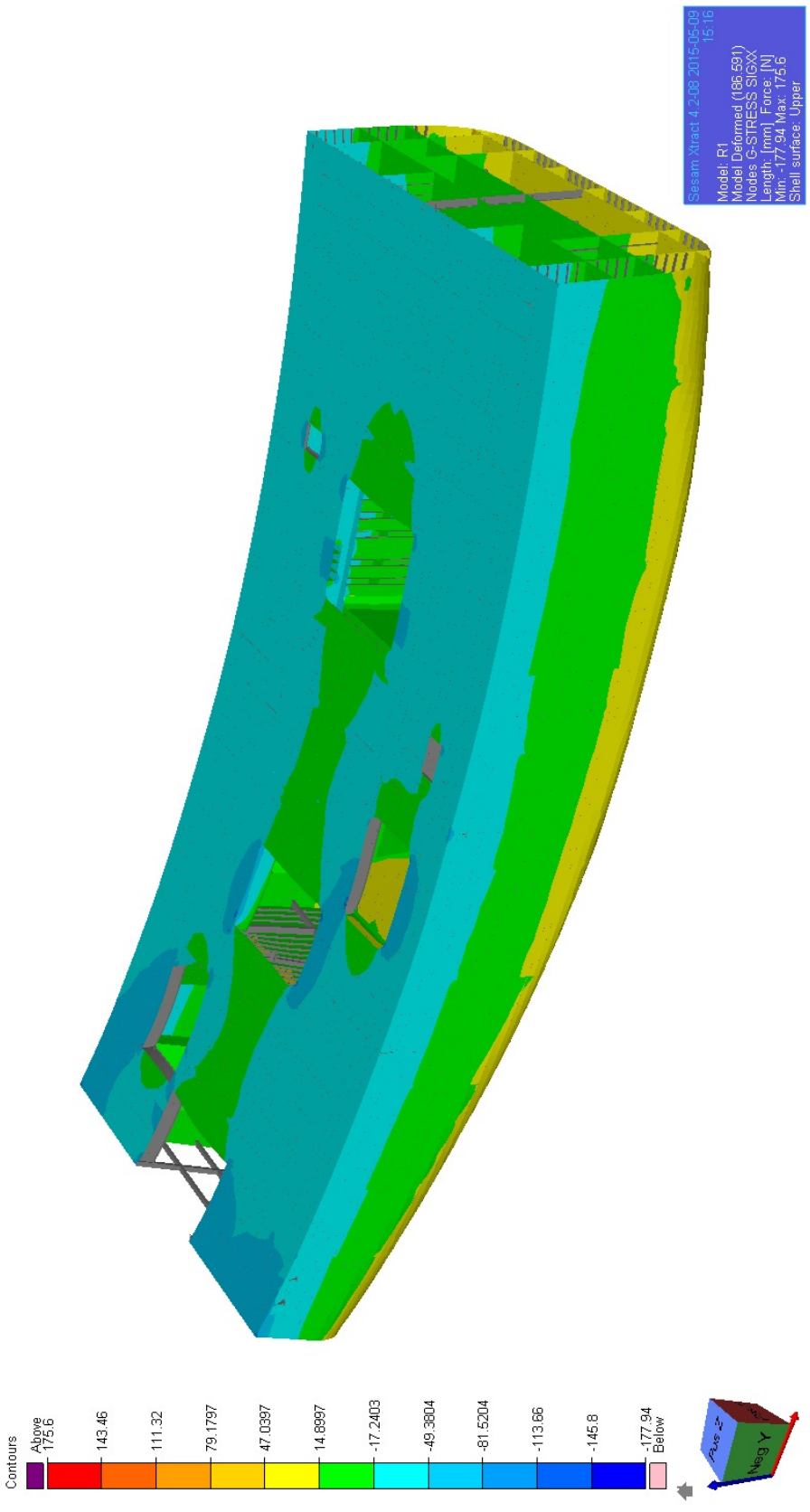

Figure F-5: Longitudinal stresses, SIGXX, in sagging condition, including hull deformation.

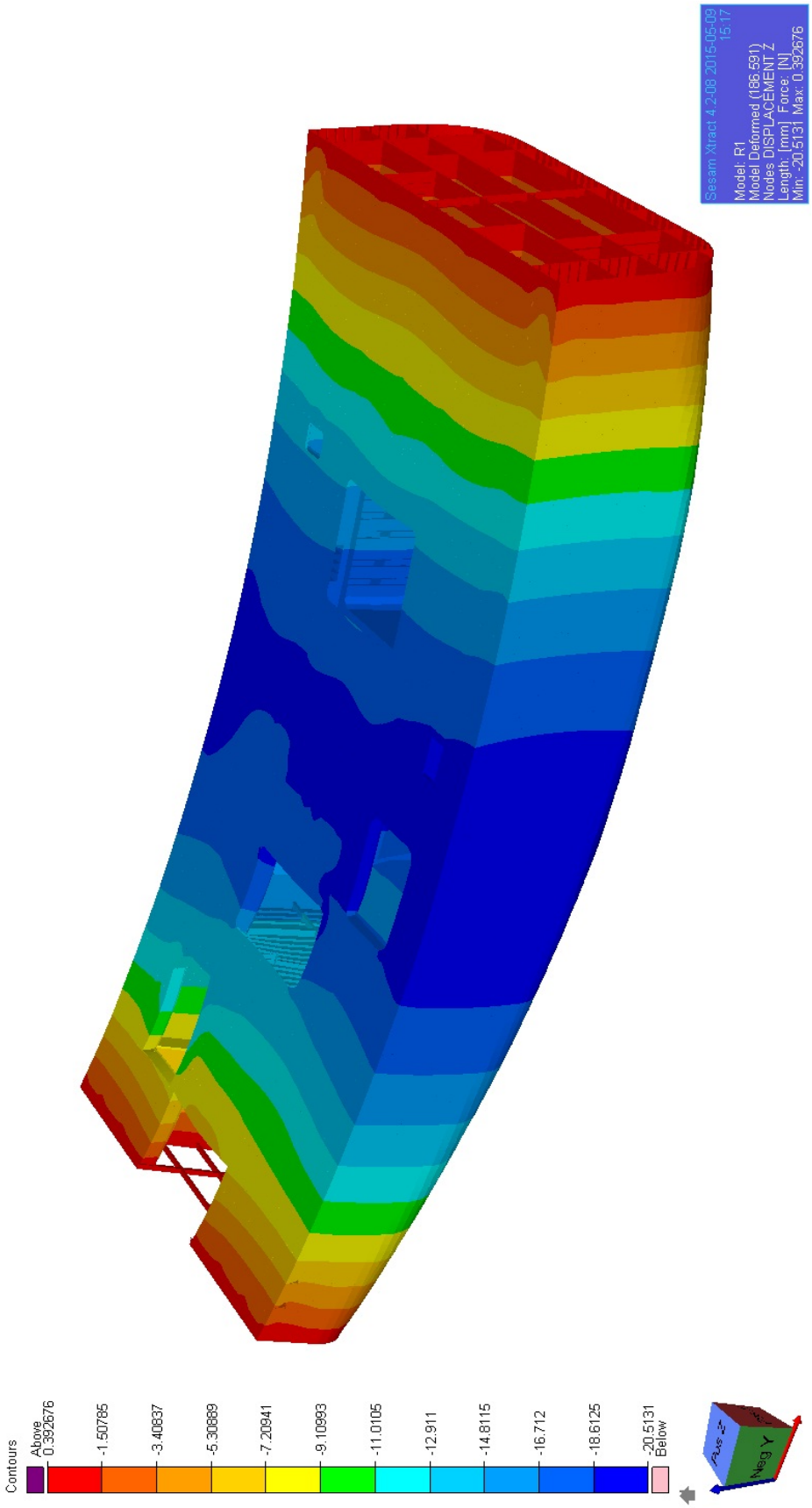

Figure F-6: vertical displacement of the hull girder due to vertical sagging moment, including hull deformation.

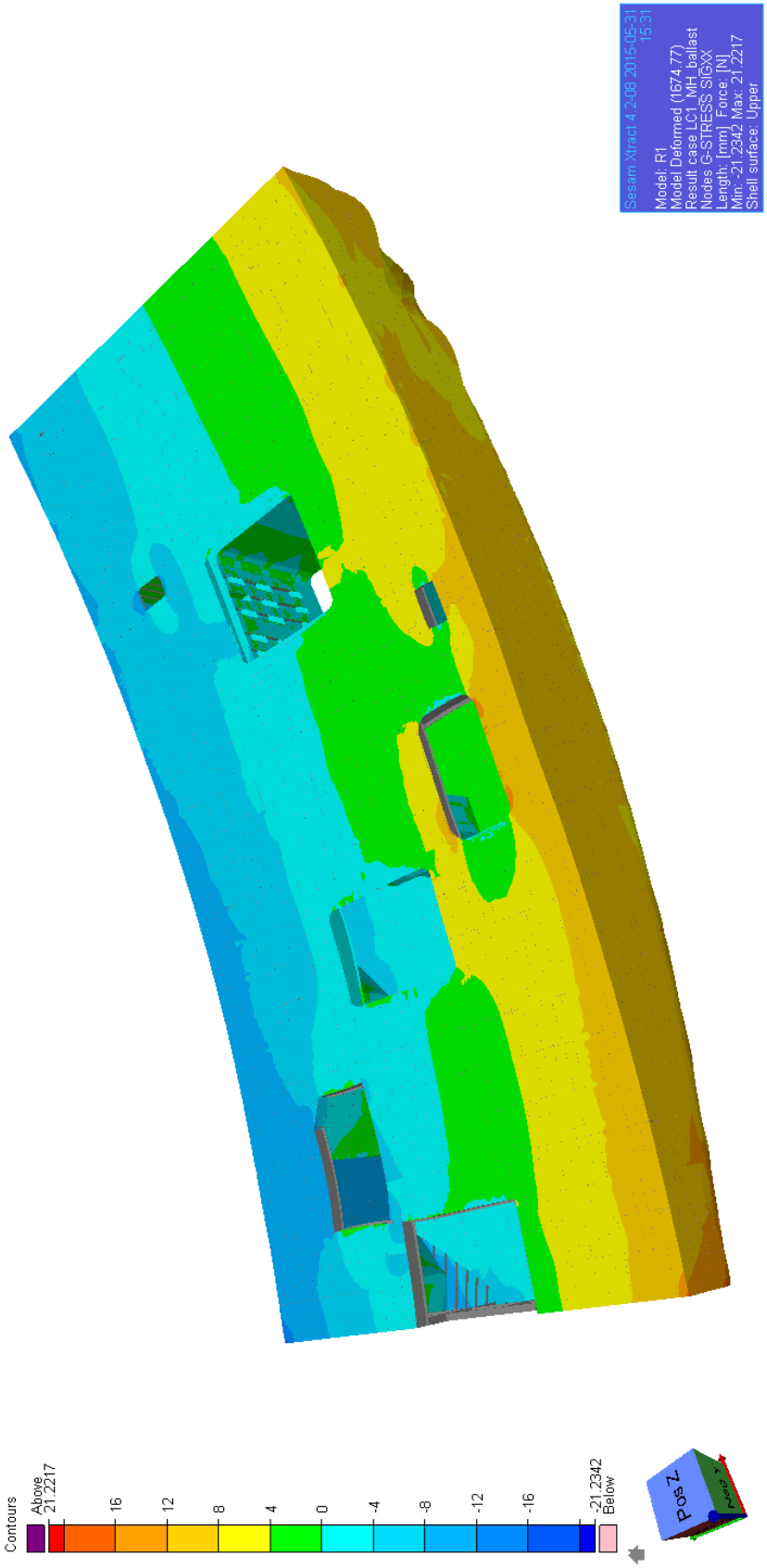

Figure F-7: Contour of longitudinal stresses, SIGXX, in the hull girder due to horizontal bending moment.

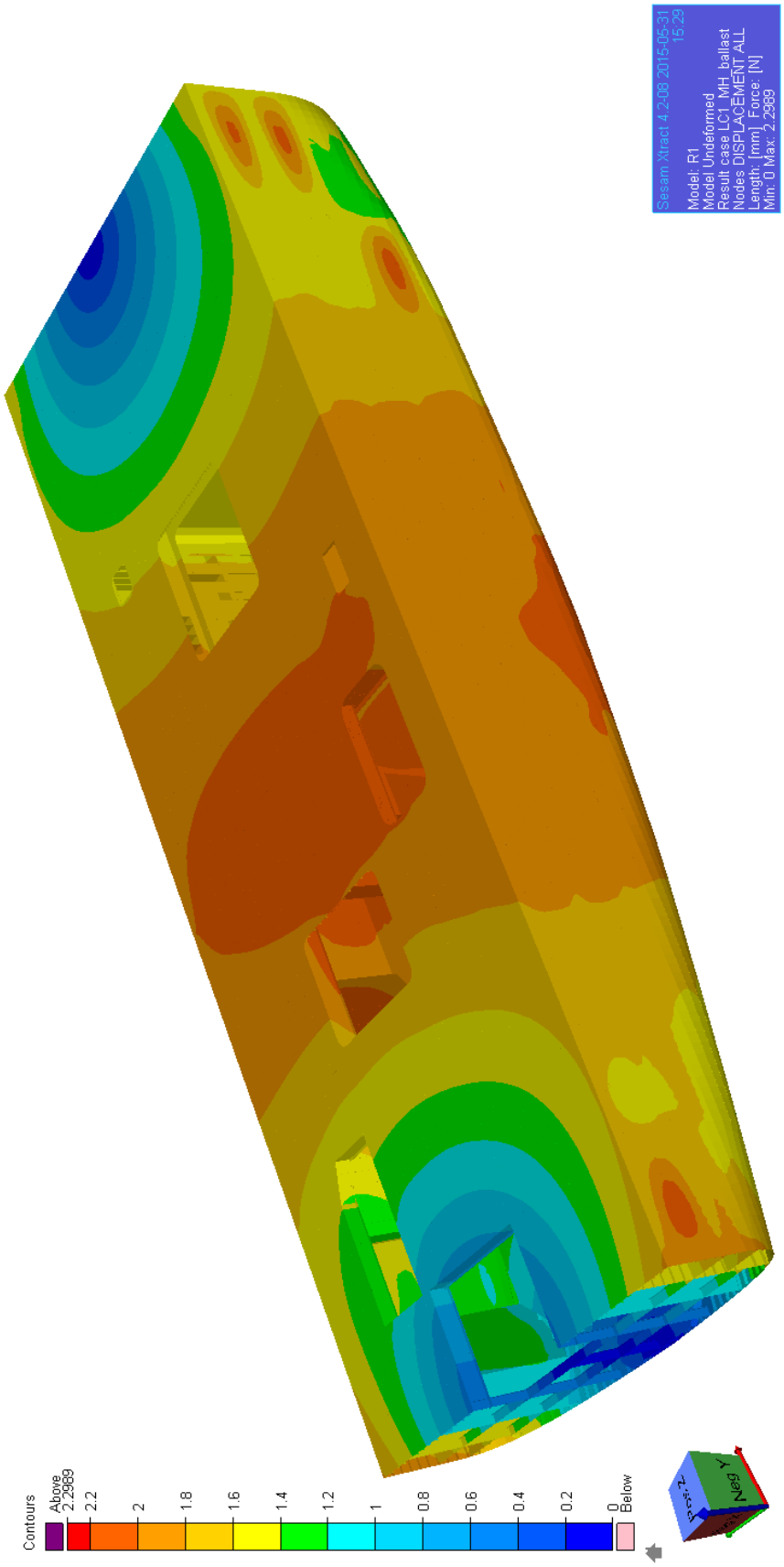

Figure F.8: Horzontal displacement of the hull girder due to horizontal bending moment, including hull deformation.

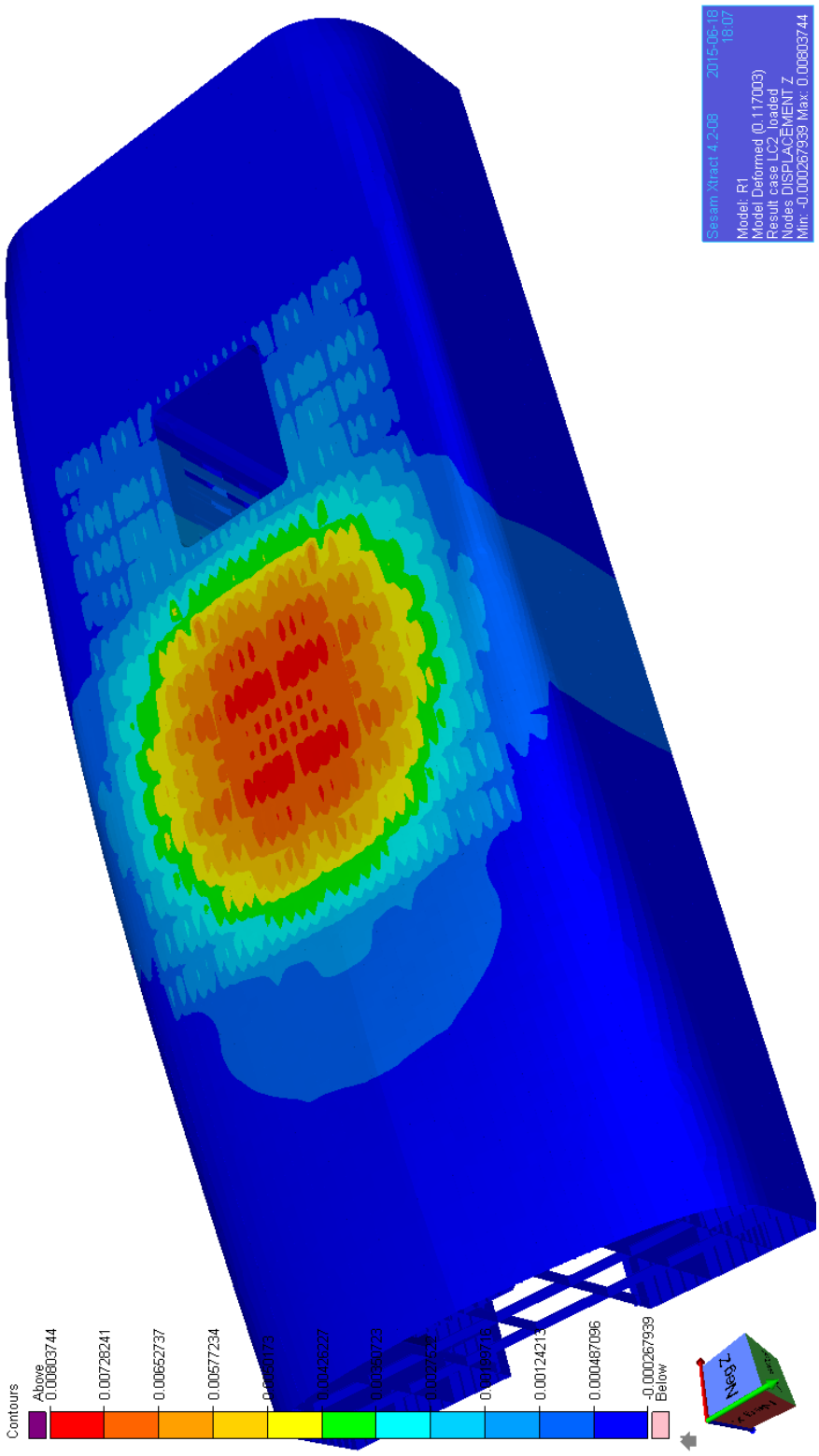

Figure F.9: Deformation of bottom when external sea pressure in ballast, is applied.

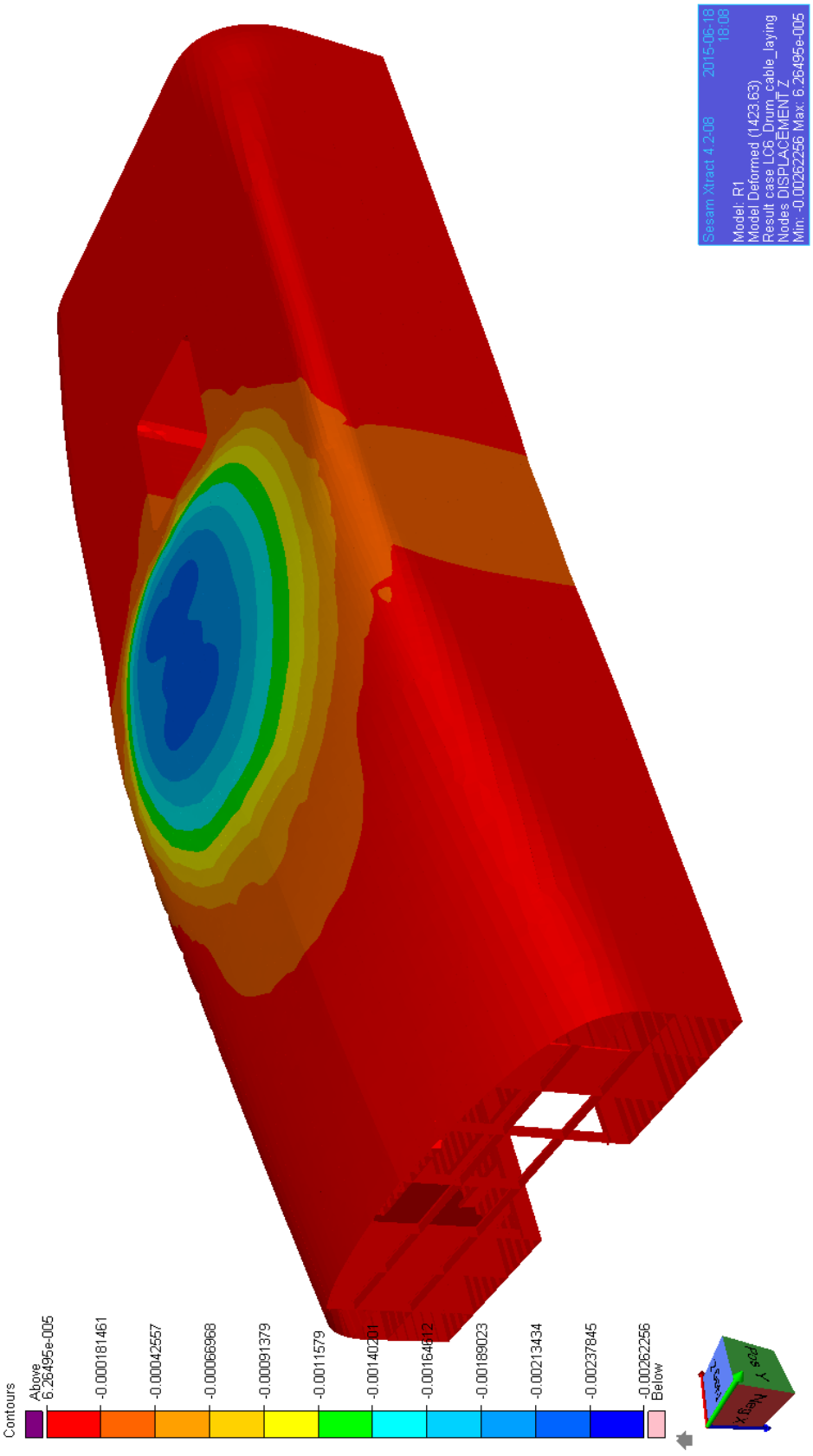

Figure F.10: Deformation of bottom when inertia loads from cable drum, is applied.

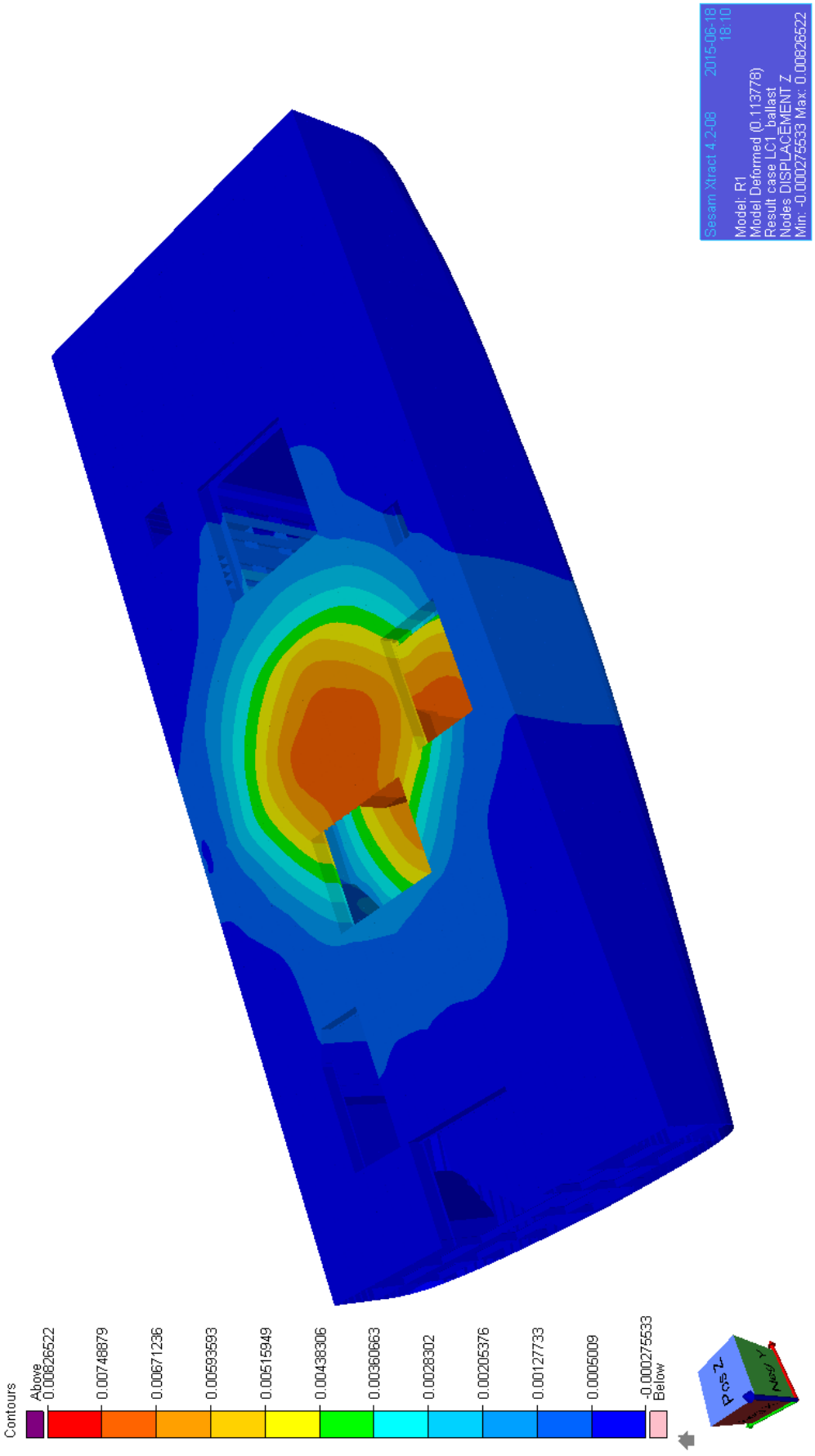

Figure F.11: Deformation in main deck due to sea pressure in ballast condition.

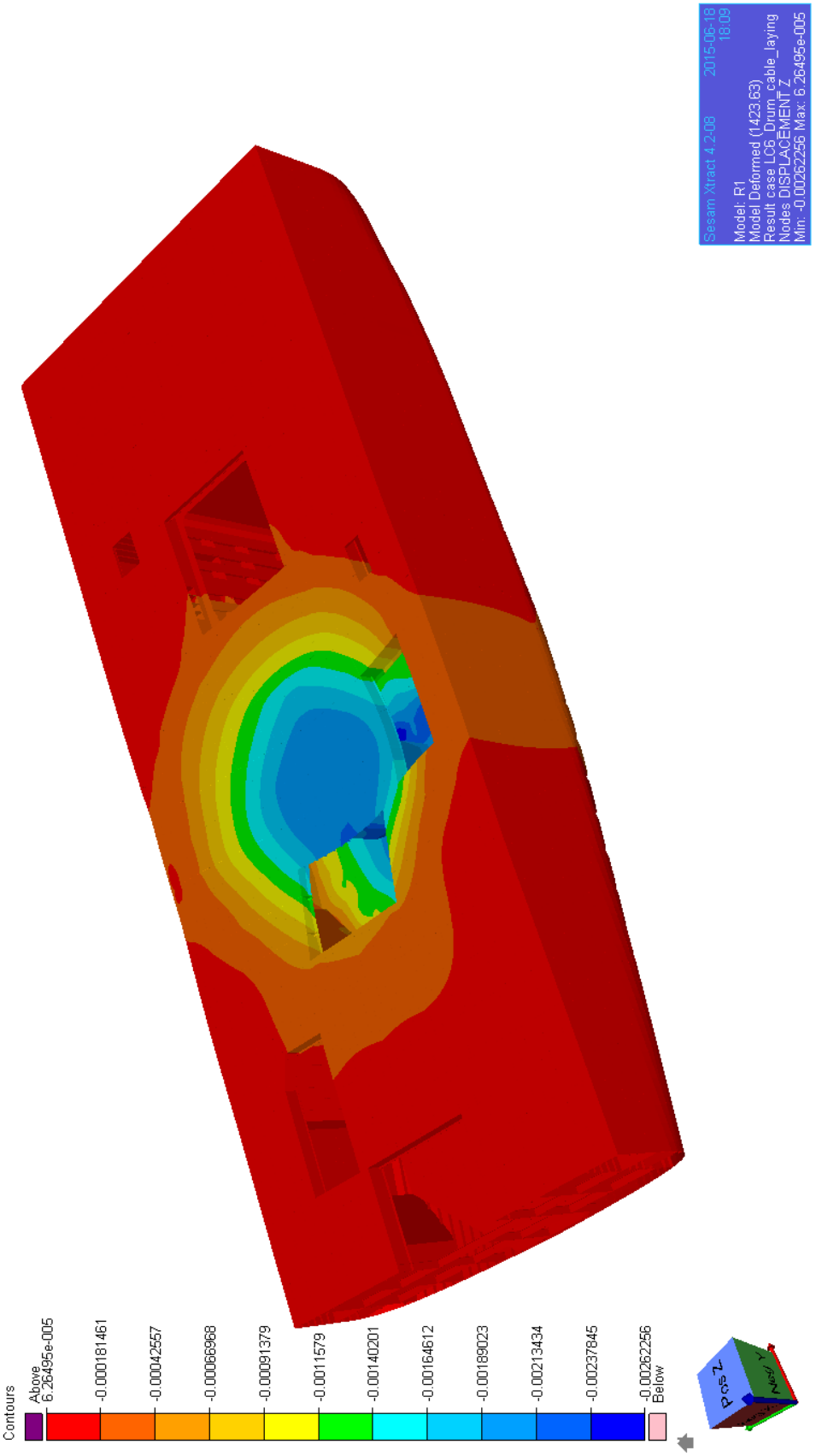

Figure F.12: Deformation in main deck when inertia loads from cable drum are applied.

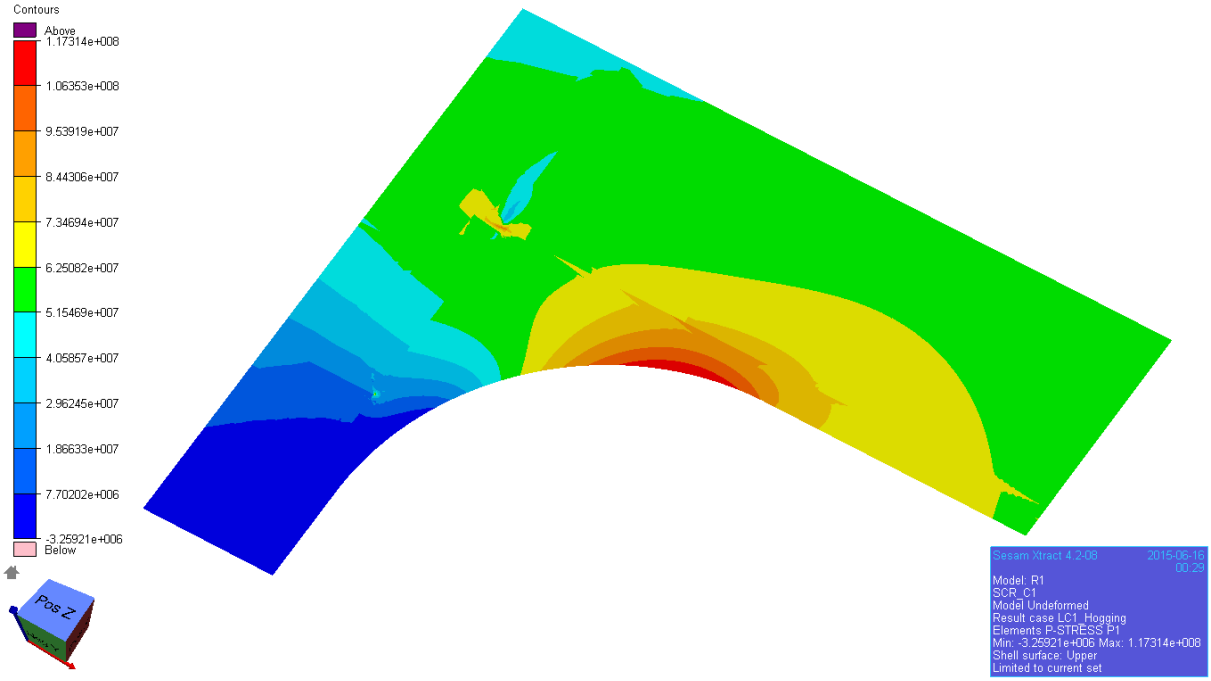

Figure F.13: Contour of Principal stress P1 for aft portside corner of the loading hatch opening in hogging condition. 8-node shell element and mesh size t x t.

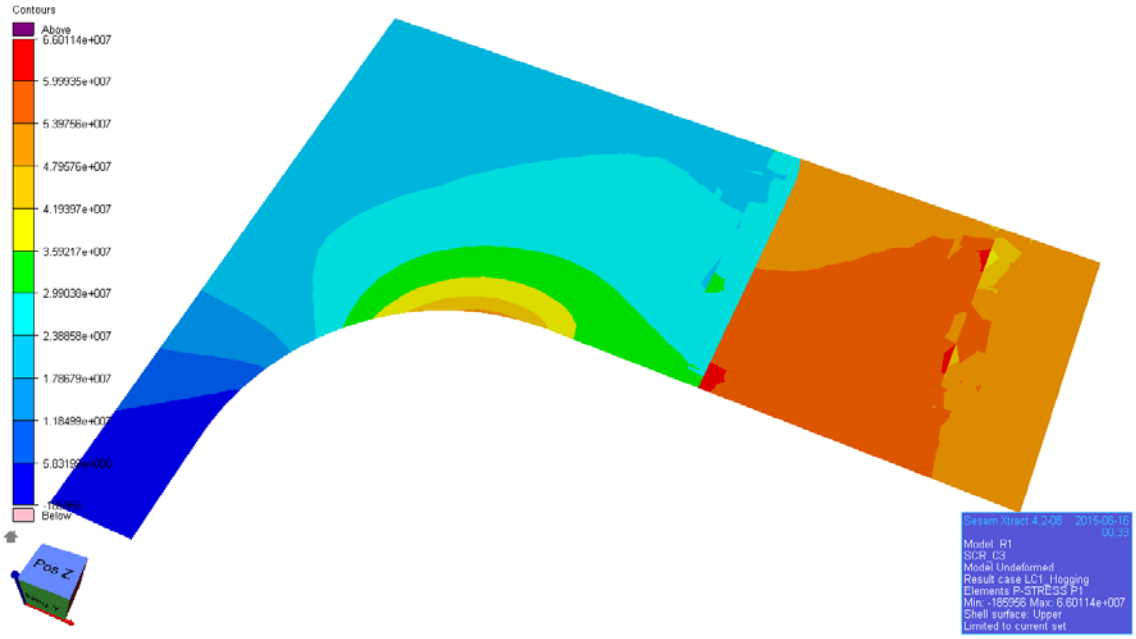

Figure F-14: Contour of Principal stress P1 for the aft portside corner of the moonpool opening in hogging condition. 8-node shell element and mesh size 50 x 50. The red/orange area is the main deck plate (t=24 mm), while the blue area is the insert plate (t=50 mm).

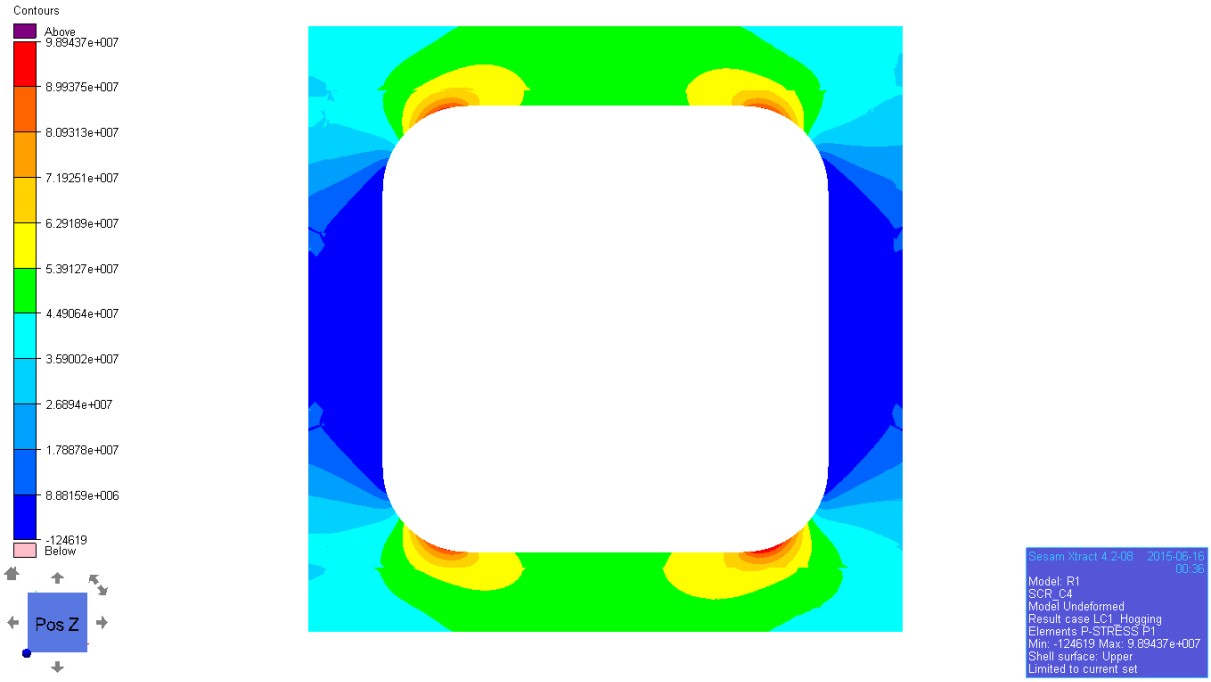

Figure F.15: Contour of Principal stress P1 for the flush hatch opening in hogging condition. 8-node shell element and mesh size t x t.

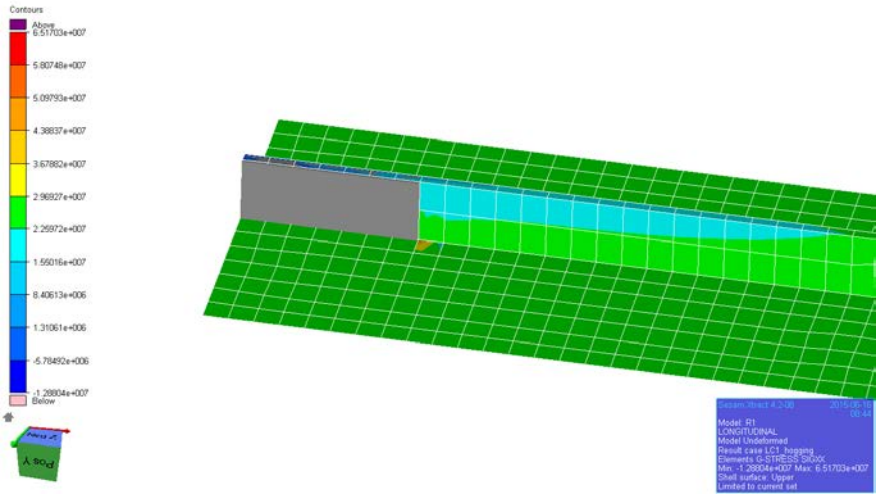

Figure F-16: Overlapping =700mm between beam element and shell elements of longitudinal in main deck. Contour for general stress, SIGXX, shown.

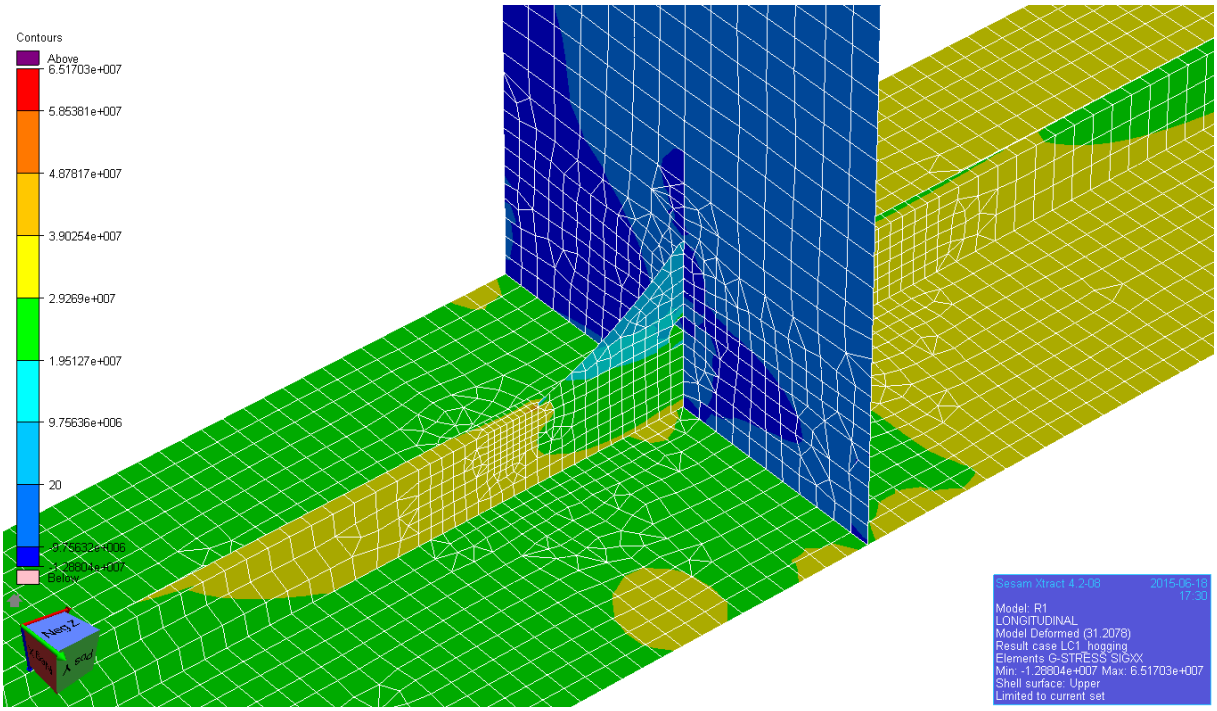

Figure F.17: The longitudinal in main deck at end support A-A. Mesh hotspot: t x t. Loading Condition: Hogging moment. Contour for General stress SIGXX is shown.

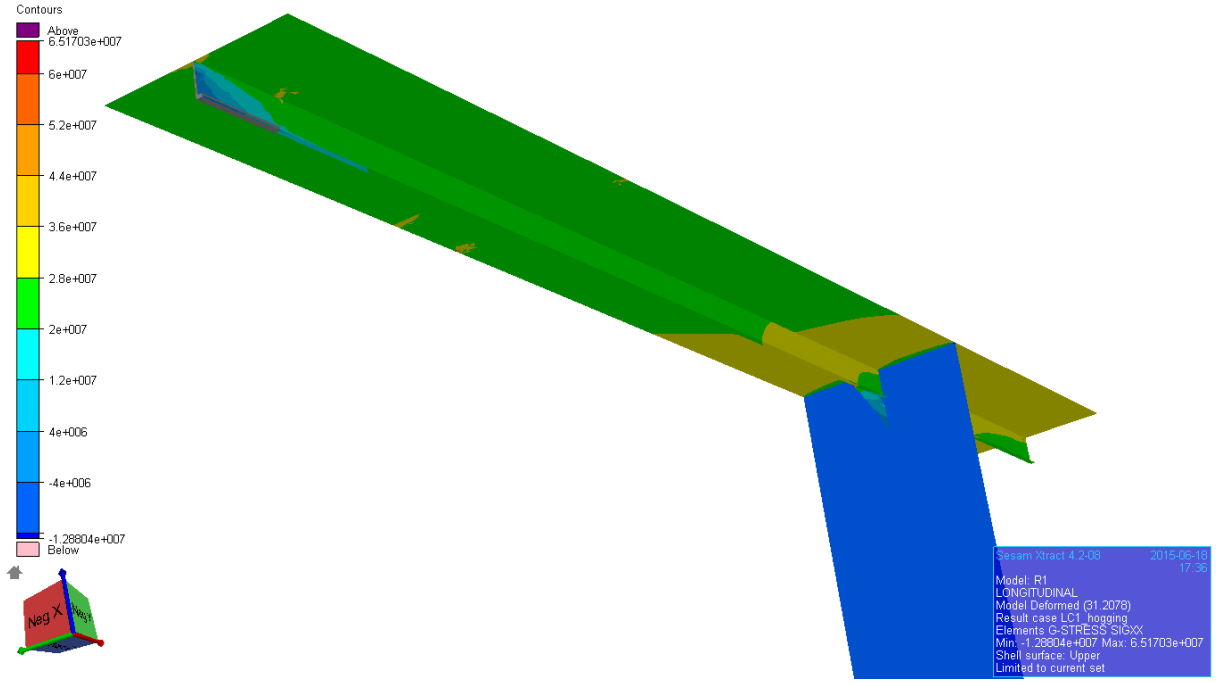

Figure F.18: Longitudinal in main deck seen in forward direction.

Appendix G – Result Comparison Study

a) Application of axial load

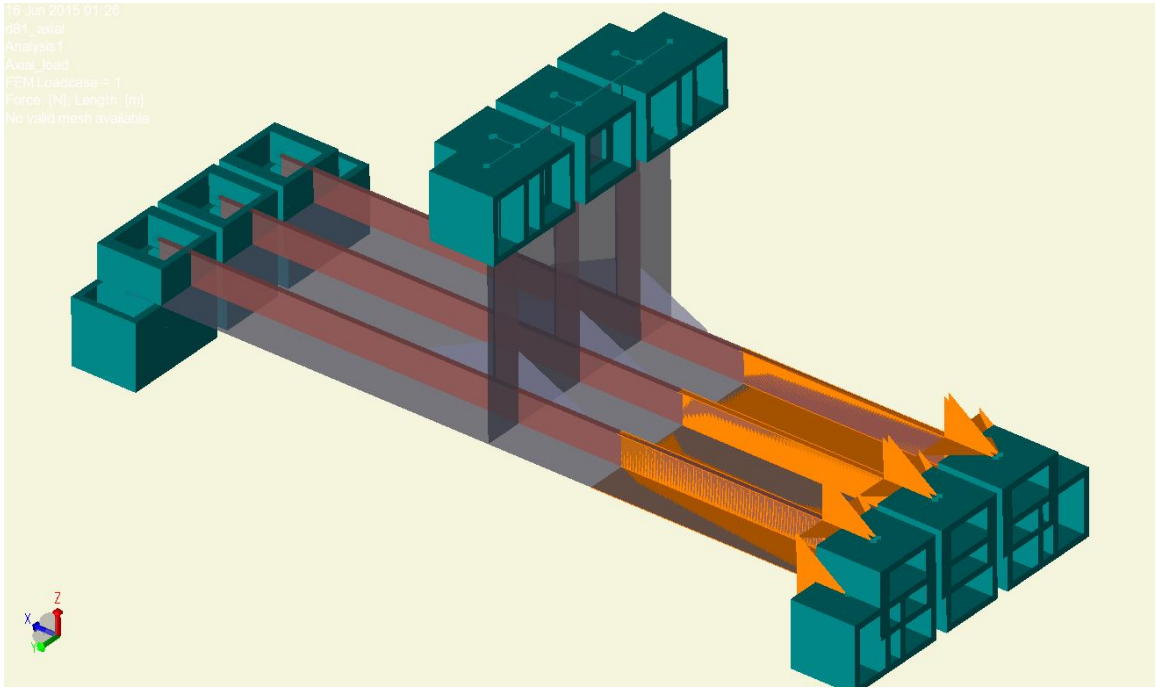

b) Application of bending load:

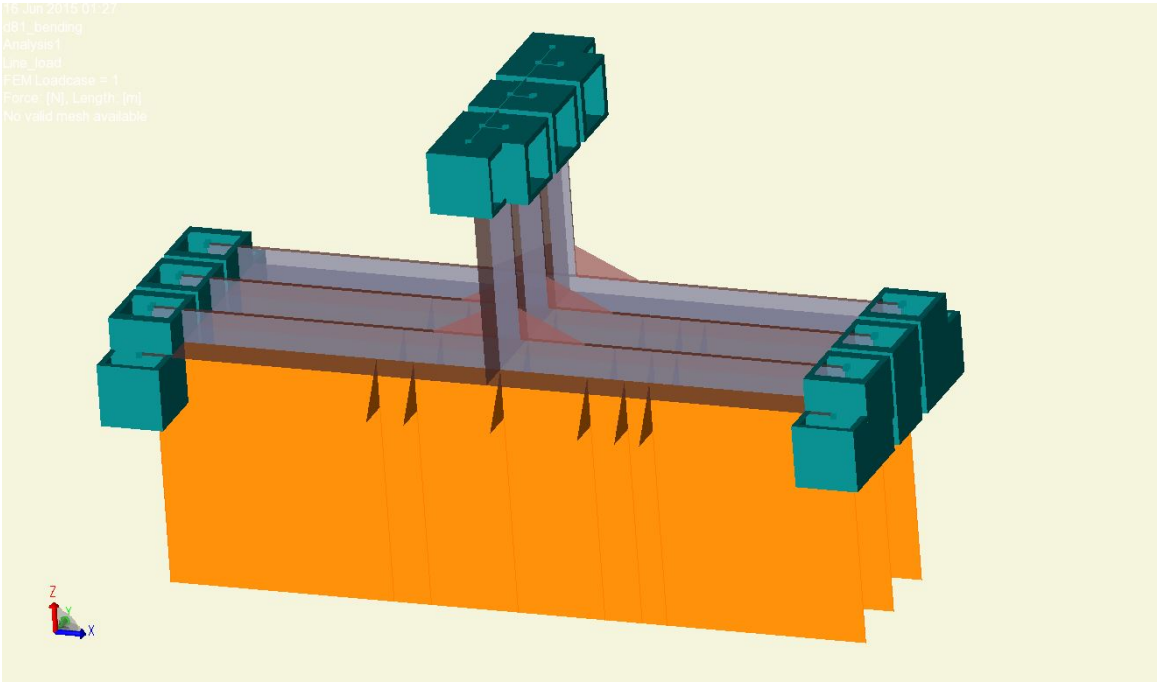

Figure: A) shows the application of axial load P = -1 N/m and b) shows the application of line load P = 1.0 N/m.

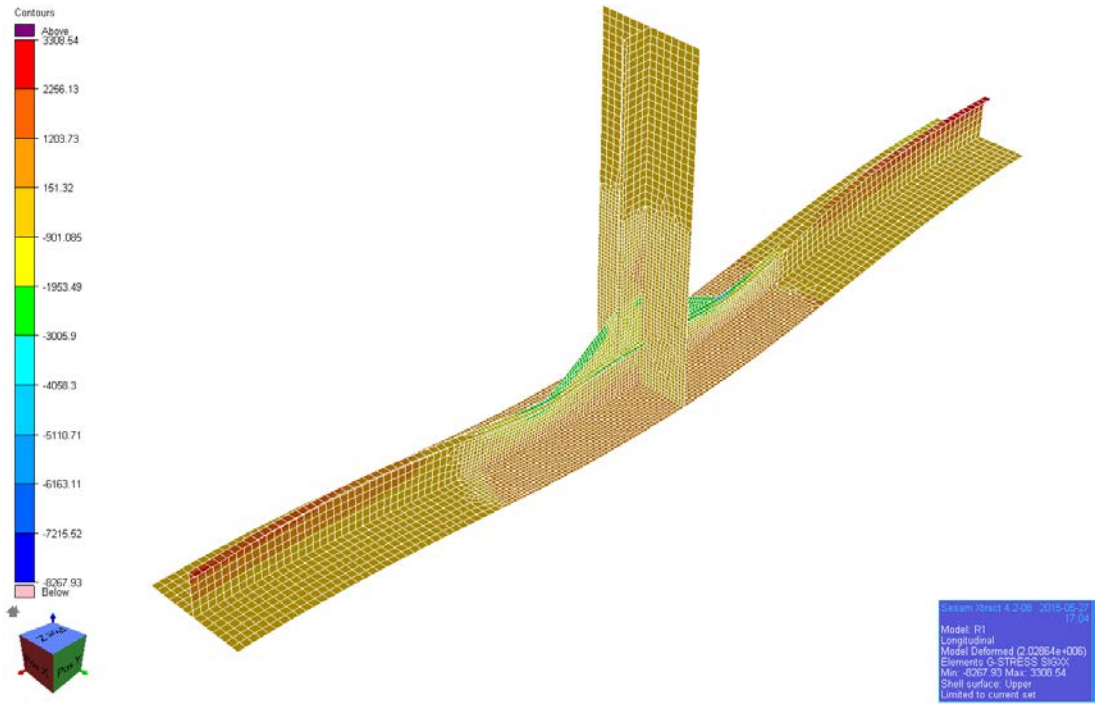

Figure: Isometric view of D81X deformed under bending. The contour represents the general stress, SIGXX and the mesh size is txt.

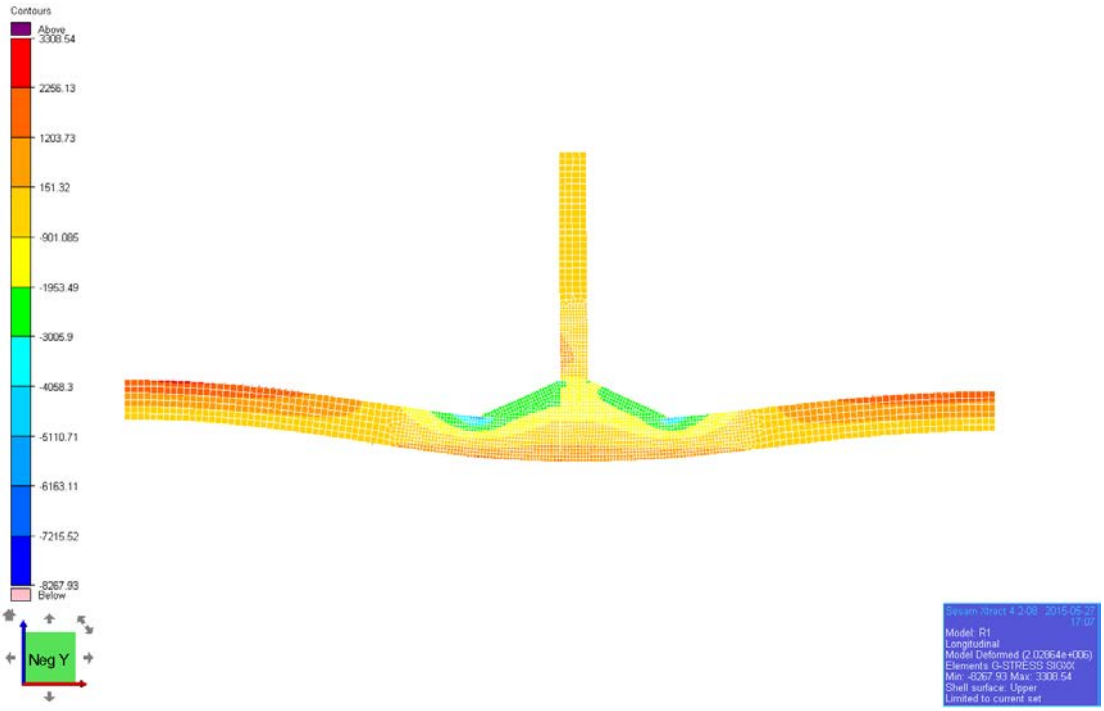

Figure: Side view of D81X deformed under bending. The contour represents the general stress, SIGXX and the mesh size is txt.

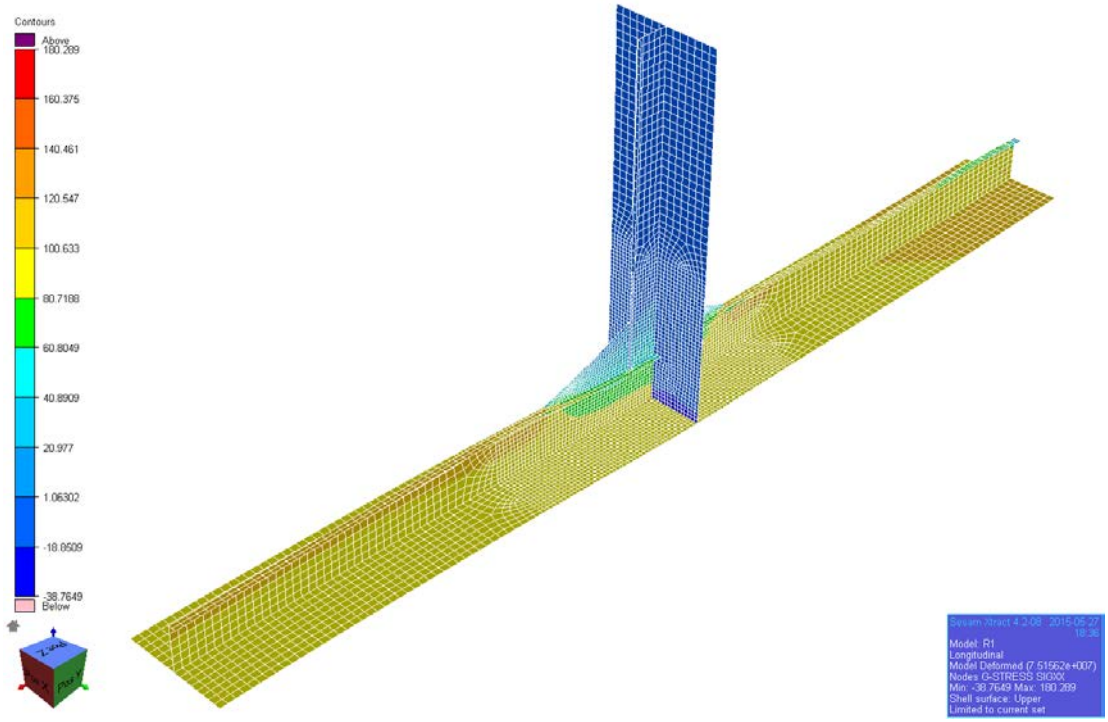

Figure: Isometric view of D81X deformed under axial loading. The contour represents general stress, SIGXX and the mesh size is txt.

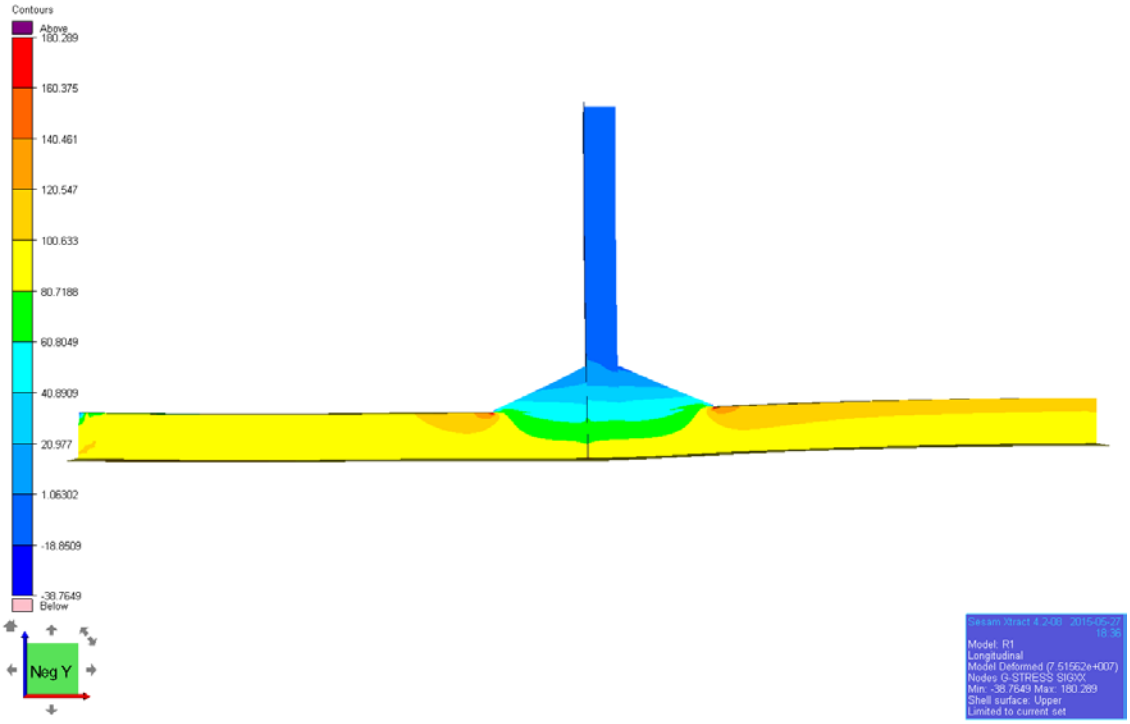

Figure: Side view of D81X deformed under axial loading. The contour represents general stress, SIGXX.

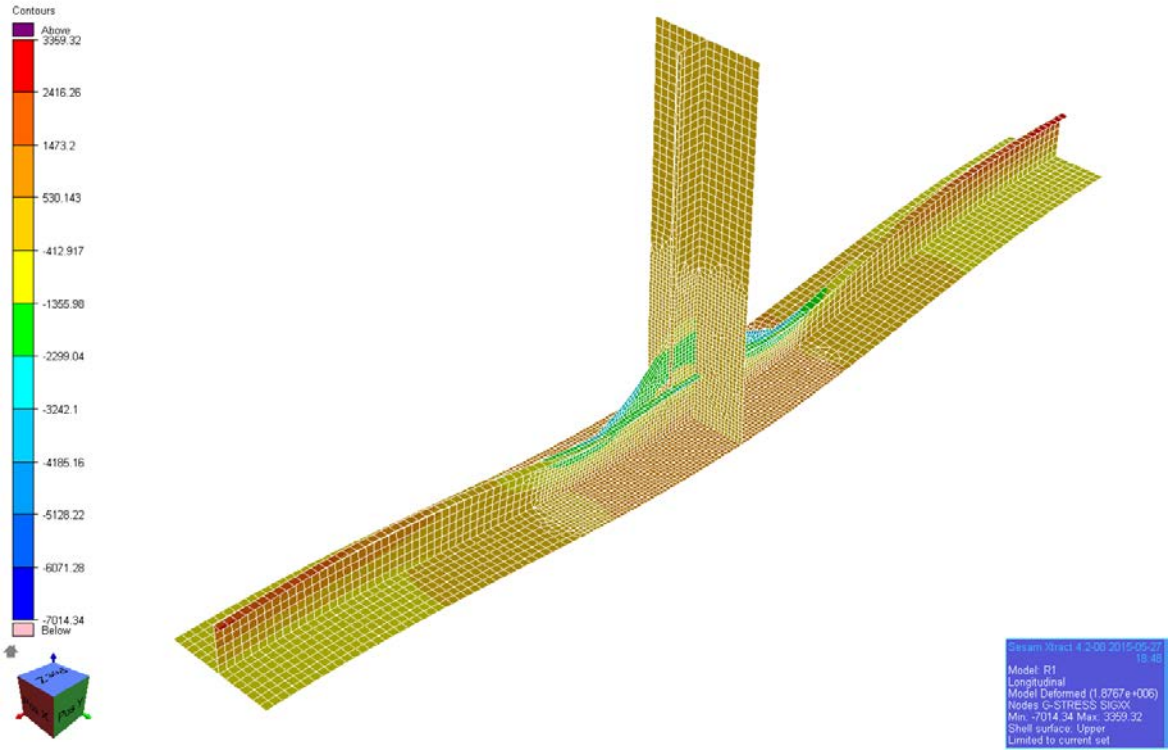

Figure: Isometric view of DA-A deformed under bending. The contour represents the general stress, SIGXX and the mesh size is txt.

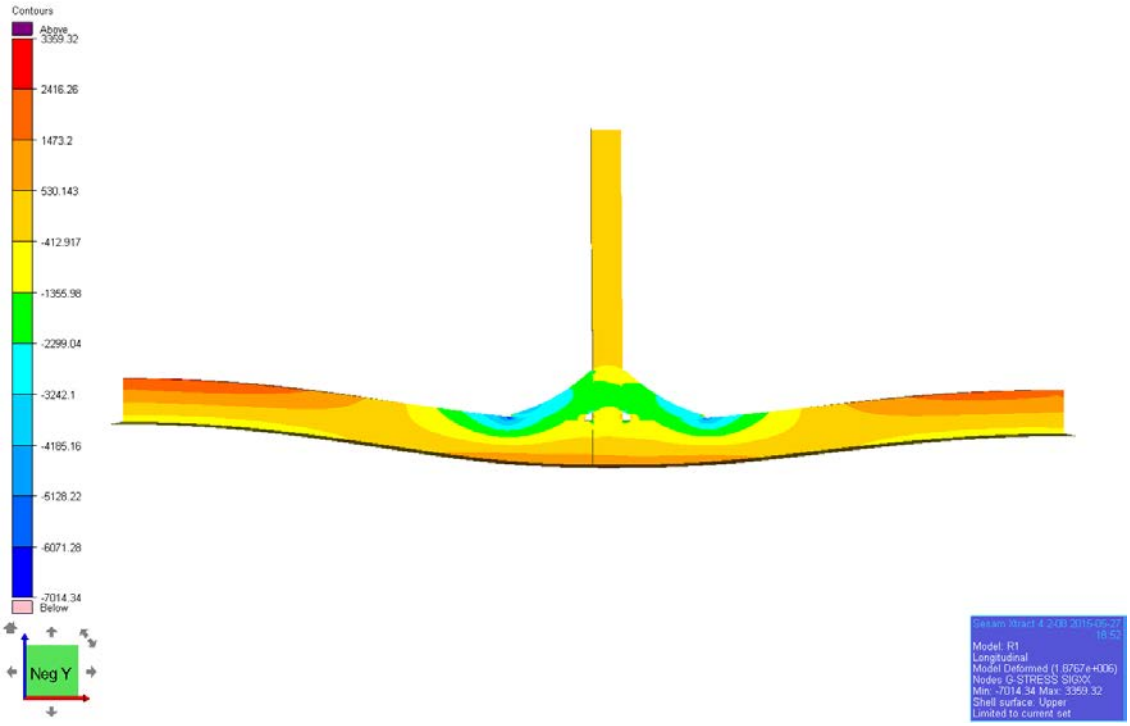

Figure: Side view of DA-A deformed under bending. The contour represents the general stress, SIGXX.

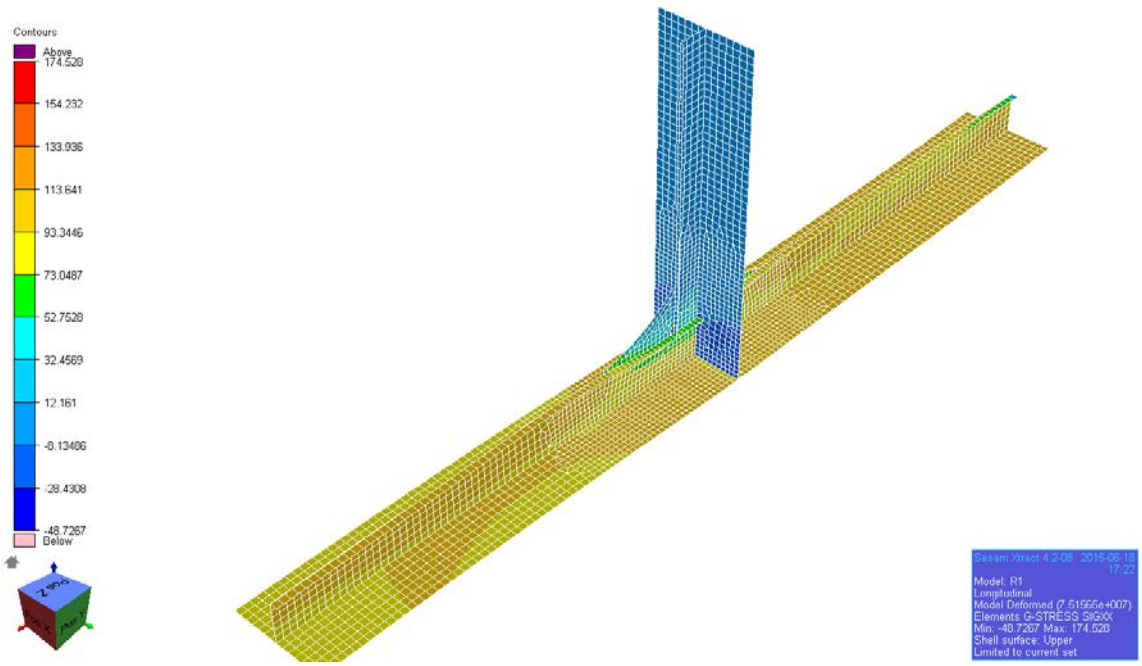

Figure: Isometric view of DA-A deformed under axial loading. The contour represents the general stress, SIGXX and the mesh size is txt.

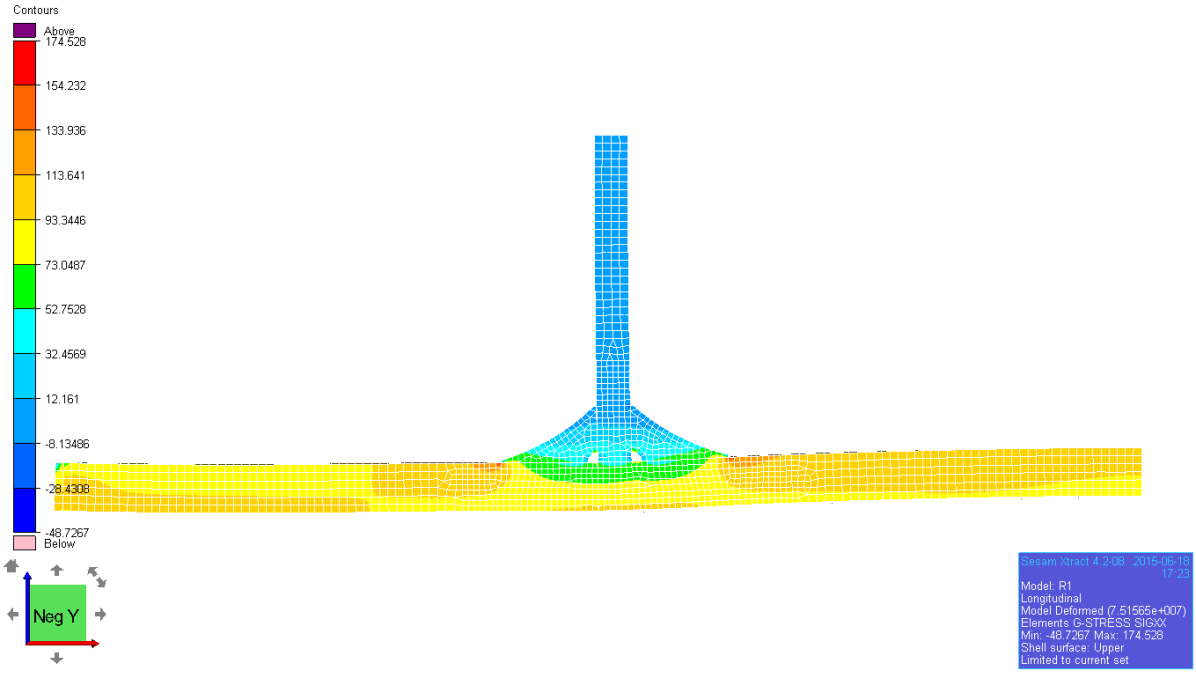

Figure: Side view of DA-A deformed under axial loading. The contour represents the general stress, SIGXX.